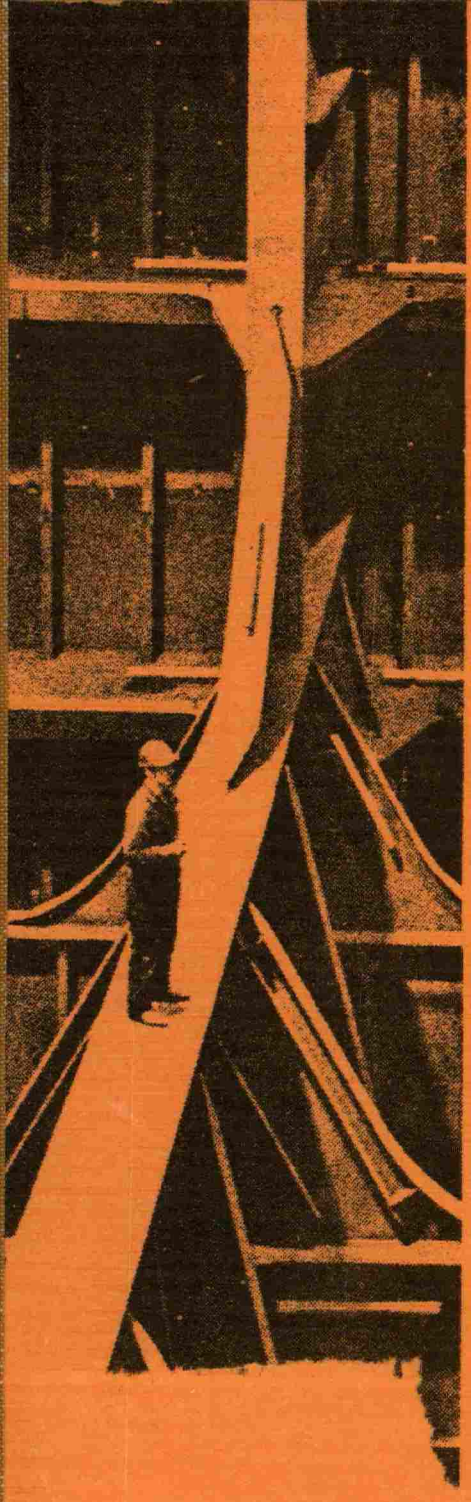

T. MOAN, K. SYVERTSEN
AND S. HAVER

STOCHASTIC DYNAMIC RESPONSE ANALYSIS OF GRAVITY PLATFORMS

REPORT SK/M 33

TRONDHEIM 1976

INSTITUTT FOR
SKIPSKONSTRUKSJONER
NORGES TEKNISKE HØGSKOLE
UNIVERSITETET I TRONDHEIM

DIVISION OF SHIP STRUCTURES
THE UNIVERSITY OF TRONDHEIM
THE NORWEGIAN INSTITUTE
OF TECHNOLOGY

MEDDELELSER

SK/M 21 Moe, J. og Gisvold, K.: "Optimization and Automated Design of Structures". 1971.

SK/M 22 Haslum, K. og Tønnessen, A.: "Torsion of Thin-Walled Non-prismatic Beams". 1971.

SK/M 23 Vinje, T.: On Viberation of Spherical Shells Interacting with Fluid". 1972.

SK/M 24 Haslum, K. og Manoharan, K.: "Transverse Frames Supported on Longitudinals Members". 1972.

SK/M 25 Sandvik, P.Chr. og Torp, S.: "Water Degradation of GRP Panels". 1972.

SK/M 26 Moe, J., Stensrud, F. og Vitiello, E.: "A Feasibility Study of Prestressed Concrete Tanker Ships". 1972.

SK/M 27 Vinje, T.: "On the Statistical Distribution of Maxima of Slightly Non-linear Stochastic Variables". 1974.

SK/M 28 Sandvik, P.Chr.: "Deck Plates Subject to Large Wheel Loads". 1974.

SK/M 29 Carlsen, C.A.: "Automated Design of Plane Transverse Bulkheads in Tankers". 1974.

SK/M 30 Lorentz, J.: "Tank Arrangement for Crude Oil Carriers in accordance with the new Anti-Pollution Regulations". 1974.

SK/M 31 Søreide, T. og Moan, T.: "Non-Linear Material and Geometric Behaviour of Stiffened Plates". 1975.

SK/M 32 Carlsen, C.A.: "INDETS - A System for Integrated Design of Tanker Structures". 1975.

SK/M 33 Moan, T., Syvertsen, K. og Haver, S.: "Stochastic Dynamic Response Analysis of Gravity Platforms". 1976.

SK/M 34 Moan, T., Carlsen, C.A., Lassen, T. og Søreide, T.: "Experimental Investigation of Stiffened and Unstiffened Circular Bulkheads Laterally Loaded to Ultimate Failure". 1975.

NTH-Trykk
Trondheim 1976

REPORT SK/M 33

STOCHASTIC DYNAMIC RESPONSE ANALYSIS OF GRAVITY PLATFORMS

BY

T. MOAN , K. SYVERTSEN AND S. HAVER

MAY 1976
TRONDHEIM

CONTENTS

ACKNOWLEDGEMENT

The authors would like to express their sincere thanks to Drs. Tor Vinje and Ragnar Sigbjørnsson for discussing the statistical developments presented in Chapter 4 of this report.

SUMMARY

The present study is concerned with the dynamic response analysis of gravity platforms subjected to random wave excitation.

The dynamic modeling involves three media, namely the soil, the structure and the sea. The modeling was planned so as to obtain a linear system. The structure is treated as the primary system, for which the response is to be determined. The dynamic behaviour of the soil and sea is represented by appropriate boundary conditions.

The structure represents stiffness, mass and damping in the system. The concrete caisson of the gravity platform is assumed to be rigid while the flexibility of the steel/concrete superstructure is modelled by beam elements accounting for bending and shear flexibility.

The transformation of the modal damping ratio for a fixed base structure into an equivalent modal damping ratio for the interaction system is commented upon.

The soil is assumed to contribute to the stiffness and the damping of the system. The soil behaviour is represented by equivalent spring and viscous damping coefficients in the point where the structure and soil interface. In general, the stiffness and damping coefficients are frequency dependent.

An elastic half-space model is adopted for the soil. The shear modulus then becomes the principal characteristic parameter.

Hysteretic losses in the soil are accounted for by an equivalent viscous damping coefficient. The effect of a potential embedment of the foundation can also be taken into account by egineering corrections devised by Novak and co-workers.

The sea primarily represents the excitation forces, but contributes also to the damping and the mass of the dynamic system.

The excitation forces are conveniently separated into forces on the slender superstructure and the caisson, respectively. The forces acting on the superstructure by a harmonic wave component is represented by the Morrison formula. The diffraction effects occuring by a short wave-length to shaft-diameter ratio are accounted for by appropriately varying the mass coefficient. Drag forces are in most cases negligible. The forces on the caisson are due to potential effects and are obtained from laboratory experiments and analysis applying source and sink techniques. Diffraction effects are accounted for.

The added mass of the surrounding water is determined in a similar way. Simplified estimates for the damping resulting from the generation of surface waves and drag are given.

The resulting linear dynamic model is utilized to compute transfer-functions (i.e. steady-state response by a harmonic wave with amplitude 1 m) for actual response quantities.

The transfer-functions provide a convenient basis for a statistical treatment of the response in the frequency domain.

In the statistical analysis the sea elevation is described as a Gaussian process with zero mean.

A stationary (short-term) sea state has a duration of some hours and is conveniently characterized by the significant wave-height, the mean wave period and the assumed duration of the storm. The first two parameters determine a wave spectrum. Pierson-Moskowitz-, Jonswap-, Derbyshire-Scott and Modified Derbyshire Scott-spectra were selected to be representative choices in the present context. A directional function to account for short-crested waves may also be included.

The long-term variation of the sea may be described as a series of short-term states with gradually changing spectrum. A complete long-term description requires the long-term distributions of the wave-spectrum parameters to be known. In addition, long-term directionality of the weather states is necessary.

The following three long-term models are discussed

- continuous distribution of short-term parameters (conventional method) [a crude approximation for the directionality of weather is proposed.]
- modified continuous distribution of short-term parameters to avoid unphysical combinations of waves [a crude approximation for long-term directionality of the weather is proposed.]
- a three-dimensional discrete "distribution" of wave parameters ($H_{1/3}$, $\bar{T}$ and direction, α). Each of the three axes is subdivided into classes ("blocks"), and a probability is associated to each three-dimensional "block", as recorded by wave observations.

The statistical treatment of the *response* may either be carried out as a short-term or a long-term analysis. Both approaches are considered herein.

Numerical studies are carried out. The structural characterics are the same in all cases. The shear modulus of the soil is varied and the effect of the direction of wave progress is investigated.

Dynamic amplification is found to be significant and must be tanken into account by the design of the actual type of structures. The magnitude of the shear modulus is of paramount importance for the response level.

Besides the magnitude of the lowest eigenfrequencies, the phase differences of forces on different shafts and the direction of wave progress are found to have a major influence on the response.

Preliminary parameter variations have been accomplished to study the effect of the choice of wave-spectrum and spectrum directionality. Significant scatter in results obtained by various spectra is found. Among the four spectra utilized none gave consistently the largest response value.

The conventional continuous long-term model and its modified version - by suppressing unphysical combinations of $H_{1/3}$ and $\bar{T}$ occuring in the conventional approach - were applied and considerable deviations were found in the respective long-term distributions. Further research will be needed in establishing reliable long-term models. The simplest and most reliable model is believed to be the discrete model, although it excludes the most extreme sea conditions.

Notation

a_0 - Dimensionless frequency $a_0 = \Omega r_0 \sqrt{\frac{\rho}{G_s}}$

A - Area

A - Parameter in the general wavespectrum

AH - Parameter in relation between $H_{1/3}$ and H_v

AT - Parameter " " " $\bar{T}$ and T_v

A_L - Work done by the damping force during a cycle

A_T - Maximum kinetic energy

BH - Parameter " " " $H_{1/3}$ and H_v

BT - Parameter " " " $\bar{T}$ and T_v

B - Parameter in the general wavespectrum

B_ϕ - Constant defining the torsianal damping coef.

C - Parameter in the Derbyshire Scott wave spectra

C_H - Coefficient for the horisontal force on the caisson

C_I - Total inertial force coefficient

c_j - Dimensionless damping coefficient

c_{rr} - Optimal damping coefficient

C_{Mi} - Inertial force coefficient
i=1 Froude-Kryloff force coefficient
i=2 Inertia force coefficient

C_D - Drag force coefficient

C_{MD} - Damping force coefficient

C_{MT} - Coefficient taking into account the overall modification of the pressure on top of the structure due to the presence of the structure

C_{MB} - Coefficient taking into account the overall modification of the pressure on the bottom of the structure due to the presence of the structure

C_T - Coefficient which takes into account the overall modifications of the pressure on the top of the structure

C_B - Coefficient which takes into account the overall modifications of the pressure under the bottom of the structure

D - Diameter (caisson, pile etc)

$\tilde{D}$ - Hysteretic damping ratio

D_j - Damping ratio for the j'th mode of vibration of loading on the caisson

e - Eccentricity of loading on the caisson $e = s_R/s_1$

E - Young modulus

E - Statistical expectation ("average")

EMARG - Statistical marinal expectation

$f(x)$ - Probability density function

$F(x)$ - Cumulative probability function

f_H - Coefficient for horizontal caisson force accounting for the shape and size of the structure. For each shape (cylindric, triangular etc), the coefficient is a function of $\sqrt{A}/\lambda$.

f_M - Coefficient for overturning moment on the caisson

f_v - Coefficient for vertical caisson force

f_j, F_j Flexibility functions

$F\bar{F}$ - Distance from equilibrium line in the joint distribution for $H_{1/3}$ and $\bar{T}$

$f(\theta)$ - Directional function

g - Accelration of gravity

g_j - Dimensionless dampingcoefficient

G - Shear modulus

h - Sea depth

h' - Depth from sea surface to the top of the caisson

$h(t)$ - Unit impulse response function

H - Wave height (peak to through distance)

$H_{1/3}$ - Significant wave height

H_o - Parameters in the Weibul distr. of visual wave height

H_c - Parameters in the Weibul distr. of visual wave height

i	-	The imaginary number $i = \sqrt{-1}$
I,J	-	Moment of inertia
IMAX	-	Number of intervals of T
JMAX	-	Number of intervals of $H_{1/3}$
k	-	Wave number, $k = 2\pi/\lambda$
k	-	Parameter in the wave spectrum
K(n)	-	Parameter in the directional function of the wave spectrum
k_j, K_j		Stiffness functions
ℓ	-	Parameter in the wave spectrum
L	-	Duratian of a short term period
m,M	-	Mass
m_i	-	Moments of the spectrum, $m_i = \int_0^\infty \omega^i S(\omega) d\omega$
n	-	Constant in the directional function
N	-	Number of maxima (peaks)
n_{ID}	-	Number of recordings in a block (I, J) in intervall ID
N_{ID}	-	Total number of recordings in interval ID
NUDIR	-	Number of directional intervals
P	-	Pressure in the water
p_1	-	$(\partial P/\partial x)max \cdot$(distance from vertical centerline to the edge of the structure)
dp	-	Force per unit length (of a shaft)
P_i	-	Nodal force
P	-	Force
P_D	-	Drag force
P_I	-	Inertial force
P_{IO}	-	Amplitude value of P_I
P_H	-	Horisontal force on the caisson
P_Y	-	Vertical force on the caisson
PDIR	-	Probability that the main direction will fall within a given interval
PVW	-	Probability that visual waveperiod, T_v, fall within a given interval

$Q(X \geq x)$ Probability exceed a value x

r - Parameter in Rayleigh distribution, $r=2 \cdot m_0$

r_0 - Radius of disc (caisson)

r_i - Nodal displacement

r_G - Coef. accounting for the embeddement of the caisson

r_m - Coef. accounting for the embeddement of the caisson

R - Allowable area of pairs of $H_{1/3}$ and T

$R(\tau)$ - Autocorrelation function

s - Vertical distance from sea bottom

s_R - Distance from bottom to the wave force resultant on the caisson

s_1 - Height of the caisson

$S(\omega,\alpha+\theta)$ Directional spectrum

$S(\omega,\alpha)$ Unidirectional spectrum

S_c - Conditional standard deviation

t - Time

T - Wave period

$\bar{T}$ - Average mean wave period

T_i - Period between: i=2 - crests
i=3 - zero upcrossing

TLIM - Boundary value according to equilibrium concept

u - Velocity in the water perpendicular to the shafts

$\partial u/\partial t$ Acceleration due to wave motion perpendicular to the shafts

V - Volume of cylindrical (caisson) structure

W - Sectional modulus of the horizontal area of the structure (caisson)

X_o - Respons level

$X(t)$ - Stochastic variable

x,y,z Cartesian coordinates

z_e - Embeddement

z_{CG} - Dist. from caisson bottom to its center of gravity

Notation (Greek letters)

α - Angle of incoming wind; Equilibrium parameter

α_i - Constants defining the dyn. stiffness coef.

β_i - Frequency ratio = $\frac{\Omega}{\omega_i}$

- Constants defining the dyn. stiffness coef.

γ - Angle defining the orientation of the structure

γ_o - Parameter in the Weibul distr. of visual wave height

γ_i - Constants defining the dyn. stiffness coef.

δ - Phase angle

δ_o - Coef. accounting for the embeddement of the caisson

ε - Parameter defined as, $\varepsilon^2 = 1 - \frac{m_2^2}{m_0 m_4}$

ε_o - Constant defining the accurancy in calculating FF

η - Parameter in wave spectrum

θ - Angle between an elementary wave and incomming wind direction

κ - Parameter in wave spectrum

λ - Wave length

λ_o - Coef. accounting for the embeddement of the caisson

ν_3 - Frequency of zero upcrossing

ξ - Damping ratio (relative to the critical damping)

ρ - Density

σ - Standard deviation

τ - Time interval

ϕ - Transfer function

ϕ^* - Complex conjugated of ϕ

ϕ_{PS} - Pseudotransfer function

ϕ^*_{PS} - Complex conjugated of ϕ_{PS}

ψ - Rotation about x-axis

θ - " " y-axis

ϕ - " " z-axis

χ_j - Corrective coefficient to structural damping ratio

ω - Circular wave frequency $\omega = 2\pi/T$

$\bar{\omega}$ - Average mean wave frequency

Ω - Circular frequency of applied loading

ω_p - Peak frequency in the wave spectrum

ω_o - Peak frequency in the Derbyshire Scott wave spectra

Matrix notation

C - Damping matrix - equivalent viscous damping matrix

F - Flexibility matrix

I - Unity matrix

K - Stiffness matrix

M - Mass matrix

P - Force vector

R(t) - Load vector (dynamic)

S - Internal force matrix

r - Displacement vector

$\dot{r}$ - Velocity vector

$\ddot{r}$ - Acceleration vector

Y - Normal coordinate vector

Φ - Modal matrix

ω^2 - Diagonal matrix of eigenfrequencies

Subscript notation

c - ref. to the structure (platform)

D - -"- drag force

E_q - -"- equilibrium wave spectrum

f - -"- fluid (environmental water)

H - -"- horizontal direction

I - -"- inertia force

ID - -"- directional interval no. ID

I	-		interval of $H_{1/3}$
J	-	-"-	interval of $\bar{T}$
i j	-	-"-	i or j the degree of freedom
L	-	-"-	interval no. L of visual wave period
m	-	-"-	mass
R	-	-"-	response spectrum
s	-	-"-	soil
v	-	-"-	vertical direction
v	-	-"-	visually estimated wave parameters
w	-	-"-	wavespectrum
xs, ys, zs θs	-	-"-	static values in directions: x,y,z and θ
xΩ yΩ zΩ θΩ	-	-"-	dynamic values in directions: x,y,z and θ
x	-	-"-	x-direction
y	-	-"-	y-direction
z	-	-"-	z-direction
ψ	-	-"-	rotation about the x-axis
θ	-	-"-	" " the y-axis
ϕ	-	-"-	" " the z-axis

Superindex notation

- (bar)	"statistical average"
· (dot)	diff. with respect to time
*	quantities in normalized eqs. of motions.

1. INTRODUCTION

Presently, numerous offshore oil and gas drilling platforms are being designed for deep water areas where environmental loadings are severe. Due to high investment and present public policy which emphasizes protection of environment against oil spills an accurate structural design is needed.

Fixed platforms of current interest in the North Sea are steel jackets and so-called gravity structures. The steel jacket is mostly a steel trusswork on a pile foundation. The gravity structure, Ref.(1) consists of a concrete caisson resting on the bottom, and a simple framed super-structure made in concrete or steel or both. The height of the caisson is typically 1/3 - 1/2 of the water depth. The frame consists of 3 - 6 shafts. Typical examples are shown in Fig. 1.1.

The platform is subjected to loadings of different types. Functional loading, e.g. equipment on the deck etc.- and environmental loading like wind and current are assumed to be static. This assumption is not correct for the wind, but since wind forces are relatively small, this simplification is premissible.
The wave loading is, however, dynamic and random in nature.

The need for more accurate prediction of response, together with the dynamic nature of the environmental loads, calls for dynamic analysis methods instead of the static analysis methods which were used in the design of shallow platform structures in the Gulf of Mexico. The need for more accurate prediction of the dynamic response of offshore platforms due to wave loading is emphasized by the fact that tall, slender structures with flexible foundations are susceptible to significant dynamic magnification of the response.

It is pertinent to know the range of fundamental periods of typical deep-water oil production platforms.

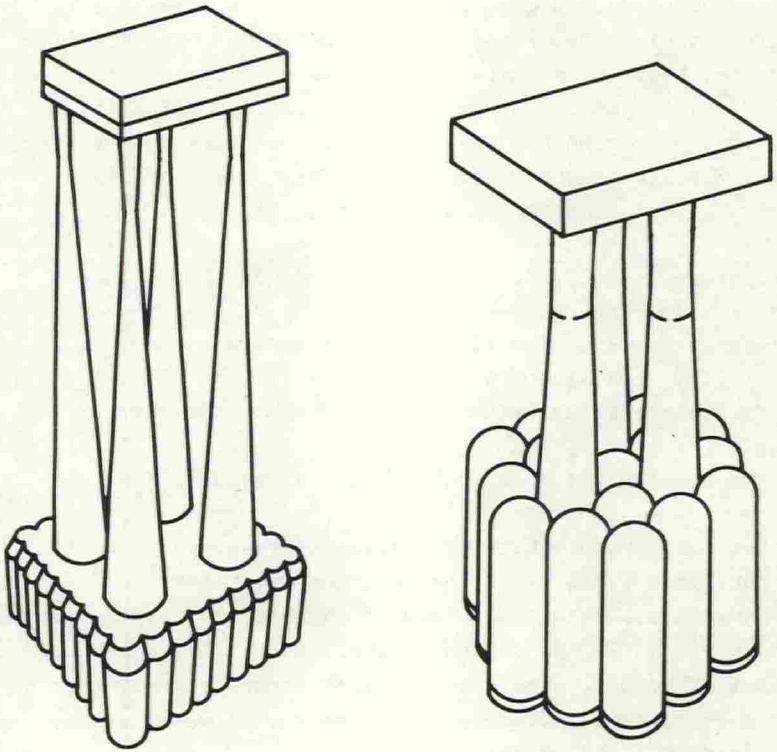

Fig. 1.1 Typical gravity type platforms

Gravity type platforms in 100 - 150 m water depth in the North Sea have fundamental periods in the range of 3.0 - 6.5 seconds depending on the foundation stiffness, which has a significant influence on the eigenfrequencies.

In the design of structures subjected to dynamic loading two different statements in the response is generally requires, depending on the corresponding mode of failure, Refs.(2.3):

- the single extreme peak response(in connection with ultimate collapse mode)
- the complete response history (in connection with fatigue or cumulative damage design)

While the prediction of a single extreme peak response is a well-defined task, the evaluation of the response for fatigue design needs some comments.
For a time history it is not obvious how relative maxima and minima should be paired to fatigue contributing stress cycles. Dowling, Ref.(8) investigated the applicability of a number of *counting methods* by making laboratory experiments with steel specimens subjected to irregular strain histories. No similar investigation is known for prestressed concrete.

In high cycle fatigue the simple mean crossing-peaks counting methods may be utilized. The range-pair and the (more complex) rain-flow method was shown to be the best fitted where most of the damage is due to a few major reversals (low cycle fatigue).

Usually the response spectrum of stresses is known. What is needed, however, is a relation between one distribution function of stress cycles and the stress spectrum. The distribution corresponding to the actual *counting method* must thus be determined.
When the response is a sufficiently narrow band process,

it is assumed that the number of cycles for each amplitude-level is accurately described by the number of peaks associated with each positive peak level. This assumption is made in this investigation.

By the structural design a satisfactory safety of the structure is ensured by introducing partial safety factors on loading, material and production tolerances, using a semi-probabilistic design method, Refs.(2-3), or by a complete probabilistic consideration of the safety, Ref.(5). The fully probabilistic methods have not been completely accepted in design codes as yet. In a semi-probabilistic design the response at a certain (low) probability level is necessary for a single excursion failure design, whilst most of the load history in a life of the structure is necessary in case of fatigue design.

The objactive of this report is to present a response analysis method which reflects the dynamic and random nature of the wave loading.

2. DYNAMIC MODELING

2.1 General Remarks

A fixed offshore structure interacts with the soil and the ocean and each of these media has to be duely considered to obtain a correct representation of the dynamic behaviour. A numerical, discrete model representing all media could be developed by means of a numerical technique such as the finite element method, Refs.(14-16).

However, in the process of formulation of the model the analyst is faced with the two conflicting requirements, namely

- make the model as *simple* as possible for case of interpretation and checking of results and for reduction of

analysis cost.
- make the model *complex* enough to represent all the possible modes of dynamic response as long as the capacity of the computer program and computer facilities is not exceeded.

The choice of model will in general depend upon the phase of design which is of interest, and the accuracy of data to put in the mathematical model.

In the present context the platform is considered to be the principal system for which response is to be evaluated. Therefore only the concrete/steel structure will be modelled. The environmental media - soil and ocean - are represented by boundary conditions for the structure. The boundary conditions are determined by imposing disturbances (corresponding to typical behaviour of the structure) on the surrounding media.

The dynamic behaviour of the soil and the ocean are determined by separate analyses or experiments.

Soil-structure interaction modelling has previously been considered for instance by Clough and Penzien, Ref.(16), Sarrazin, Roesset and Whitman, Ref.(23), Krizak, Gupta and Parmelee, Ref. (24) and Roesset, Whitman and Dobry, Ref.(25), Novak, Ref.(36) among others.
Soil-structure-ocean interaction modelling has been treated by Bell, Ref.(102),Moan, Ref.(104), Holand, Ref.(105), Eatock-Taylor, Ref.(106), Moan, Haver and Vinje, Ref.(107) and Larsen, Ref.(110) among others.

The structure-ocean interaction problem for fixed offshore structures has been investigated by Dean and Harleman, Ref.(66), Nath and Harleman, Ref.(67), Wilson and Muga, Ref.(68), Malhotra and Penzien, Ref.(69), Foster, Ref.(70), Selna and Cho, Ref. (71) and Berge, Ref. (72) among others.

2.2 Equations of Motion

The equations of motion for a multi-degree-of-freedom system (see e.g. Fig. 2.1) with viscous damping may be expressed in matrix notation as, Refs.(14 - 16):

$$M\ddot{r} + C\dot{r} + Kr = R(t) \qquad (2.1)$$

The finite element method has proven to be the most effective technique for general matrix formulation of governing equations and subsequently digital computer analysis, and it will be assumed here that the discretization is of this type. In this method, the structure is formulated by idealizing the structure into an assemblage of discrete finite elements with mass, damping and stiffness properties.

2.3 Structural Idealization

General Remarks

The structure contributes to the stiffness, mass and damping properties of the system. The caisson in general is made of concrete. The superstructure is of steel or concrete or a combination of both materials.

Stiffness and Mass

The slender superstructure is modelled by beam elements accounting for axial-, bending- and shear flexibility.

The cross-sectional stiffness of the *concrete* members is constituted by the concrete itself and the reinforcement steel. It must, however, be recognized that part of the concrete cross-section may crack even in serviceability limit state.

Fig. 2.2 displays the variation of rigidity of a hollow circular cross-section with the relative magnitude of axial force and

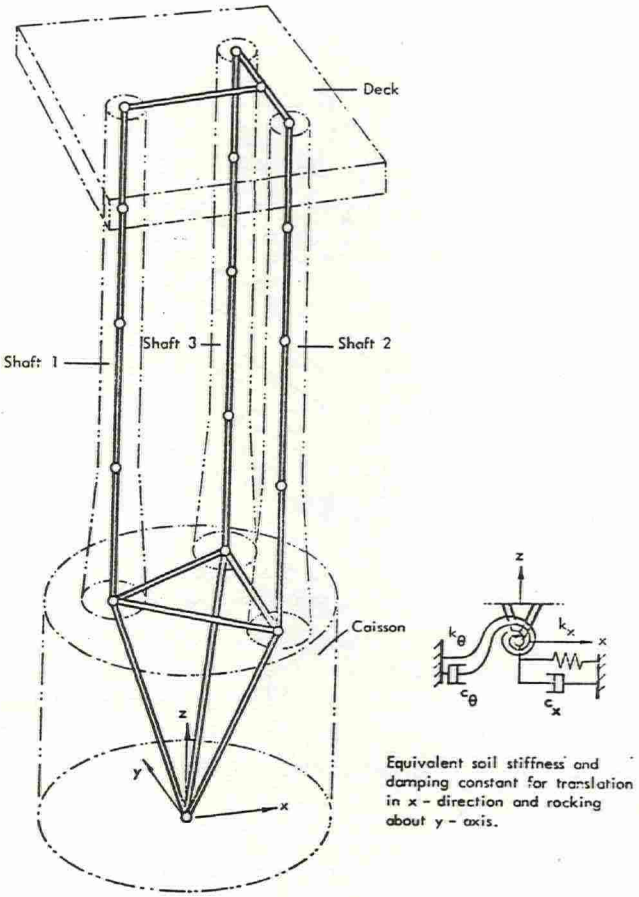

Fig. 2.1 Structural idealization of a three-column concrete gravity type platform

moment, and the percentage of steel reinforcement.

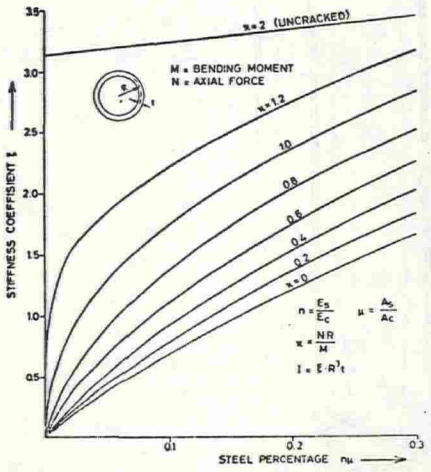

Fig. 2.2 Bending stiffness of cracked circular ring section subjected to bending and axial force

The diagram is based on the assumption that the concrete has no tensile strength.

The effect of repeated loading on Youngs modulus must also be accounted for.

The stiffness properties of a potential steel superstructure is well defined as long as the behaviour is within the elastic range.

The main motion of the platform is rocking and sliding. Thus, horizontal grillages may be considerably simplified. For instance the deck structure which may consist of several crossing girders

may be simplified as shown in Fig. 2.1 by making the original and new one equivalent by flexibility considerations.

A primary assumption is that the caisson is completely rigid. Only six degrees of freedom (in one node) are thus needed to describe the behaviour of the caisson. Even if the caisson is almost rigid the nodes of the superstructure and the bottom node are connected by elements with stiffness 50 times the stiffness of the column. This introduces satisfactory rigidity without causing numerical ill-conditioning by the solution of the governing equations. The choice of mesh in the superstructure primarily depends on the ability of the beam element to represent variation in stiffness and mass. A particular point is whether "lumped" or "consistent" mass is used. In general the "lumped" mass formulation yields a larger discretization error than the consistent formulation for the same number of degrees of freedom. For the same computer costs, a more refined mesh can be applied for the "lumped" mass formulation; thereby compensating for the initial benefit of the "consistent" formulation. For the modeling shown in Fig. 2.1 the lower eigenfrequencies will be insignificantly influenced by this approximation. As later will be shown, it is the lower (few) eigenmodes that give the major contribution to the dynamic behaviour. This fact justifies a lumped mass formulation even with a rather coarse beam idealization.

Damping

Structural damping is due to internal friction within the material itself (hysteretic damping) and is proportional to the deflection. The structural damping is small as compared to the damping in soil and surrounding waters. Reported values for damping in uncracked *prestressed concrete* beams are 0.5 - 1 % of critical damping, Refs (10-12)

The damping, however, varies significantly with the development of cracking. Therefore, the damping is indirectly related to

the amount of prestress since the level of prestressing governs the extent of cracking. The references quoted report damping ratio in the range 1 - 2 % for beams with extensive cracks but still with linear overall behaviour.

Bare steel has an extremely low value of damping, namely in the range 0.05 - 0.15 %. Damping of full-scale structures is found to be of the order 0.2 - 0.8 %, Refs.(12,13). A reasonable damping ratio may be 0.5 % for a steel frame.

If the structure is not of monolitic type additional damping may occur in the joints, Ref.(13).

When accounting for the structural damping in the system equation for the interaction problem, the damping ratio must be appropriately modified, cfr. Appendix A.

2.4 Soil Idealization

2.4.1 General Remarks

In the present case the soil is treated as a substructure of the dynamic model, i.e. it is necessary to know the relation between the stress resultants $P_j(t)$ and the corresponding displacements $u_j(t)$ at the contact area between the soil and the structure. This relation is clearly dependent upon the properties of the soil and the geometry of the structure-soil interface. A rigid structure and a perfect bond between the footing and the soil will be assumed.

The primary soil property is the dynamic stress-strain relations. Other important dynamic soil characteristics such as excess pore pressure development, vibratory compaction and liquefaction etc. are not considered.

The cyclic shear stress-strain relationship in most soils is a hysteresis curve, Fig. 2.3a, which is conveniently described in terms of the two parameters

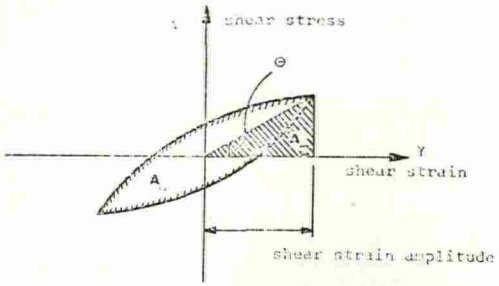

$$G = \operatorname{tg} \theta$$

$$\tilde{D} = \frac{A_L}{4\pi A_T}$$

a) Measure for hysteretic damping

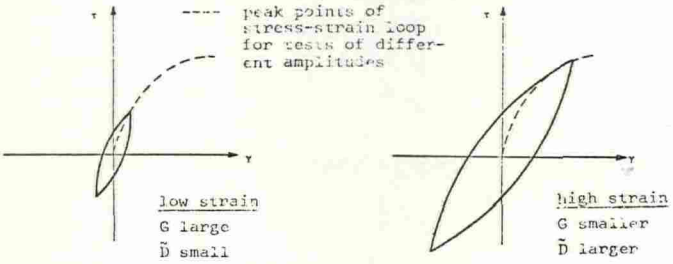

b) Influence of shear strain on the damping material properties

Fig. 2.3 Cyclic shear deformation

- the peak-to-peak slope, or, the equivalent shear modulus, G_s
- the energy absorbed per cycle, non-dimensionalized by analogy to a viscous material, as expressed by the damping ratio $\tilde{D}$ (see below).

The soil will basically be treated as a *linear isotropic elastic* half-space. However, hysteretic energy losses will be considered in a simplified manner.

The extreme cross-section shapes of the footing of current interest are the circle and the square. A rigid-footing has 6 degrees of freedom. The elastic soil is characterized by density (ρ_s), the shear modulus (G_s) and Poisson's ratio (μ_s) and contributes to the *stiffness* and the *damping* in the lower nod. of the discretized structure only. The elastic half-space

assumption provides an equivalent spring-dashpot model. The response of the soil to harmonic oscillations should be determind for the following modes of motion:

- vertical motion
- rotation about a vertical axis
- horizontal displacement (sliding)
- rotation about a horizontal axis (rocking)

In the case of wave-excitation the rocking motion is most important. The sliding and rocking motion will in general be coupled, but uncoupled behaviour is often assumed, when the structure is resting on the soil (with no embedment).

Impedance functions for dynamic soil behaviour have been considered in Refs.(17,40).

2.4.2 Stiffness and (geometrical) Damping of the Soil

Vertical Motion

Let P_j be the amplitude of a generalized (*horizontal* or *torsional*) harmonic moment acting on the disc along the j coordinate, and let u_j be the amplitude of the corresponding displacement, see Fig. 2.4. The relationship between the force and displacement may be stated as

$$P_j = K_j \cdot u_j \tag{2.2}$$

or

$$u_j = F_j \cdot P_j \tag{2.3}$$

in which K_j is a complex valued stiffness (impedance) function of the form

$$K_j = k_{js}(k_{j\Omega} + ia_0 c_{j\Omega}) \tag{2.4}$$

and

$$F_j = \frac{1}{k_{js}}(f_{j\Omega} + ia_0 g_{j\Omega}) \qquad (2.5)$$

The quantity k_{js} represents the static stiffness of the disc. $k_{j\Omega}, c_{j\Omega}, f_{j\Omega}$ and $g_{j\Omega}$ are dimensionsless functions of Poisson's ratio for the half-space material, μ_s and of the dimensionless frequency parameter

$$a_0 = \Omega r_0 \sqrt{\frac{\rho_s}{G_s}} \qquad (2.6)$$

where

G_s - shear modulus of the soil
ρ_s - density of the soil
r_0 - radius of the disc
Ω - circular frequency of the applied harmonic loading

Coupled Sliding and Rocking Motion

Consider the (coupled) translation and rocking motion in the x-z (or y-z) plane(s).

Having described completely the mathematical model for the soil material the relation between reaction force $P_x(t)$ and moment $P_\theta(t)$ and the footing displacements u and θ, may now be obtained by superposition of the various components of the total soil reaction. The following form

$$\begin{bmatrix} P_x(t) \\ P_\theta(t) \end{bmatrix} = \begin{bmatrix} K_{xx}(\omega) & K_{x\theta}(\omega) \\ K_{\theta x}(\omega) & K_{\theta\theta}(\omega) \end{bmatrix} \begin{bmatrix} u(\omega) \\ \theta(\omega) \end{bmatrix} \qquad (2.7)$$

or

$$P = KU$$

expresses the relation between steady-state-harmonic force to produce displacements, u and θ at frequency ω.

For the footing and soil material under consideration the

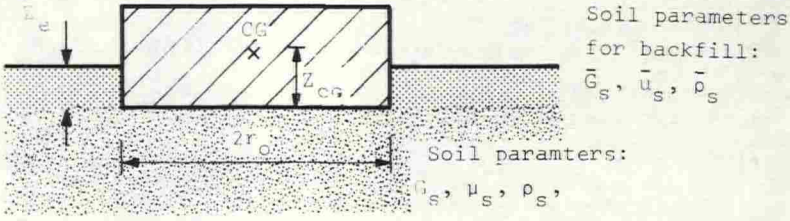

a) Rigid embedded foundation

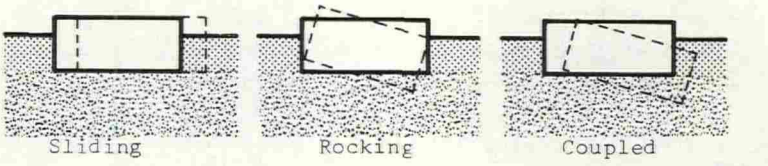

b) Vibrational modes

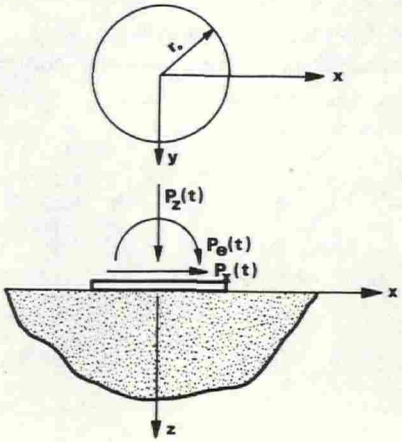

c) Simple foundation-soil system

Fig. 2.4 Basic notation for the soil-structure interaction problem

impedance functions are

$$K_{xx} = k_x(a_0) + ia_0c_x(a_0)$$

$$K_{\theta\theta} = k_\theta(a_0) + ia_0c_\theta(a_0) \qquad (2.8a\text{-}c)$$

$$K_{x\theta} = K_{\theta x} = k_{x\theta} + ia_0c_{x\theta}(a_0)$$

Hsieh, Ref.(17) has shown that the k_x, k_θ and $k_{x\theta}$ may be interpreted as the stiffness of frequency-dependent linear springs, whereas c_x, c_θ and $c_{x\theta}$ are associated with viscous dampers, also functions of frequency.

The stiffness and damping coefficients (k_j,c_j) may be written as

$$k_j = k_{js}k_{j\Omega}(a_0)$$

$$c_j = r_0\sqrt{\frac{\rho_s}{G_s}}\, k_{js}\cdot c_{j\Omega}(a_0) \qquad (2.9a\text{-}b)$$

$$j = x,y,z,\theta,$$
$$x\theta,\ y\psi,$$

It is convenient to have the dynamic properties of the soil by an equivalent spring-, dashpot-model. The coefficients may then be directly added into the system stiffness and damping matrix, respectively.

2.4.3 Equivalent Stiffness and Damping Coefficients

Stiffness for an Embedded Circular Footing on an Elastic Half-Space

In this investigation k_j and c_j were calculated from the approximate closed-form solutions presented by Veletsos and Wei,

Ref. (20), Luco and Westman, Ref.(26) and Veletsos and Verbic, Ref.(31), and Novak, Ref.(36)

The equivalent spring stiffnesses may be expressed as

$$
\begin{aligned}
k_x &= k_{xs}\,(k_{x\Omega} + \Delta k_{x\Omega}) && \text{(sliding)}\\
k_y &= k_x\\
k_z &= k_{zs}\,(k_{z\Omega} + \Delta k_{z\Omega}) && \text{(vertical)}\\
k_\theta &= k_{\theta s}\,(k_{\theta\Omega} + \Delta k_{\theta\Omega}) && \text{(rocking)}\\
k_{x\theta} &= k_{xs}\,(\Delta k_{x\theta\Omega}) && \text{(coupled sliding and rocking)}\\
k_\psi &= k_\theta\\
k_{y\psi} &= k_{x\theta}\\
k_\phi &= k_{\phi s}\,(k_{\phi\Omega} + \Delta k_{\phi\Omega}) && \text{(torsion)}
\end{aligned}
\qquad (2.10a\text{-}h)
$$

k_{xs}, k_{zs}, $k_{\theta s}$ and $k_{\phi s}$ are the static constants defined by

$$
\begin{aligned}
k_{xs} &= \frac{8}{2-\mu_s}\, G_s\, r_0\\
k_{zs} &= \frac{4}{1-\mu_s}\, G_s\, r_0\\
k_{\theta s} &= \frac{8}{3(1-\mu_s)}\, G_s\, r_0^3\\
k_{\phi s} &= \frac{8}{3(1-\mu_s)}\, G_s\, r_0^3
\end{aligned}
\qquad (2.11a\text{-}d)
$$

The coefficients $k_{x\Omega}$, $k_{z\Omega}$, $k_{\theta\Omega}$ and $k_{\phi\Omega}$ all express the variation of stiffness with the frequency Ω (frequency of applied harmonic loading). The coefficients $\Delta k_{x\Omega}$, $\Delta k_{z\Omega}$, $\Delta k_{\theta\Omega}$ and $\Delta k_{\phi\Omega}$ are corrections due to the embedment of the structure.

The frequency dependence of the stiffnesses $k_{j\Omega}$ are displayed in Figs.(2.5-7). The functions in Eqs. (2.12a-d) represent fits to the actual functions.

$$k_{x\Omega} = 1.0$$

$$k_{z\Omega} = 1.0 - \gamma_1 \frac{(\gamma_2 a_0)^2}{1+(\gamma_2 a_0)^2} - \gamma_3 a_0^2 \qquad (2.12a\text{-}d)$$

$$k_{\theta\Omega} = 1.0 - \beta_1 \frac{\beta_2 a_0}{1+(\beta_2 a_0)^2} - \beta_3 a_0^2$$

$$k_{\phi\Omega} = 1.0$$

The coefficients β_i and γ_i are displayed in the Table 2.1.

Table 2.1 Values of α_1, β_i and γ_i in Eqs. (2.12a-d,2.17a-d) From Ref.(31).

Quantity	$\mu_s = 0$	$\mu_s = 1/3$	$\mu_s = 0.45$	$\mu_s = 0.5$
α_1	0.775	0.65	0.60	0.60
β_2	0.525	0.5	0.45	0.4
β_1	0.8	0.8	0.8	0.8
β_3	0	0	0.023	0.027
γ_1	0.25	0.35	-	0
γ_2	1.0	0.8	-	0
γ_3	0	0	-	0.17
γ_4	0.85	0.75	-	0.85

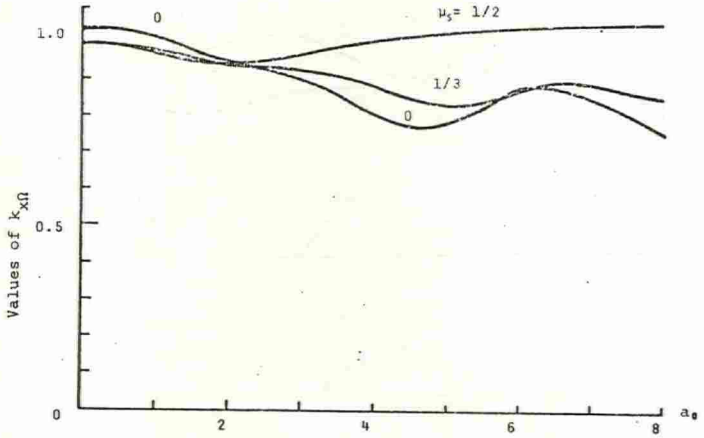

Fig. 2.5 Variation of stiffness coefficient $k_{x\Omega}$ with frequency a_0

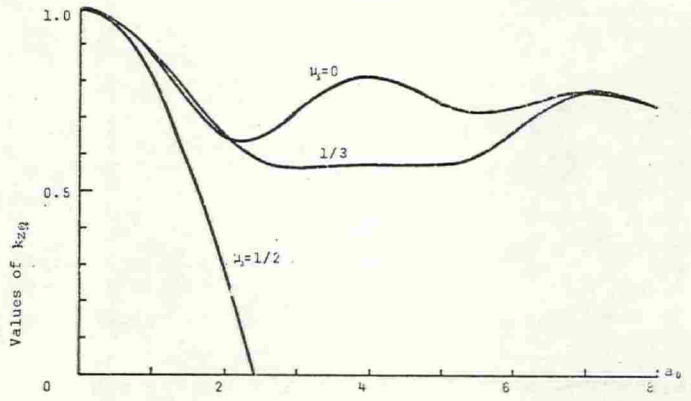

Fig. 2.6 Variation of stiffness coefficient $k_{z\Omega}$ with frequency a_0

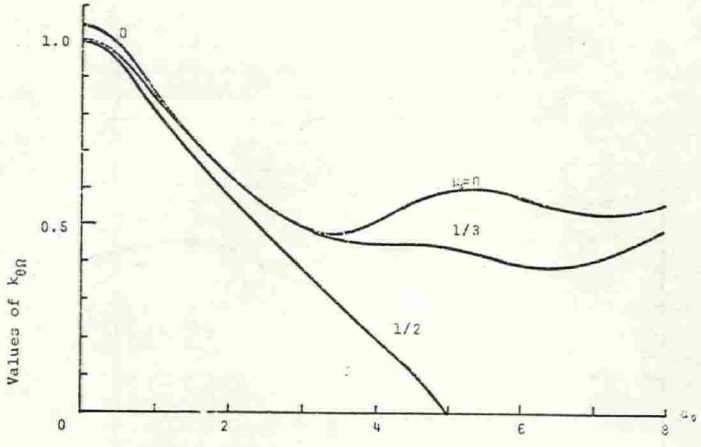

Fig. 2.7 Variation of stiffness coefficient $k_{\theta\Omega}$ with frequency a_0

The effect of embedment on damping and stiffness coefficients was studied in Ref.(22.32-36). Introducing the simplification proposed by Novak, Ref.(36) give the following correction coefficients:

$$\Delta k_{x\Omega} = 0.5\delta_{,} r_G(2-\mu_s)$$
$$\Delta k_{z\Omega} = 0.6\delta_{,} r_G(1-\mu_s)$$
$$\Delta k_{\theta\Omega} = 3\lambda^2\frac{1-\mu_s}{2-\mu_s} + \delta\, r_G[0.9+1.5(\frac{\delta^2}{3} - \delta\lambda+2)]\,(1-\mu_s)$$
$$\Delta k_{x\theta\Omega} = \lambda_{,} + 0.5\delta\, r_G(\lambda-\tfrac{1}{2}\delta)(2-\mu_s)$$
$$\Delta k_{\phi\Omega} = 3.75\delta\, r_G(1-\mu_s) \qquad (2.13a\text{-}e)$$

where

$$\delta = \frac{Z_e}{r_0}\ ,\quad \lambda_{,} = \frac{Z_{CG}}{r_0}\ ,\quad r_G = \frac{\bar{G}_s}{G_s} \qquad (2.14a\text{-}c)$$

The above formulas are based on fully effective "backfill". If the backfill has cohesion the rocking motion may push the soil away from the foundation permanently so that the *beneficial* effects of embedment are lost. The effect of the embedment should be carefully judged.

Geometrical Damping for an Embedded Circular Footing on an Elastic Half-space

The geometrical damping may be described as

$$c_x = c_{xs}(c_{x\Omega} + \Delta c_{x\Omega}) \quad \text{(sliding)}$$
$$c_y = c_x$$
$$c_z = c_{zs}(c_{z\Omega} + \Delta c_{z\Omega}) \quad \text{(vertical)}$$
$$c_\theta = c_{\theta s}(c_{\theta\Omega} + \Delta c_{\theta\Omega}) \quad \text{(rocking)} \qquad (2.15a\text{-}h)$$
$$c_{x\theta} = c_{xs}(\Delta c_{x\theta\Omega}) \quad \text{(coupled sliding/rocking)}$$
$$c_\psi = c_\theta$$
$$c_{y\psi} = c_{x\theta}$$
$$c_\phi = c_{\phi s}(c_{\phi\Omega} + \Delta c_{\phi\Omega}) \quad \text{(torsion)}$$

where

$$c_{xs} = k_{xs}\, r_0 \sqrt{\rho_s / G_s}$$

$$c_{zs} = \frac{3.4 r_0^3}{1-\mu_s} \sqrt{\rho_s \cdot G_s} \qquad (2.16a\text{-}d)$$

$$c_{\theta s} = k_{\theta s}\, r_0 \sqrt{\rho_s / G_s}$$

$$c_{\phi s} = \frac{\sqrt{k_{\phi s} \cdot m}}{1+2B_\phi} \quad , \quad B_\phi = \frac{I_\phi}{\rho\, r_0^5}$$

where

I_ϕ - torsional moment of inertia with respect to z-axis
m - mass of the whole structure including "added mass"

The variation of the coefficients $c_x \rightarrow c_\phi$ with Ω is shown in Figs. 2.8 - 2.10.

Analytical function fits to these functions are displayed in Eqs.(2.17a-d).

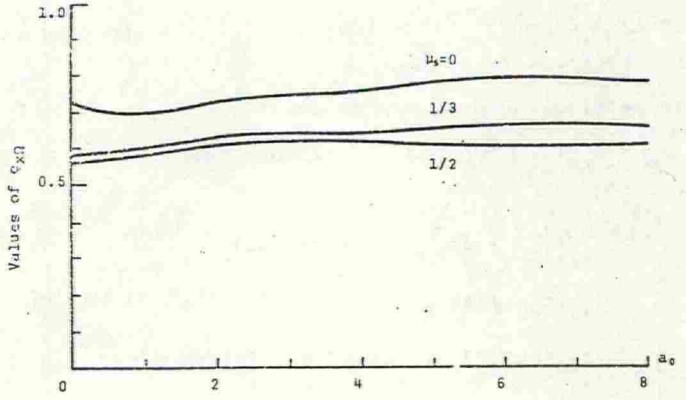

Fig. 2.8 Variation of damping coefficient $c_{x\Omega}$ with frequency a_0

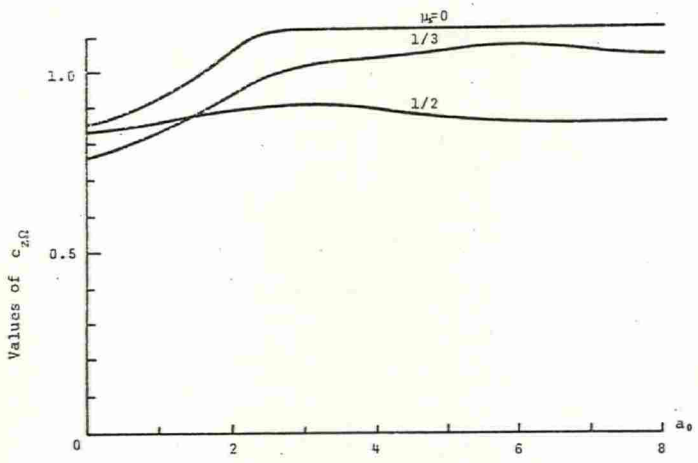

Fig. 2.9 Variation of damping coefficient $c_{z\Omega}$ with frequency a_0

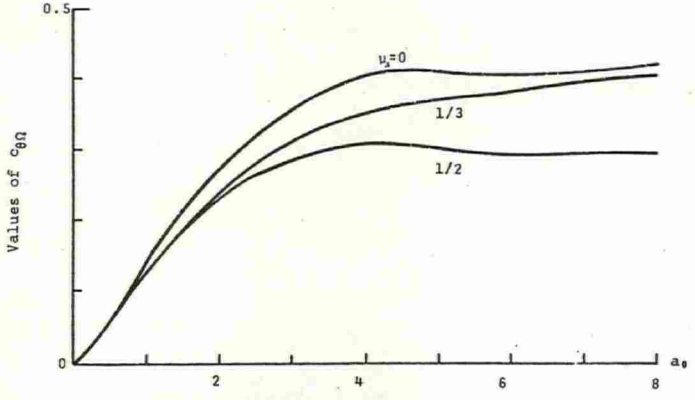

FIg. 2.10 Variation of damping coefficient $c_{\theta\Omega}$ with frequency a_0

$$c_{x\Omega} = \alpha_1$$

$$c_{z\Omega} = \gamma_4 + \gamma_1\gamma_2 \frac{(\gamma_2 a_0)^2}{1+(\gamma_2 a_0)^2} \qquad (2.17a\text{-}d)$$

$$c_{\theta\Omega} = \beta_1\beta_2 \frac{(\beta_2 a_0)^2}{1+(\beta_2 a_0)^2}$$

$$c_{\phi\Omega} = 1.0$$

The constants α_1, β_i and γ_i depend on Poisson's ratio and may be found in Table 2.1.

The effect of embedment yields the following corrections:

$$\Delta c_{x\Omega} = 1.1\delta_c r_m(2-\mu_s)$$

$$\Delta c_{z\Omega} = 0.3\delta_c r_m$$

$$\Delta c_{\theta\Omega} = \delta_c r_m(0.7+\frac{\delta_c^2}{3}-\delta_c\lambda_c+\lambda_c^2)(1-\mu_s) + 3\frac{1-\mu_s}{2-\mu_s} c_{x\Omega} \lambda^2 \qquad (2.18a\text{-}e)$$

$$\Delta c_{x\theta\Omega} = c_{x\Omega} \lambda + 1.1\delta_c r_m(\lambda-\tfrac{1}{2}\delta_c)(2-\mu_s)$$

$$\Delta c_{\phi\Omega} = 8.0\ \delta_c r_m$$

where

$$r_m = \sqrt{\frac{\bar{\rho}_s \bar{G}_s}{\rho_c G_c}} \qquad (2.19)$$

A typical range for a_0 in connection with offshore gravity platforms may be 0 - 0.4. It is seen that while stiffness and geometrical damping coefficients for translational motions vary little with frequency, the rocking motion coefficients and particularly the damping coefficient are sensitive to a change in frequency.

Stiffness and Damping Coefficients for Foundations of other Shapes

The equivalent stiffness and damping for a strip foundation and a rectangular footing resting on an elastic half-space may be found in e.g. Refs.(19,26-29), respectively.

Some guidelines for the choice of equivalent radius of rectangular footings can be found in Refs. (19.28).

Stiffness and Damping Coefficients in the Case of Soil Layering

The elastic half-space approach was applied to determine the impedance functions for a circular foundation on a layered elastic medium in Ref.(30). In general, the rocking impedances are the least affected by layering, while the vertical impedances are the most affected. The impedances for a layered medium show a stronger frequency dependence than the impedances for the half-space. For an intermediate or a high contrast between elastic properties of the layers there is a considerable reduction in radiation damping and the effect should be properly accounted for.

2.4.4 Hysteretic Energy Dissipation

The geometrical damping is due to the fact that energy forced onto the footing and then transmitted into the half-space, is not reflected from the boundaries infinitely far away from the source of excitation, see Ref.(19), pp.91 - 92.

If the soil were a linear elastic body, the shear modulus, G_s, Poisson's ratio, μ_s and the mass density, ρ_s, characterize its dynamic response using elastic half-space theory.

While linearity is ensured when the cycle strain level is low, the stress-strain relation depends significantly on the amplitude of cyclic strain for higher load levels. In the present context linearity is assumed by introducing equivalent elastic characteristics, characterized by the hysteretic damping ratio,

(loss factor), Refs. (21a-b)

$$\tilde{D} = A_L / 4\pi A_T \qquad (2.20)$$

A_L is the area of the closed hysteresis loop during a cycle of deformation, and A_T is the strain energy density at maximum shear strain, see Fig. 2.3.

This type of damping is in particular associated with the rocking motions. The damping ratio $\tilde{D}$ is a function of several soil and loading parameters.

Half-space Models with Hysteretic Losses (Simplified Approach)

The hysteretic energy loss can be accommodated by assuming a linear vicsoelastic material in the half-space.
The following equivalent shear modulus is then introduced

$$\tilde{G}_s = G_s[1 + i \cdot 2\pi \frac{\omega G'_s}{G_s}] \qquad (2.21)$$

where

$$2\pi \frac{\omega G'_s}{G_s} = \frac{A_L}{A_T} \qquad (2.22)$$

G_s and G'_s are the shear moduli of elasticity and viscosity, respectively.
Experiments have justified the assumption of a constant hysteretic soil, (i.e. $\omega G'_s$ is constant) and hence A_L/A_T is independent of ω. Veletsos and Verbic, Ref.(39), have shown that the principal effects of the hysteretic ("structural") damping are to *increase the damping capacity* of the foundation and to *reduce* the stiffness.

For normalized frequencies (a_0) below 2.0 the effect is principally to increase the damping. For low frequency excitations the hysteretic damping may be introduced by transforming it into an equivalent viscous damping coefficient, $\bar{c}_j$, by assuming the dissipated energy in one cycle for the two models to be equal for a one-degree-of-fredom system, Ref.(39).

The equivalent viscous damping coefficient for the j'th degree of freedom for the foundation then is

$$\bar{c}_j = \frac{2k_j\tilde{D}}{\Omega} \quad j = x,\theta,x\theta, \ldots \qquad (2.23)$$

In this manner the equivalent damping coefficient is determined for each of the six degrees of freedom (in the node at the soil - structure interface). However, only the contribution to rotational degrees of freedom is significant.

It is clear that the steady-state response of two 1-DOF systems with the same mass and stiffness but one with viscous damping and the other with (equivalent) hysteretic damping, the motions will be equal only at one frequency. However, if the $\tilde{D}$ is not too large this error is negligible, Ref.(25).
The above (simplified) approach to incorporate the effect of internal damping should be used with caution when extreme soil layering and a high level of internal damping is present.

2.4.5 Comments on the Parameters in the Present Soil Idealization

General Comments

Among the parameters G_s, μ_s and ρ_s, G_s is the most important one. Satisfactory evaluation of G_s is difficult. A general approach is devised by Richart et al, Ref. (19). Poisson's ratio may simply be estimated at a value ranging from 0.3 for dry granular soil to 0.5 for soft saturated clay. The error made by using μ_s in all calculations is small compared to other uncertainties. The determination of ρ_s is straight forward.

Comments on the Shear Modulus and the Hysteretic Damping Ratio

Fig. 2.3b shows the influence of shear strain amplitude on the dynamic properties graphically. As strain amplitude increases, the effective shear modulus decreases while the damping ratio increases.

In strong-motion earthquake problems ($\gamma \in 10^{-2}$ - 1%) and the analysis of offshore facilities under severe storm conditions ($\gamma \in 10^{-3}$-10^{-1}%) the reduction in G_s with load amplitude must be duely considered.

Further, $G_{s\ max}$ (at $\gamma \doteq 0$) varies approximately with 0.5 power of the mean effective stress (octahedral normal stress) for the soil. Another important parameter is the void ratio. Hardin and Drnevich, Refs.(21a-b) proposed empirical relationships for the shear modulus and the damping ratio as dependent upon the important soil properties. A concise summary is recently presented by Öner, Ref. (109).
Applying the method proposed in Refs.(21a-b) $\tilde{D}$ is estimated to be in the range 0.02 - 0.05 for North-Sea soils.

2.4.6 Improved Representation of the Soil Behaviour

Better soil modelling is primarily obtained by including a physically more correct (non-linear) soil material description and geometry interface description. The variation of soil strength and stiffness in the half-space also should be accounted for.

The dynamical soil response may be determined either by an analytical continuum approach, or, numerical techniques such as finite element methods.

The applicability of the analytical continuum approach is limited. Complex material and geometry representation require numerical tools to be applied. The finite element method may be adopted in for that purpose.

The level of analysis sophistication must be consistent with the quality of the input data. For soil-structure interaction problems, the properties of the soil profile required are the geometry of the layering, the shear modulus, Poisson's ratio, density and damping characteristics of each layer.

Due to a wide scatter of the soil data the analyses with a range of values is usually recommended. This, together with the fact that there is inherent non-uniformity in most soil deposits should be determinant for the choice of methodology of analysis.

2.5 Representation of the Ocean

2.5.1 General Remarks

The ocean environment contributes to the equations of motion in several ways. First of all, the waves represent the source of dynamic excitation (wave forces). But the ocean environment also contributes to the mass and damping of the vibratory system.

2.5.2 Wave Forces in Regular Waves

General Comments

In the present section (2.5) the wave forces in the dynamic interaction problem will be described considering a regular wave. In section 4 the random nature of the sea elevation is recognized.

The wave forces on a floating or a fixed structure in a fluid which is supposed to be incompressible, irrotational and inviscid, can be classified as potential or viscous, Ref (41). The forces may be determined by analysis or experiments or both.

The general analytical treatment of the forces is very difficult. In particular, the determination of viscous forces is not yet possible. Potential effects are easily accessible by means of the source-sink techniques, Refs.(45, 46).

Several approximate formulas are used in the evaluation of inertial and drag forces. The Morrisom formula was originally developed for circular cylindrical piles, Ref.(42). The classical Morison formula is applicable when the dimensions of the object is small compared to the wave length. (which holds true for the superstructure of the gravity platforms). For larger objects (such as the caisson) the

stronger wave-structure interaction makes the load evaluation more complex. However, systematic analysis and experiments for the load evaluation on larger objects are available.

A gravity structure is conveniently splitted into two parts. The first consists of structural components which are large enough to diffract waves or otherwise interact. The second group consists of structural members of small diameter. In that case the flow is only locally affected.

In the subsequent sections various aspects in connection with analytical and experimental treatment of wave loading will be summarized.

Before the discussion of wave forces the choice of kinematic theory for the waves is commented upon.

Comments on Wave Theory

The analytical determination of forces requires that the kinematics of the waves must be known. There are a large number of wave theories to describe particle velocities and accelerations, ranging from the simple linear Airy theory to more refined non-linear theories, see e.g. Refs. (51,52).

The choice of theory depends on several factors. The primary factor is, of course, which theory represents the physical behaviour most correctly. It is often that the nonlinear theories are the best. However, there are other reasons for prefering the linear theory. For instance linearity simplifies the calculations of forces, in particular when diffraction effects must be taken into account. Furthermore, for a Morison type approach to the forces, there must be consistency between the method for obtaining particle velocities and accelerations and the method for determining mass and drag force coefficients. This statement also may imply preference of the linear theory.

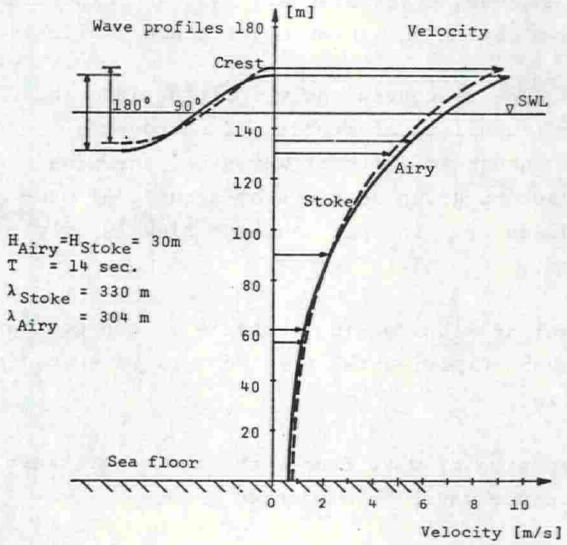

Fig. 2.11 Velocity distribution at the crest in a regular wave.

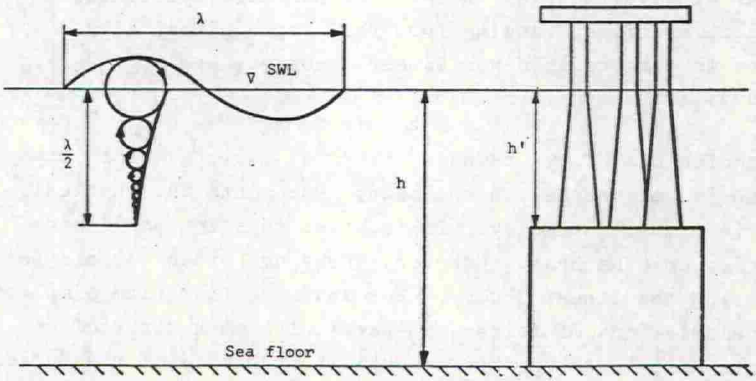

Fig. 2.12 Schematic representation of the region of influence for a regular wave.

Velocity distributions corresponding to the linear Airy theory and Stokes fifth order theory are compared in Fig. 2.11. Higher order theories generally predict higher velocities (and drag forces) although accelerations (inertia forces) are not too much different.

Fig. 2.12 shows the distribution of velocity over the depth. Practically no force will act on the caisson when $\lambda/2 < h'$, where λ is the wave length, see Fig. 2.12.

Finally, the statistical treatment of the response is considerably simplified by assuming the linear wave theory.

2.5.3 Wave Forces on Slender Members in Regular Waves

General Approach

The classical Morison formula, Ref. (42) may be reformulated to give the distributed forces normal to a cylinder by a drag and inertia terms, as

$$dp=\tfrac{1}{2}\rho_f C_D D(u-\dot{r})|u-\dot{r}|+\rho_f C_{M_1}\frac{\pi}{4}D^2\frac{\partial u}{\partial t}+\rho_f C_{M_2}\frac{\pi}{4}D^2\left(\frac{\partial u}{\partial t}-\ddot{r}\right) \quad (2.24)$$

(symbols are explained in the list of notations)

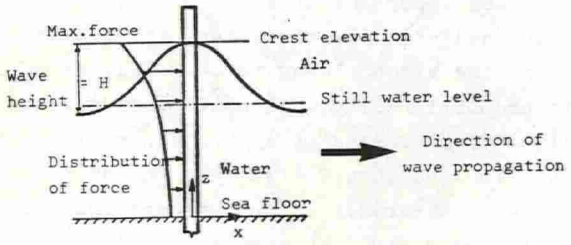

Fig. 2.13 Definition sketch of wave and wave forces on single vertical pile

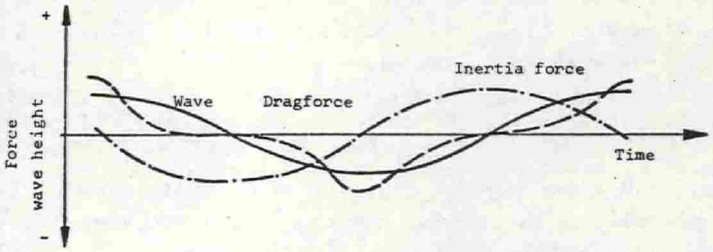

Fig. 2.14 The relation between wave-height, drag- and total inertia-force

The problem of wave force prediction is then reduced to determining u and $\partial u/\partial t$ from wave kinematics, and the choice of drag and mass coefficients. As a result of the scatter in the magnitude of these coefficients,a careful consistent choice must be made in an actual case.

The total force on a vertical pile is obtained by integrating the distributed force, dp. The total force consists of one drag term from viscous effects and two inertia terms from potential effects. The two inertia terms are of a linear harmonic nature whilst the drag term in nonlinear. The drag and inertia terms are 90° out of phase as shown in Fig. 2.14.

Comments on Viscous Effects (the Drag Term)

The viscous effects are important on structures which are small compared to the wave height. The first term in Morison formula, $\frac{1}{2}\rho_f C_D u|u|$, represent the viscous drag force. This term is nonlinear due to its proportionality with $u|u|$. The drag coefficient C_D, is empirically determined and is a function of the Reynold number, $Re = uD/\nu$. For the actual structure the drag coefficient is in the range 0.5 - 1.0. In the present analysis the viscous drag term is neglected. The error this introduces is discussed in a subsequent subsection.

In addition to the drag term, the viscous effects generates lift forces normal to the flow direction. These effects occurs when the flow separates unsymetrical from the sylinder and oscillating eddies are formed. This lift force is also proportional to $u \cdot u$ and is accordingly nonlinear. For slender structures the lift force may generat not negligible forces having relative high frequency compared to the wave frequency. In the present analysis this force is neglected.

Comments on Potential Effects (the Inertia Terms)

The forces related to the mass terms in the Morison formula may be devided into

- undisturbed wave pressure forces (Froude-Krilov force) (in phase with the absolute acceleration)
- inertia force (in phase with the relative acceleration)

In addition a potential damping force in phase with the velocity acts on a vertical cylinder.

The wave forces on a vertical rigid circular cylinder piercing the water surface and extending to the sea bottom were obtained in Ref. (44) by means of diffraction theory, based on the following assumptions.

- frictionless and irrotational (no viscous forces)
- linear wave theory

  (i.e. $\frac{\text{wave height}}{\text{wave length}}$ = sufficient small)

- the wave is reflected at the vertical surface of the cylinder without loss of energy

The total "mass" force may be written as

$$P_I = [(C_{M_1} + C_{M_2})\cos\omega t + C_{MD}\sin\omega t]P_{I_0} \qquad (2.25)$$

C_{M_1} and C_{M_2} represents the Froude-Krilov and the inertia force, respectively. C_{MD} is the potential damping force coefficient. Due to diffraction of waves, these coefficients depend upon the ratio $\pi D/\lambda$. Fig. 2.15 shows their depence on $\pi D/\lambda$.

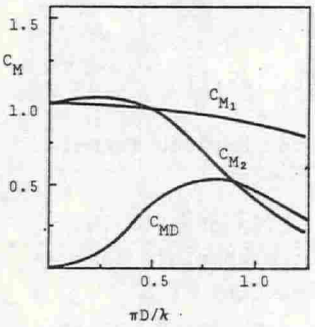

Length of cylinder = water depth = ∞
Diameter of cylinder = D
Wave length = λ

C_{M_1} = Undisturbed pressure force coefficient

C_{M_2} = Inertia force coefficient

C_{MD} = Damping force coefficient

Fig. 2.15 Components of wave excited forces on a vertical cylinder according to Havelock, Ref.(41.b)

Furthermore, the force coefficients are subjected to corrections due to the presence of the caisson and interaction effects between the different cylinders, Ref.(50). No such corrections will be made in the applications presented in this report.

Normally the potential damping force coefficient, C_{MD}, for small bodies is negligible as compared to the terms due to accelerations. Fig. 2.16 shows the error made by neglecting the damping force. The error is less than 5% of the total force when $\pi D/\lambda < 0.65$, and at decreasing values of $\pi D/\lambda$ the error is completely negligible. Thus in the present analysis this potential damping is neglected.

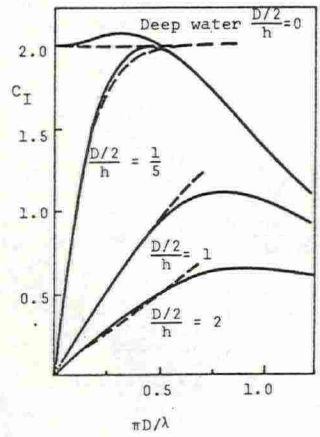

Lenght of cylinder = water depth = h

Diameter of cylinder = D

——— Exact solution (inertia and damping)

------ Approximation (neglecting the damping term in the potential forces)

C_I = Total force coefficient

Fig. 2.16 The total horizontal wave excited force X_a on a vertical circular cylinder

Comments on Relative Magnitude of Drag and Inertia Forces

An estimate of the relative magnitude of wave force components may be obtained for a vertical pile in an undisturbed regular wave. Since the drag and inertia force are ninety degrees out of phase, the amplitude of resulting force may be approximated by

$$P_{max} = (P_{I\ max}^2 + P_{D\ max}^2)^{\frac{1}{2}} \qquad (2.26)$$

$$P_{I\ max} = \rho_f C_I \frac{\pi D^2}{4} \left(\frac{H}{2}\omega^2 \frac{\cosh kz}{\sinh kh}\right) \qquad (2.27)$$

$$P_{D\ max} = \rho_f C_D \frac{D}{2} \left(\frac{H}{2}\omega \frac{\cosh kz}{\sinh kh}\right)^2 \qquad (2.28)$$

Equations (2.27) and (2.28) provide a convenient means by which the relative magnitudes of the maximum inertia and drag components of the Morison equation may be compared. The desired comparison ratio is:

$$R = \frac{\int_{h'}^{h} P_{D\,max}\, dz}{\int_{h'}^{h} P_{I\,max}\, dz} = \frac{1}{2\pi}\frac{C_D}{C_I}\frac{H}{D}\left(\frac{(\sinh 2kh-\sinh 2kh')+2k(h-h')}{2(\sinh kh-\sinh kh')\sinh kh}\right) \quad (2.29)$$

Let 0.8 and 2.0 be representative values for C_D and C_I, respectively. For H/D smaller than 2.5, R then is smaller than 0.16.

The nature of Eq. (2.26) is such that if any component is equal to or less than 0.16 times the other, the influence of the smaller component is only 0.015. This statement on the relative magnitude of forces is valid for a regular wave. However, in a random sea the relative effect of the drag force amounts to a value between 0.16 and 0.015, depending on the spectrum width.

As a first approximation, the drag forces can be neglected. An improved representation of the drag forces is obtained by including a linearized drag term of Eq. (2.24).

Comments on Interaction Effects

When the superstructure consists of several columns, interaction effects should be accounted for when using the Morison formula.

For waves penetrating down to the caisson, the particle velocity and acceleration will be influenced by the caisson. A very conservative estimate of the influence of the caisson may be obtained in the following way: The sea depth in the actual region may be assumed to be h' (see Fig. 2.12) and the wave height may be transformed to an equivalent height, H', assuming continuity. In this way the wave is assumed to pass the caisson neglecting three-dimensional effects. Systematic calculations and measurements reported in Ref.(47) displayed that interaction effects are relatively small. In the present applications these effects are neglected.

2.5.4 Wave Forces on the Caisson in Regular Waves

General Approach

For waves of length, λ, which is larger than $2h'$ (inertial) forces on the caisson have to be considered, (see Fig. 2.12.).

Due to the relative dimensions of the caisson the Morison formula is not directly applicable for this case since radiation and scattering of the water waves occur. More elaborate techniques of load evaluation need to be considered. For large objects with smooth surfaces, the forces may be theoretically evaluated by potential theory and an approximate numerical method, see for example Refs.(44-46). Alternatively, experimental investigations may be carried out, Refs.(46-49).

Experimental Case Study

In the present context the experimental results in Ref.(47) were used. In the present wave-structure-soil interaction study the caisson is supposed to be rigid. Thus, the loading could be conveniently expressed by the wave-pressure resultants: the horizontal force, and the overturning moment (including the

effect of the horizontal and vertical pressure on the caisson). For the purpose of illustration a typical pressure distribution on a caisson is shown in Fig. 2.17.

In the present context the experimental results in Ref.(47) were used. The results are expressible as an horizontal force, and an overturning moment, including the effect of the horizontal and vertical pressure on the caisson. A typical pressure distribution on a caisson is shown in Fig. 2.17.

Assuming a structure with cross-section close to a circle, a hexagon or a triangle the forces may be correlated to a Morison-type formula using the Airy wave theory.

The coefficients in the formula are determined from the experiments reported in Ref.(47):

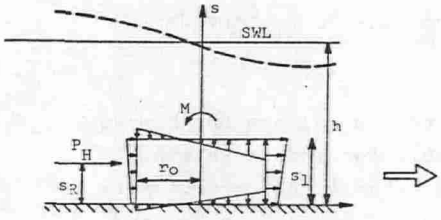

Fig.2.17 Typical pressure distribution

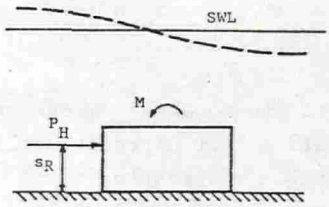

Fig. 2.18 Statically equivalent system to the model in Fig. 2.17

The pressure in the wave then is:

$$p = \rho_f \frac{H}{2} \frac{\cos ks}{\cosh kh} \cos(kx - \omega t) \qquad (2.30)$$

The horizontal force is

$$P_H = -\rho_f C_H \frac{H}{2} \cdot V \frac{k}{\cosh kh} \frac{\sin ks_1}{ks_1} \sin \omega t \qquad (2.31)$$

The overturning moment is

$$M_0 = P_H \cdot s_R - C_{MT} p_1(0, s_1, t) \cdot W \cdot f_M + C_{MB} p_1(0,0,t) W \cdot f_M \tag{2.32}$$

The vertical force is

$$P_V = -\rho_f \frac{H}{2} V \frac{k}{\cosh kh} \frac{C_T \cosh ks_1 - C_B}{ks_1} f_V \cos \omega t \tag{2.33}$$

Comments on the Coefficients of the Caisson Loading

Figs. 2.19 and 2.20 display the variation of the pressure resultant coefficients C_H, C_T, C_B, C_{MT} and C_{MB} as a function of the normalized cross-section are $(\sqrt{A}/\lambda)$, for a given height of the structure to water depth ratio (s_1/h).

The coefficients are also influenced by the steepness of the waves. Results for three different wave steepnesses are shown.

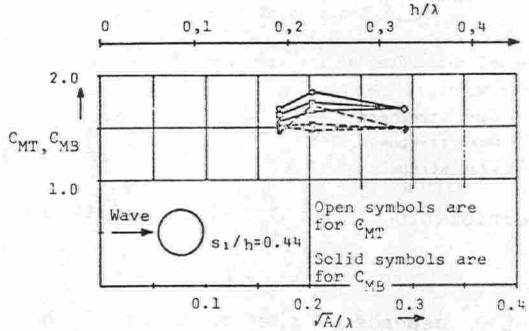

A-horizontal area of the structure
λ-wave height
o - wave steepness 0.03
Δ - wave steepness 0.05
□ - wave steepness 0.07

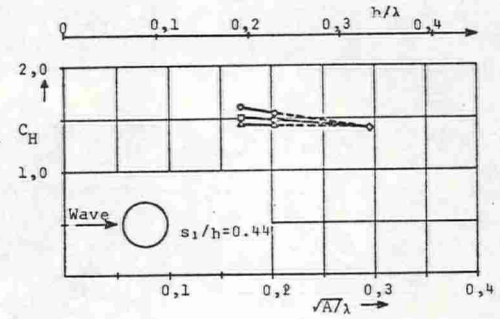

A-horizontal area of the structure
λ-wave height
o - wave steepness 0.03
Δ - wave steepness 0.05
□ - wave steepness 0.07

Fig. 2.19 Coefficients C_{MT}, C_{MB} and C_H (From Ref.(47)

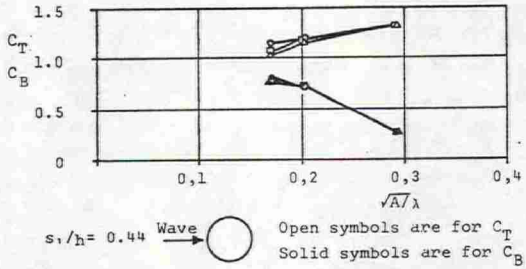

A-horizontal area of the structure
λ-wave height
o - wave steepness 0.03
Δ - wave steepness 0.05
□ - wave steepness 0.07

Fig. 2.20 Coefficients C_T and C_B (From Ref.(47))

The coefficient C_B depends on the embedment of the structure. The value shown in Fig. 2.20 is obtained when the water pressure is free to act under the structure. If the structure was embedded in fine soil, the wave induced pressure under the bottom may be neglected, i.e. $C_B = 0$.

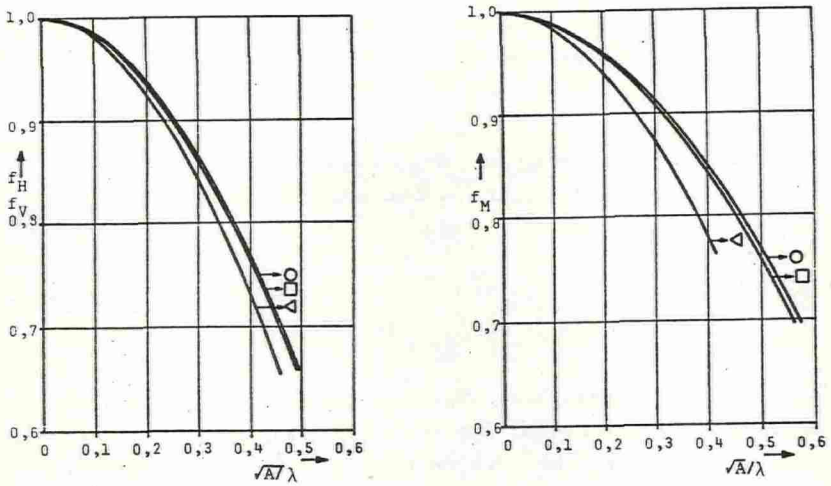

Fig. 2.21 Coefficients f_H, f_V and f_M (From Ref.(47))

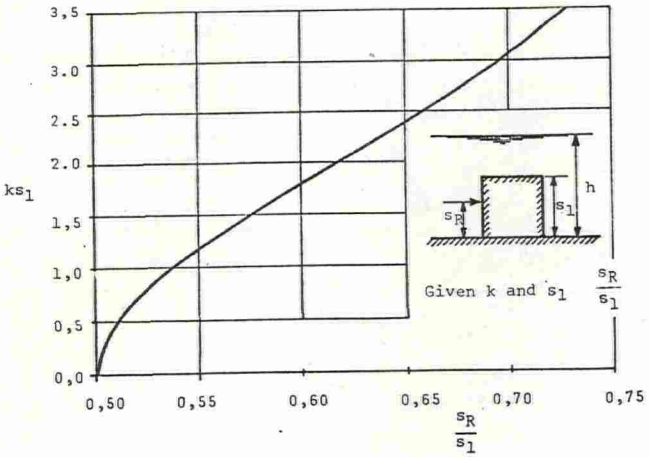

Fig. 2.22 Point of application of horizontal force (From Ref. (47))

Fig. 2.21 shows the theoretical variation of the coefficients f_H, f_M and f_V, which account for the variation of the pressure gradient over the structure.

To find the overturning moment, M_0, the application point for f_H must be determined. The characterizing distance s_R may be obtained from Fig. 2.22.

The variation of the force resultants as dependent upon the ratio (s_1/h) may be found in Refs. (47,49).

Fig. 2.23 shows the phase angles between wave profile, horizontal- and vertical forces. Defining the time, t_0, as a reference point, the wave height has its maximum at t_0. The horizontal force is 90° out of phase and the vertical force is 180° out of phase. The overturning moment due to the horizontal force is as the force 90° out of phase. The overturning moment due to pressure on top of the caisson is 270° out of phase whilst the moment due to pressure on bottom of the structure is 90° out of phase.

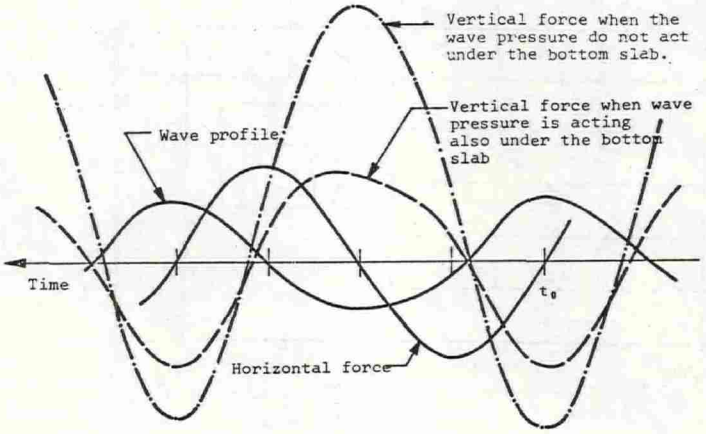

Fig. 2.23 Sample of wave and force measurements (From Ref./47/)

The force and moment calculated according to the reported procedure, are all assumed to be of an harmonic nature. This implies that drag forces, sloshing and other non-harmonic forces are neglected. These modifications will generally not effect the result as their contribution to the overall loading is negligible.

The reported calculation procedure is based on an experimental fitment of the theoretical force and moment equations. The results obtained by this procedure depends to a large extend of the reliability of the experimental results.

2.5.5 Hydrodynamical Mass

General Remarks

The water contributes to the mass by enclosed water and added mass due to the motions of the platform. The added mass may be derived from the general expression for the loading, see the previous sections on wave forces.

Slender Members

Neglecting the drag force in the Morison formula, Eq.(2.24) the intensity (load per unit length) of the inertia wave loading on the superstructure members may be expressed as

$$dp = C_{M_1} \cdot \rho_f \cdot dV \cdot \frac{du}{dt} + C_{M_2} \rho_f dV \frac{d}{dt}(u-\dot{r}) \qquad (2.34)$$

By considering this force in conjunction with the equations of motion, dp can be separated into two components, namely an excitation force:

$$d\bar{p} = C_{M_1} \rho_f dV \frac{du}{dt} + C_{M_2} \rho_f dV \frac{du}{dt} \qquad (2.35)$$

and an added mass term (on left hand side of the equations of motion)

$$dm = C_{M_2} \rho_f dV \tag{2.36}$$

Possible magnification of equivalent added mass due to sloshing in the tanks, frequency dependency and variation due to variation in the surface elevation are neglected in the present applications.

Caisson

The forces on the caisson must be determined by analytical or numerical methods such as the source-sink technique, Ref. (45) or by experiments. Similarily, the added mass term must be determined in a more elaborate way than the Morison formula. Assuming the caisson to behave as a rigid body and defining the degrees of freedom as shown in Fig. 2.24, the added mass matrix may in principle be written as

$$\mathbf{M} = \rho_f V \begin{bmatrix} M_{11} & M_{12} & M_{13} \\ M_{21} & M_{22} & M_{23} \\ M_{31} & M_{32} & M_{33} \end{bmatrix} \tag{2.37}$$

when only two-dimensions are considered.

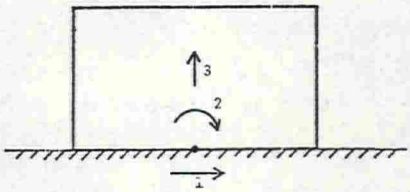

Fig. 2.24 Definition of degrees of freedom for the caisson motion.

The horizontal tranlation and the rotational motion are coupled. However, no coupling between the vertical and the

other motions exists when the body is cylindrical. Hence the matrix is reduced to the form

$$\mathbf{M} = \rho_f V \begin{bmatrix} M_{11} & M_{12} & 0 \\ M_{21} & M_{22} & 0 \\ 0 & 0 & M_{33} \end{bmatrix} \qquad (2.38)$$

Fig. 2.25 displays the mass matrix coefficients associated with horizontal translation and rotation as determined by experiments, Ref.(48b)for an actual structure/depth configuration.

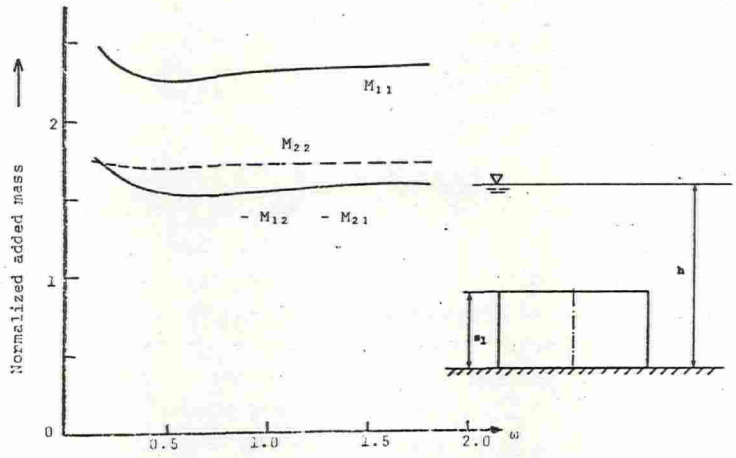

Fig. 2.25 Case Study on hydrodynamical added mass for the caisson.

It is clear from Fig. 2.25 that frequency dependency of the added mass can be neglected. The added mass for vertical translation, which is of less importance, is also assumed to be frequency independent.

2.5.6 Hydrodynamical Damping

General Remarks

The hydrodynamical damping is due to (potential) diffraction - and drag effects. The diffraction damping is due to wave generation from the vibrating structure. Drag-damping is caused by viscous effects and separation of the potential flow. Hydrodynamical damping therefore is frequency and amplitude dependent.

Slender superstructure

Both drag and diffraction damping contribute to the hydrodynamical damping of the slender members. The drag damping may be estimated from the Morison equation, while a diffraction theory must be used to determine the diffraction damping. To estimate the magnitude of the damping, the platform can be assumed to rotate as a rigid body about the mudline. The resulting damping ratio, $\xi = c/c_{critical}$ is then determined. McCamy & Fuchs theory is used to determine the diffraction damping.

Fig. 2.26 displays the resulting damping ratio for an actual case. The diffraction damping depends significantly upon the frequency, but does not vary with the amplitude. The drag damping varies with amplitude and frequency. Drag damping is displayed for 3 different amplitudes. The amplitude, δ, is defined as the horizontal displacement amplitude of the deck. The upper curve , δ = 1 meter, should be regarded as an upper bound and is only expected to be found at low frequencies. A more realistic displacement amplitude at high frequencies is δ = 0.25 meter or less. Consequently the error made by neglecting the drag damping is not significant.

Caisson

In the caisson the diffraction damping is predominant. A source-sink model, Ref. (45), should be applied to determine this damping. Coupling exists between damping for

horizontal and rotational motion. The damping matrix associated with the 1 and 2 degrees of freedom in Fig. 2.24, may be written as

$$C = \begin{bmatrix} C_{11} & C_{12} \\ C_{21} & C_{22} \end{bmatrix} \qquad (2.39)$$

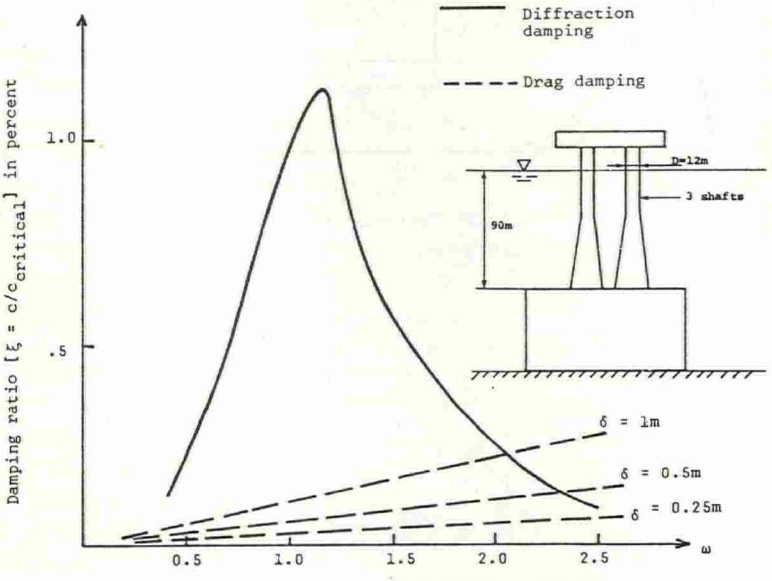

Fig. 2.26 Case Study on hydrodynamical damping associated with the slender members

where the damping associated with the vertical motion is neglected. The case displayed in Fig. 2.27 shows that the diffraction damping is heavily dependent upon the frequency. It is, however, noticed that the damping on the caisson is significant for frequencies below 0.8 in this case.

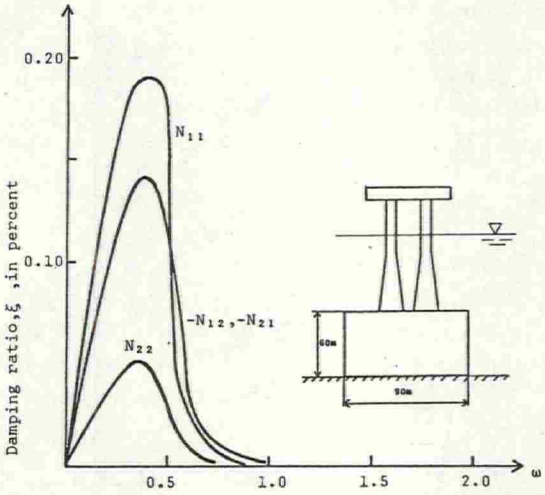

Fig. 2.27 Case Study on hydrodynamical damping associated with the caisson.

3. EVALUATION OF DYNAMIC RESPONSE (transfer functions)

3.1 Summary of the Dynamic Modeling

The equations of motion, Eq.(2.1) are based on a lumped mass matrix (M) which includes the mass of the members, the mass of the enclosed or entrapped water, the added or virtual mass of the surrounding ocean and the mass of the equipment on the deck.

The damping matrix (C) consists of geometrical and hysteretic dissipation in the soil and hysteretic and viscous damping in the structure and the sea,respectively.

The stiffness matrix is the assembled stiffnesses of the structural members and an equivalent soil stiffness as represented by springs in the lower node of the model. The exciting force vector (R(t)) is due to the effect of waves.

The representation of the *structural* properties is accomplished without particular problems. Also the *soil* is easily modelled since it is associated with the lower node of the model. However, at this point the incorporation of the *ocean* needs some comments.

The intensity (load per unit length) of the wave *loading* on the *superstructure members* may be expressed by the Morison formula as

$$dp = C_{M_1} \rho_f dV \frac{du}{dt} + C_{M_2} \rho_f dV \frac{d}{dt}(u - \dot{r}) + \tfrac{1}{2} C_D \rho_f dA (u - \dot{r}) |u - \dot{r}| \qquad (3.1)$$

The components of the (nodal) load vector may then be determined by the conventional procedure (as a lumped or a consistent load vector).

A typical equation of motion for a node in the superstructure thus reads

$$M_i\ddot{r}_i + C_i\dot{r}_i + \sum_j k_{ij}r_j = R_i$$

$$aA = C_{M_1}\rho_f V_i \frac{du_i}{dt} + C_{M_2}\rho_f V_i \frac{d}{dt}(u_i-\dot{r}_i) \qquad (3.2)$$

$$+ \tfrac{1}{2}C_D\rho_f A_i(u_i-\dot{r}_i)|u_i-\dot{r}_i|$$

r_i may be a translational or a rotational degree of freedom.

M_i is correspondingly a mass or mass moment, etc.

Rearranging the terms

$$(M_i + C_{M_2}\rho_f V_i)\ddot{r}_i + C_i\dot{r}_i + \sum_j k_{ij}r_j$$

$$= (C_{M_1}+C_{M_2})\rho_f V_i\frac{du_i}{dt} + C_D\rho_f A_i(u_i-\dot{r}_i)|u_i-\dot{r}_i| \qquad (3.3)$$

Eq. (3.3) expresses that the waves besides resulting in exciting forces provides added mass and viscous damping forces.

The drag term provides a non-linear fluid-structure interaction. The hydrodynamical damping forces are small for submerged slender members, although these effects increase with size and proximity to the free surface.

The drag term in Eq.(3.1) is assumed to account both for viscous and turbulence effects. In addition, radiation damping must be considered.

The *loading* on the *caisson* is primiarily constituted by inertial effects. Therefore only terms analogous with the first two terms in Eq.(3.1) will be present. As mentioned in Section 2.5.4, the loading on the caisson is expressed by force resultants (forces and moments) associated with the translational and rotational degrees of freedom in the lower node, cfr.

Fig. 2.24.

Having the force on "Morison" type form, Eq. (3.1), the inertia term consists of a Froude-Kryloff and an "added mass" type term. The Froude-Krilov mass coefficient can always be assumed equal to 1.0. The remaining thus represents the added mass inertia coefficient.

Further remarks on the formulation are given in Section 3.2 where the implications by the choice of method of solution on the formulation is discussed.

3.2 Solution of the Equations of Motion

3.2.1 General Remarks

The methods for solution of the equations of motion may be categorized as

- modal superposition techniques
- direct integration by step-by-step procedures
- special methods

Excellent reviews of these methods have been given in Refs. (14,16,54-57,62-65 and 111).

The choice of numerical solution procedure mainly depends on three factors, namely

- linearity of the equations of motion
- frequency dependence of stiffness, damping and mass properties
- the form in which wave (or wind) data for the structure is to be used (deterministic versus stochastic and time domain versus frequency domain approach).

These two aspects will be discussed subsequently.

The principal *nonlinearities* in the equations of motion may be summarized by the following list of effects:

- geometrical and material nonlinearities in the structure
- nonlinear material properties in the soil
- changes of the added (hydrodynamical) mass due to water surface variation
- wave-structure interaction by drag effects.

It is clear that only a step-by-step procedure can yield an "exact" solution to problems with pronounced nonlinearities. However, for some types of nonlinearities modal techniques with appropriate modifications have been utilized, see for example Ref. (72).

Further,

- soil stiffness and damping
- hydrodynamical damping

are *frequency dependent*. The first category is the most important in this connection. The response to an *harmonic* excitation is easily traced both by modal techniques and step-by-step techniques in the case of a linear problem with frequency dependent properties. It will be difficult, however, to achieve the response through a time domain analysis when dealing with frequency dependent dynamic properties and a random excitation.

The *statistical analysis* of the wave response may either be obtained through a time domain or a frequency domain approach. The latter is generally preferable in linear problems, while the first often must be resorted to when the problem involves heavy nonlinearities.

A frequency domain analysis requires the dynamic analysis to be carried out for a range of wave frequencies.

Since the response must be traced through several cycles until the steady-state condition is attained, the use of a step-by-step procedure will be relatively costly as compared to modal superposition with a few contributing modes.

However, since the magnitude and type of damping varies considerably within the interaction system the classical modal analysis does not strictly apply. This problem can be circumvented by turning to damped modal analysis, Ref.(14). The solution of the governing equations then requires the handling of twice as many unknowns as in the classical approach. Alternatively, by modifying the classical modal analysis method it can be made applicable, see Section 3.2.2.

For a linear problem the response can be rigorously computed by transform methods such as The Fast-Fourier-Transform, Ref. (54), or Foss' method, ref. (55). Step-by-step numerical integration methods, Ref. (16) can be applied both to linear and nonlinear problems. However, such methods sacrifice the considerable advantages of modal superposition. The modal analysis permits a good visualization from the values of the natural frequencies and the modal shapes of the significance of the flexible foundation on the response. Furthermore, the truncation of the number of degrees of freedom reduces computer costs.

In general, in the case of linear stochastic response analysis a classical normal mode superposition technique with appropriate modifications or a combination of modal superposition and step-by-step procedure is prefered. When large nonlinear effects are present the step-by-step procedure is often the only applicable method.

3.2.2 Modal Superposistion

Formulation and Solution of the Free Vibration Problem

The stiffness and mass matrices are established in a straight forward manner and the generalized free vibration problem (obtained by assuming a harmonic motion $r = \phi \sin\omega t$ and putting

damping and excitation forces equal to zero in Eq. (3.1))

$$K\phi = \omega^2 M\phi \tag{3.4}$$

is solved by a standard subroutine to give the natural circular frequencies, ω_i, and the corresponding mode shapes ϕ_i. In this case an inverse simultaneous iteration process is used, Ref. (16) p. 250.

For a_0 in the range (0-0.5) the frequency dependence of the soil stiffness coefficients may be neglected with an error less than 3 percent.

For a wider range of variation of a_0 the frequency depency of the soil stiffness can be accommodated by solving Eq . (3.4) for a few (say 3) frequencies, a_0, and storing the corresponding eigenfrequencies and eigenmodes.

When subsequently the forced response analysis are undertaken a linear interpolation procedure may be utilized to determine the actual eigenfrequencies and the eigenmodes.

It is preferable to normalize the modal matrix. Among the alternatives of current interest it is simplest to normalize such that the generalized mass matrix is an identy matrix when calculating structural response. Calling the modal matrix obtained by solving Eq.(3.4) ϕ and the corresponding generalized mass matrix M^* an identity matrix is obtained by pre- and postmultiplying M^* by $(M^*)^{-\frac{1}{2}}$.

$$\begin{aligned} I &= (M^*)^{-\frac{1}{2}} M^* (M^*)^{-\frac{1}{2}} \\ &= (M^*)^{-\frac{1}{2}} \phi^T M \phi (M^*)^{-\frac{1}{2}} = \tilde{\phi}^T M \tilde{\phi} \end{aligned} \tag{3.5}$$

where

$$\tilde{\phi} = \phi (M^*)^{-\frac{1}{2}} \tag{3.6}$$

is the modal matrix wanted.

The relationship between the discretized system coordinates r and the modal coordinates Y is given by

$$r = \phi \cdot Y(t) \tag{3.7}$$

where ϕ represents the set of significant undamped free-vibration mode shapes of the combined soil-structure-ocean-system. In general only a limited number (p) of the modes will contribute to the response, that is, $p << N$ (total number of degrees of freedom). Therefore, ϕ is a rectangular matrix with many more rows than column.

Formulation and Solution of the Forced Vibration Problem

Now, if Eq.(3.7) is substituted into Eq.(2.1) and both sides are pre-multiplied by ϕ^T, the result is the set of p normal-coordinate equations of motion which may be written

$$M^*\ddot{Y} + C^*\dot{Y} + K^*Y = P^*(t) \tag{3.8}$$

where M^*, C^* and K^* are generalized mass, damping and stiffness matrix, respectively. Both the generalized mass and stiffness matrices are diagonal matrices, while the generalized damping matrix normally is a full matrix.

Assuming that the mode shapes are normalized so that the generalized mass for each mode is unity

$$M^*_{nn} = \tilde{\phi}_n^T M \tilde{\phi}_n = 1 \tag{3.9}$$

Eq.(3.8) may be written as

$$\ddot{Y} + C^*Y + \omega^2 Y = P^*(t) \tag{3.10}$$

Correspondingly, the generalized stiffness for each mode becomes the modal frequency squared

$$\omega^2 = \begin{bmatrix} \omega_1^2 & & & \\ & \omega_2^2 & & \\ & & \ddots & \\ & & & \omega_p^2 \end{bmatrix} \tag{3.11}$$

The generalized damping matrix in Eq.(3.10) is defined by

$$C^* = \phi^T C \phi \tag{3.12}$$

If the damping matrix of the combined soil-structure-ocean system is such that the mode shapes are orthogonal with respect to it, Eq.(3.12) has the form

$$C^{*(D)} = \begin{bmatrix} 2\xi_1\omega_1 & & & \\ & 2\xi_2\omega_2 & & \\ & & \ddots & \\ & & & 2\xi_p\omega_p \end{bmatrix} \tag{3.13}$$

In this case Eq.(3.10) becomes a set of independent modal response equations which can be solved separately. Since the actual time variation of the loading is harmonic and only steady state response is wanted, the solution is explicitly stated.

For mode (j) the steady state response to the loading

$$P_j^* = P_{0j} e^{i\Omega t} \tag{3.14}$$

is

$$Y_j(t) = \frac{P_{0j}}{\omega_j^2} \frac{[(1-\beta_j^2)\sin\Omega t - 2\xi_j\beta_j\cos\Omega t]}{((1-\beta_j^2)^2+2\beta_j\xi_j)^{\frac{1}{2}}} \tag{3.15}$$

$$\beta_j = \frac{\Omega}{\omega_j} \tag{3.15a}$$

Even if the damping matrix does not satisfy the orthogonality conditions, the transformation to normal coordinates still may be beneficial. Since the number of (coupled) equations in Eq.(3.8) is smaller than in the original Eq.(2.1), the solution of Eq.(3.8) by for instance a step-by-step numerical integration method is cheaper than solving the complete set (2.1) In this case the only approximation is the trunctation of (insignificant) higher modes. The corresponding internal forces in the structure may, when r is found,be calculated according to

$$S = Kr + S_0 \qquad (3.16)$$

where S is the internal force vector. S_0 is the equivalent nodal forces due to external loading. By choosing a rather fine element mesh, the S_0 forces become negligible as compared to the"elastic forces"Kr.

Comments on the Modeling of Damping Properties

The representation of the damping is the most uncertain item by the dynamic modeling.

All three media- soil, structure and ocean contribute to the damping in the interaction system.

For the *soil* an equivalent viscous damping coefficient representing geometric and hysteretic damping is derived. The error by representing the hysteretic damping by an equivalent viscous one is negligible. The damping coefficients are introduced in the C matrix. The corresponding C* matrix (Eq.(3.13)) in general will have large off-diagonal terms.

The damping in the *structure* is most often known from measurements as modal damping by pure structural vibrations (i.e. for fixed base structures). The structural damping - most often known in terms of the damping ratio - must be modified when introducing it into the interaction model. As the foundation flexibility

changes the vibration modes the amount of energy dissipated in the structure itself also changes.

The equivalent damping ratio for the interaction mode (j) due to damping in the structure may be obtained by multiplying the bare structural damping ratio by a correction factor χ_j, (see Appendix A.1.). For the modes corresponding to the lowest frequencies χ_j may be taken as $(\omega/\bar{\omega})^3$ where $\bar{\omega}$ and ω are the corresponding eigenfrequencies of a structure on rigid and flexible soil, respectively.

The *hydrodynamical* (damping) may be treated either in the same way as the soil or the structural damping.

The conditions under which the C^* matrix will be diagonal requires C expressible as a polynomial of K, Refs.(60,61).

A possible full damping matrix, C^* may be replaced by a diagonal matrix $C^{*(D)}$ in various ways, namely

1) The elements $C^{*(D)}$ are equal to the diagonal elements of C^*, i.e. off-diagonal terms are ignored, Refs. (25, 36).

2) The diagonal elements in $C^{*(D)}$ are determined so that the transfer function for a characteristic response quantity obtained by the rigorous and the classical normal mode solution match for all eigenfrequencies within the frequency range of interest.

   The transfer function for a given quantity - as defined in Section 3.3 - for the rigorous and the normal mode solution is denoted $\phi(\omega)$ and $\tilde{\phi}(\omega)$, respectively. $\phi(\omega)$ is given by the numbers computed while $\tilde{\phi}(\omega)$ is a linear combination of terms of the type (3.15) where the ξ_j's are unknown. Notice that $\tilde{\phi}(\omega)$ will be a nonlinear function of ξ_j. The ξ_j's are then determined by solving the equations

$$|\phi(\omega_k)| = |\tilde{\phi}(\omega_k)| \qquad (3.17)$$

$$k = 1,2,.... \ell$$

The set of simultaneous nonlinear, algebraic equations can be solved by iteration. The iteration is started by neglecting the contributions from all modes other than the k'th itself when evaluating $|\tilde{\phi}(\omega_k)|$.

The reason for achrieving the matching at the eigenfrequencies, ω_k, is that the response is most sensitive to the magnitude of the damping at these frequencies.

Because the response at the deck is usually more sensitive to damping, the deck displacement may be chosen as the basis for transfer function matching.

The number of frequencies to be considered is in general less than 10.

The use of this technique - requiring both a rigorous (step-by step) and normal modal analysis - is justified when a large number of transfer functions are to be evaluated and each transfer function requires the computation of the response for a number of frequencies of the order 20 - 50 and the technique (1) mentioned above yields too large errors. The approach was applied by Tsai, Ref.(58) in conjunction with a soil- structure interaction problem.

3) For the normal mode approximation there are several empirical methods available for computing the composite modal damping for the interaction system. Bigg's method, Ref.(56), computes the composite modal damping as a weighted average of the respective damping values of the foundation and the structure, the weighting factor being the strain energy. Johnson and McCaffey's

method, Ref.(57), also computes the weighted average of the respective damping values, but the weighted factor is the mass, the mode shape or the product of both.

3.2.2 Step-by-step Integration

Formulation of the Equations of Motion

In this case the stiffness and mass matrices are constructed in a conventional way. The damping matrix consists of the soil and ocean damping coefficients which are directly added in the matrix. The (modal) structural damping is transformed into the damping matrix by

$$C^S = M[\sum_{n=1}^{n} \phi_n^S \xi_n' \phi_n^{ST}]M \tag{3.18}$$

where ξ_n' are the damping ratio for the structural mode number n.

Alternatively, the damping matrix resulting from structural damping is calculated, Refs. (60,61) as

$$C = \sum_{j=\ell}^{\ell+n} \alpha_j M(M^{-1}K)^j \tag{3.19}$$

in which ℓ is an arbitrary integer, and the coefficients α_j are obtained from the solution of the system of equations

$$2\xi_j'\omega_i = \sum_{j=\ell}^{\ell+n} \alpha_j \omega_i^{2j} \tag{3.20}$$

If the structure consists for instance of materials with essentially different damping properties the damping (sub-) matrix may be constructed for each structure separately and added in the global damping matrix.

Selection of Integration Method

The transient response may be obtained by direct "step-by-step" method for the coupled equations of motions (2.1). In connection with stochastic response analyses it will often be beneficial to contract the general equations (2.1) to the form (3.10) before carrying out the step-by-step procedure. It is assumed that the boundary conditions have already been incorporated into the equation above and that the initial displacements $\{r(0)\}$ and initial velocities $\{\dot{r}(0)\}$ also are known. The dynamic equilibrium equations are a set of second order ordinary differential equations in time, which is usually the highest order encountered in engineering applications.

Time integration of initial value problems has an extensive literature. The book by Richtmyer and Morton (62) provides an excellent theoretical foundation. In the context of structural dynamics Argyris et al, Ref.(63), and Bathe and Wilson, Ref.(64) Nickell, Ref.(65),and Langen, Ref.(111) have contributed recent reviews of methods.

The methods are based on numerical differentation (finite differences) or numerical integration.

Among the finite difference based methods, the second central difference method and the Houbolt method are the most popular.

Newmark β-methods (including the Wilson modification) are the most widely used methods based on numerical integration.

The choice of method should in general be based on an efficiency criterion.

The method which can solve the problem with a given accuracy for minimum costs is then preferable.

The accuracy mainly depends on the following factors:

- time discretization (or truncation) error (degree of consistency of the approximation with respect to the exact differential equations)
- time stability

The costs are mainly characterized by the following factors:

- number of calculations for each time step
- computer storage requirements

The choice of solution method is problem dependent. The type of structure, the spatial and time-wise variation of the loading will influence the choice. A time domain solution through step-by-step methods will be particularily of interest when the problem is nonlinear. In the choice of method due consideration should be given to the degree of nonlinearity.

Since the "best" method depends on the problem to solve, a computer code should provide for a possible choice between different step-by-step methods. This is in most cases a simple task.

The commonly used methods can be written on an explicit form. The coefficient (pseudostiffness matrix) then need only be triangularized once if the structural problem is linear and constant time-step is chosen. Due to the large costs of the triangularization constant time-step is most convenient in linear problems.

3.3 Transfer-functions (response to regular waves)

The structural response (i.e. displacements or stresses in certain points and directions) may be described by the transfer-functions, $\phi(\omega,\alpha+\theta)$. A transfer-function is the ratio between the amplitude of the steady-state response to a regular wave of arbitrary amplitude and wave amplitude at a given frequency ω and wave direction. The transfer function there-

fore is expressed as a function of the frequency , ω, and the wave direction, $\alpha + \theta$. It is, however, implicit that the transfer function depends on the dynamical properties (stiffness, mass and damping) of the actual system.

In practice, each transfer function is determined by calculating the harmonic response for about 20 - 30 wave frequencies. The harmonic response is for convenience calculated for a wave height of 2 m (wave amplitude of 1 m) for all periods. Harmonic nodal force amplitudes and phase angles are determined for an arbitrary structure according to Section 2.5.

The response is evaluated by the normal mode technique as described in Chapter 3.2.2. First, the displacement vector is determined by solving Eq.(3.10) with $C^* = C^{*(D)}$ (uncoupled equations). Amplitudes and phase angles are stored in the computer.

The total displacement response is obtained directly by superimposing the modal displacements. Forces and moments are obtained from Eq.(3.16) by determining the forces S for each mode and superimposing. In practice, the beam element lengths are chosen so small that the forces and moments, S_0 can be discarded in Eq.(3.16).

The transfer functions must, in a general non-symmetric structure, be calculated for waves progressing in several directions, β, in the range $0 < \beta < 2\pi$. When the structure exhibits symmetry about one or two axes, the computations are considerably reduced. In the present analysis twelve directions have been chosen.

4. STATISTICAL ANALYSIS

4.1 Description of the Sea as a Random Process

A stochastic process, $X(t)$, is said to be weakly stationary if its autocorrelation function $R(t,t+\tau) = E(X(t+\tau) \cdot X(t))$ is independent of t, i.e. $R(t,t+\tau) \equiv R(\tau)$.

If $R(t,t+\tau)$ is slowly varying with t, the process can be devided into periods where the autocorrelation function is independent of t. Hence the long-term stochastic process, in which $R(t,t+\tau)$ is slowly varying with t, could be treated as composed of a series of short-term weakly stationary stochastic processes, see Refs. (78,81,83), and Section 4.3. Within a period of 30 min. to some hours the sea elevation can be assumed to be a stationary Gaussian process with zero mean, Ref.(43). The statistical properties then are completely described by the spectrum, $S(\omega)$ of the process, which is the Fourier transform of $R(\tau)$, Ref. (73). Defined in this way $S(\omega)$ is a two-sided spectrum, i.e. valid for all values of ω. The physically realisable one sided spectrum is defined through.

$$S_w(\omega) = \begin{cases} 2S(\omega) & \omega \geq 0 \\ 0 & \omega < 0 \end{cases}$$

It is $S_w(\omega)$ which may be measured experimentally.

4.2 Short-term Description of the Waves

General Remarks

As mentioned above the spectrum is the primary characterization of a short-term state of irregular waves.

According to the elementary wave theory, the surface elevation is due to incoming waves from any direction, and hence the spectrum has to be given both in terms of the frequency and the angle, β, which can be divided into two parts: $\beta = \alpha+\theta$, where α is the mean direction of the incoming waves and θ is the angular deviation from α for the elementary waves, see Fig. 4.1.

Hence the wave spectrum (defined for positive frequencies, ω) is written: $S_w(\omega,\alpha+\theta)$. $S_w(\omega,\alpha+\theta)$ is commonly assumed to be given on the form

$$S_w(\omega,\alpha+\theta) = f(\theta) \quad S_w(\omega,\alpha) \tag{4.1}$$

where

$S_w(\omega,\alpha+\theta)$ - two-dimensional wave spectrum
$S_w(\omega,\alpha)$ - one-dimensional wave spectrum
$f(\theta)$ - directionality function
ω - circular frequency
α - angle of incoming waves
θ - angle between elementary wave and mean direction of incoming waves.

It is clear that the moments (m_n) of the spectrum can be utilized to characterize the sea state instead of the spectrum

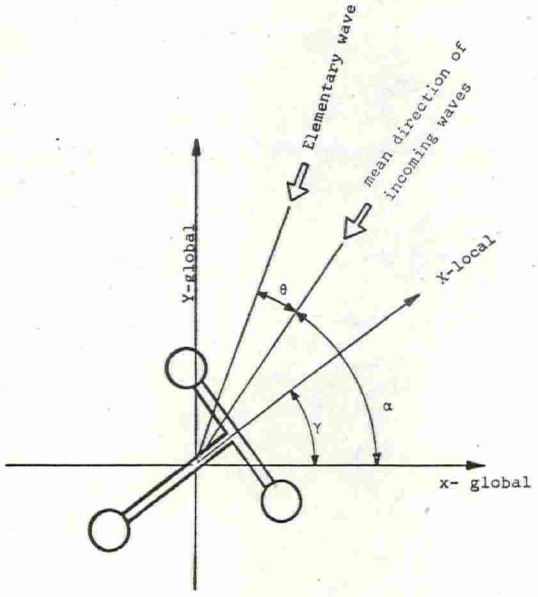

Fig. 4.1 Definitions of angles α,θ,γ.
γ-orientation of the structure

$$m_n = \int_{\omega} \omega^n S(\omega,\alpha+\theta)d\omega \quad ; \quad n = 0,1, \ldots \infty \qquad (4.2)$$

Most of the information needed in practice is contained in the lower order moments ($n \leq 4$).

Wave Spectrum

A mathematical model of the real one-dimensional wave spectrum may be written on the following form, see Refs.(88,92).

$$S_w(\omega,\alpha) = A\omega^{-k}\exp(-B\omega^{-\ell}) \exp\{-\frac{(\omega-\omega_p)^2}{2\kappa^2\omega^2}\}^{\eta} \qquad (4.3)$$

A,B,k,ℓ,η,κ and ω_p are parameters of the wave spectrum. In general A,B,η,κ, and ω_p are functions of the directions α.

Pierson-Moskowitz Spectrum.

With $\eta = 1$, $k = 5$ and $\ell = 4$, Eq. (4.3) reduces to the Pierson-Moskowitz spectrum

$$S_w(\omega,\alpha) = A\omega^{-5}\exp(-B\omega^{-4}) \qquad (4.4)$$

It can be shown that the parameters A and B may be written

$$A = 0.11\, H_{1/3}^2\, (\frac{2\pi}{\bar{T}})^4$$
$$B = 0.44\, (\frac{2\pi}{\bar{T}})^4 \qquad (4.4a)$$

and the wave spectrum is written (ISSC-form):

$$S_w(\omega,\alpha) = 0.11\, H_{1/3}^2\, (\frac{2\pi}{\bar{T}})^4\omega^{-5} \exp\{-0.44\, (\frac{2\pi}{\bar{T}})^4\omega^{-4}\} \qquad (4.5)$$

where

$H_{1/3}$ - significant wave height defined as the mean of the upper third crest to through wave height (see Fig. 4.2)

$\bar{T}$ - average mean period, given as

$$\bar{T} = 2\pi \frac{m_0}{m_1}$$

$\bar{T}$ is a commonly used estimator for the period between crests, T_2, see Fig. 4.2 .

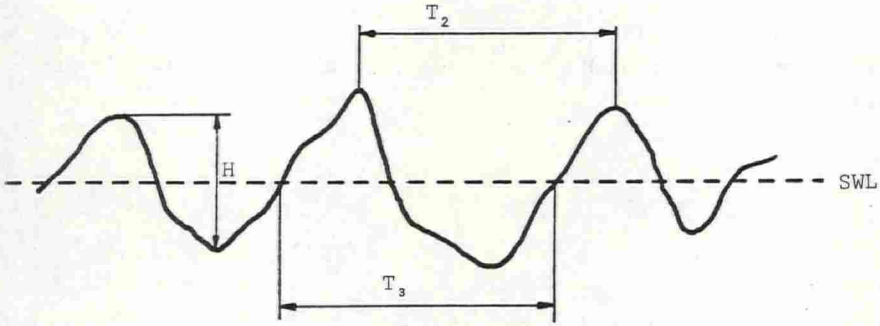

Fig. 4.2 Definition of crest to through wave height, H, and period between crests T_2, and zero-up crossing period T_3

JONSWAP Spectrum.

With k = 5 and ℓ = 4 Eq.(4.3) reduces to the sharply peaked JONSWAP-spectrum

$$S_w(\omega,\alpha) = A\omega^{-5} \exp(-B\omega^{-4}) \eta \exp\{-\frac{(\omega-\omega_p)^2}{2\kappa^2\omega_p^2}\} \qquad (4.6)$$

η is a peakedness parameter, ω_p is the peak frequency, and κ defines the width of the "spectral peak".

η is found to vary between 1 and 7 with an average value of 3.3. For $\eta = 1$ the JONSWAP-spectrum Eq.(4.6) reduces to the shape of the Pierson-Moskowitz spectrum, Eq.(4.5).

The JONSWAP-spectrum seems to be a better fit to North Sea wave data. However, little information about the statistical distribution of its parameters is available. Hence the Pierson-Moskowitz spectrum will be applied in most of the present context.

A possible way to study the influence of this peakedness would be to use the Pierson-Moskowitz spectrum given as Eq.(4.5) multiplied with

$$\eta^{\exp\{-\frac{(\omega-\omega_p)^2}{2\kappa^2\omega_p^2}\}} \tag{4.6a}$$

ω_p is determined as a function of $\bar{T}$ as

$$\omega_p = \frac{2\pi}{\bar{T}} (0.352)^{1/4} \tag{4.6b}$$

and κ given as

$$\kappa = \begin{cases} \kappa_a = 0.07 & \omega \leq \omega_p \\ \kappa_b = 0.09 & \omega > \omega_p \end{cases} \tag{4.6c}$$

Other proposed wave-spectra that have to be mentioned are the *Derbyshire-Scott spectrum* and the *modified Derbyshire-Scott*. These spectra are given by

$$S_w(\omega,\alpha) = \begin{cases} 0 & \omega-\omega_0 < -0.26 \\ A \cdot H_{1/3}^2 \exp\{-[\frac{(\omega-\omega_0)^2}{B(\omega-\omega_0+C)}]^{\frac{1}{2}}\} & -0.26 \leq \omega-\omega_0 \leq 1.65 \\ 0 & \omega-\omega_0 > 1.65 \end{cases} \tag{4.7}$$

where

$$\omega_0 = 3.15 \cdot \bar{T}^{-1} + 8.98 \cdot \bar{T}^{-2} \qquad (4.7a)$$

The parameters A,B,C are given as:

Derbyshire-Scott spectrum:

$$\begin{aligned} A &= 0.214 \\ B &= 0.065 \\ C &= 0.26 \end{aligned} \qquad (4.7b)$$

Modified Derbyshire-Scott spectrum:

$$\begin{aligned} A &= 0.300 \\ B &= 0.03534 \\ C &= 0.26 \end{aligned} \qquad (4.7c)$$

Up to now there is no general agreement on which formulation that represents the best fit to the real wave spectrum. Most likely no spectrum will be the best in any situation. The influence of the choice of spectrum on the response therefore will be illustrated by some example cases.

The Directionality Function

According to Refs.(81,82,92) directionalty function may be chosen as

$$f(\theta) = \begin{cases} K(n) \cos^n\theta & -\frac{\pi}{2} \leq \theta \leq \frac{\pi}{2} \\ 0 & \text{elsewhere} \end{cases} \qquad (4.8)$$

K(n) is determined from Eq.(4.9)

$$\int_{-\frac{\pi}{2}}^{\frac{\pi}{2}} f(\theta)\, d\theta = 1 \qquad (4.8a)$$

Most commonly the following functions have been applied:

Pierson: $$f(\theta) = \frac{2}{\pi} \cos^2\theta \quad -\frac{\pi}{2} \leq \theta \leq \frac{\pi}{2} \qquad (4.9)$$

Mark: $$f(\theta) = \frac{8}{3\pi} \cos^4\theta \quad -\frac{\pi}{2} \leq \theta \leq \frac{\pi}{2} \qquad (4.10)$$

Other directionality functions are given in Ref.(72)

4.3 Short-term Response Statistics

Response Spectrum

The sea is, as mentioned in Section 4.1, assumed to be composed by a series of stationary Gaussian processes with zero mean. The response will thus be given as a series of stationary processes being Gaussian with zero mean. The spectrum of the response process then completely characterizes its statistics. The response spectrum, $S_R(\omega,\alpha+\theta)$ can be obtained from the transfer function, $\phi(\omega,\alpha+\theta)$ and the wave spectrum in the following manner, Ref.(73):

$$S_R(\omega,\alpha+\theta)=\phi(\omega,\alpha+\theta)\phi^*(\omega,\alpha+\theta)\ S_w(\omega,\alpha+\theta) \qquad (4.11)$$

where the symbol * denotes complex conjugation. ϕ obviously is independent of $\bar{T}$ and $H_{1/3}$, but dependent of $\alpha+\theta$, and of the angular orientation γ, of the structure (γ refered to the same global axis as α). Hence, ϕ is formally written

$$\phi = \phi(\omega,\alpha+\theta-\gamma) \qquad (4.12)$$

θ can be eliminated from the response spectrum in the following way:

$$S_R(\omega;\alpha,\gamma)=\int_\theta \phi(\omega,\alpha+\theta-\gamma)\phi^*(\omega,\alpha+\theta-\gamma)\ f(\theta)S_w(\omega,\alpha)d\theta \qquad (4.13)$$

Introducing the pseudo-transferfunction, $\phi_{ps}(\omega,\alpha,\gamma)$, Eq.(4.13) may be written

$$S_R(\omega;\alpha,\gamma)=\phi_{ps}(\omega,\alpha,\gamma)\ \phi^*_{ps}(\omega,\alpha,\gamma)\cdot S_w(\omega,\alpha) \qquad (4.14)$$

where

$$\phi_{ps}(\omega;\alpha,\gamma)\ \phi^*_{ps}(\omega,\alpha,\gamma)=\int_\theta \phi(\omega,\alpha+\theta-\gamma)\phi^*(\omega,\alpha+\theta-\gamma)\cdot f(\theta)d\theta \qquad (4.14a)$$

In the following γ is chosen equal to zero, see Fig. 4.1. Hence Eqs. (4.14) and (4.14a) are written

$$S_R(\omega,\alpha)=\phi_{ps}(\omega,\alpha)\ \phi^*_{ps}(\omega,\alpha)\ S_w(\omega,\alpha) \qquad (4.15)$$

$$\phi_{ps}(\omega,\alpha)\ \phi^*_{ps}(\omega,\alpha)=\int_\theta \phi(\omega,\alpha+\theta)\ \phi^*(\omega,\alpha+\theta)f(\theta)d\theta \qquad (4.15a)$$

Distribution of Individual Maxima

The response processes of current interest are characterized by a wavy form with varying amplitude and frequency. The maximum value and the number of cycles corresponding to each amplitude level are the response quantities of primary interest in the design. The distribution of individual maxima ("amplitudes") rather than the distribution of the wave elevation is the most appropriate statistical measure for characterizing these quantities. For stationary Gaussian processes this distribution has been discussed in detail in Refs.(73,75,76,82,83), and is found to be dependent on the parameters m_o and ε defined as

$$\varepsilon^2 = 1 - \frac{m_2^2}{m_0 m_4} \quad ; \quad 0 < \varepsilon < 1 \qquad (4.16)$$

where the moments (m_n) of the response spectrum are defined in the same manner, Eq.(4.2) as the moments of the wave spectrum. In the case $\varepsilon = o$ the maxima are Rayleigh distributed, while $\varepsilon = 1$ gives the Gaussian distribution. For $o < \varepsilon < 1$ the probability density function for the *greater* maxima is found to

become approximately $\sqrt{1-\varepsilon^2}$ times that of the Rayleigh distribution. The frequency of the *greater* maxima for $0 < \varepsilon < 1$ is found to be approximately $1/\sqrt{1-\varepsilon^2}$ of the frequency of maxima for $\varepsilon = 0$. Hence the probability of exceedance of some level by a given number of maxima within a given time interval is the same for all values of ε (reasonably less than 1). Hence the Rayleigh distribution will be assumed for the short-term distribution of individual maxima. This distribution is given by the following probability density function.

$$f_R(x) = \begin{cases} \frac{2x}{r^2} \exp(-x^2/r^2) & x \geq 0 \\ 0 & \text{elsewhere} \end{cases} \qquad (4.17)$$

where

$$r^2 = 2m_0 = 2 \int_0^\infty S_R(\omega;\alpha)d\omega \qquad (4.17a)$$

The probability to exceed some amplitude-level x may be calculated from Eq.(4.17) as

$$Q_S(X \geq x) = \int_x^\infty f_R(x)dx = \exp\{-(\frac{x}{r})^2\} \qquad (4.18)$$

Eq. (4.18) gives the distribution of the response *amplitude* when r is known.

The Rayleigh parameter, r, for the response is a function of the sea-state parameters $H_{1/3}$, $\bar{T}$ and α, and the dynamical properties of the interaction system. Eq. (4.18) may be written as a conditional probability of exceedance:

$$Q_S(X \geq x | H_{1/3}, \bar{T}, \alpha) = \exp\{-(\frac{x}{r})^2\} \qquad (4.19)$$

In Eq. (4.19) only the dependence on the sea-state parameters are incorporated. This equation will be useful when extending the statement on probability of exceedance to a long-term state- in Section 4.5.

Within time-interval where the sea elevation is assumed to be weakly stationary, the distribution of response is described by Eq.(4.19). These intervals could be of duration 1 - 24 hours, a very short period compared with the life-time of the structure.

Extreme Value of the Response

The evaluation of the extreme value of the response is decisive for the design against ultimate collapse and similar modes of failures. By means of order statistics, the following quantities can be computed from the distribution of the largest peak within the short-term period considered, Refs, (74.-76).

Mean extreme value:

$$E[X_{max}] = \sqrt{m_0}\left[\sqrt{2\ln N} + \frac{0.5772}{\sqrt{2\ln N}}\right] \qquad (4.20)$$

where N is the number of cycles in the short-term state

$N = \nu_3 L = \frac{1}{2\pi}\sqrt{\frac{m_2}{m_0}}\, L$, L is the duration of the short term period.

Standard deviation of the extreme value

$$\sigma_{X_{max}} = \sqrt{m_0}\,\frac{\pi}{\sqrt{6}\sqrt{2\ln N}} \qquad (4.21)$$

Since the standard deviation (4.21) of the largest peak value is relatively small as compared to the mean value (4.20) when N is of the order 10^4, the mean value is a representative design value, Ref.(74).

It should be noticed, however, that the quantity (4.20) is conditional upon the sea-state. To ensure that (4.20) is the desired peak response occuring with a return period equal to the estimated life-time of the structure (20 - 50 years) the corresponding "worst in the life-time" sea state should be used. However, no consistent rule exists by which this state can be

found. Therefore the long-term description of the waves (Section 4.3) and the subsequent long-term response statistical treatment of the response (Section 4.4) are believed to be more consistent way of establishing the extreme response.

Furthermore, this long-term model yields an estimate on the response to be used to check against fatigue failure.

4.4 Long-term Description of the Waves

General Remarks

Each set of $H_{1/3}$, $\bar{T}$ and α, describes a short-term state of the sea, and therefore the long-term description of the sea will be obtained from a three-dimensional probability density function of $H_{1/3}$, $\bar{T}$ and α, $f(H_{1/3},\bar{T},\alpha)$. The directions at a given location is divided into a finite number of intervals, and the probability density function may be written as:

$$f(H_{1/3},\bar{T},\alpha) = \sum_{ID} f_{ID}(H_{1/3},\bar{T}|\alpha)\ PDIR_{ID}(\alpha) \qquad (4.22)$$

where

$f_{ID}(H_{1/3},\bar{T}|\alpha)$ - conditional probability density function of $H_{1/3}$ and $\bar{T}$ given direction-interval no. ID

$PDIR_{ID}(\alpha)$ - probability that the principal direction of the incomming wave system fell within interval no. ID

Conventional Model for Long-term Distribution of Wave Data

In most wave statistics, the data for stationary sea states are given in terms of visually estimated wave period, T_v, and visually estimated wave height, H_v.

The long-term conditional distribution of H_v, (within a given interval of visual wave period T_v and a given direction interval α_{ID}) is according to Ref. (81) described by a three-parameter Weibull-distribution.

Prob ($H_v \leq H_v | T_v$ within interval no. L, direction no. ID)

$$= F_{ID,L}(H_v|T_v,\alpha) = 1-\exp\{-(\frac{H_v-H_{oID,L}}{H_{cID,L}-H_{oID,L}})^{\gamma_{ID,L}}\} \quad (4.23)$$

$H_{oID,L}$, $H_{cID,L}$, and $\gamma_{ID,L}$ are parameters of the distribution.

Nordenstrøm, Ref.(81) has found that there is a relationship between H_v and $H_{1/3}$ satisfying Eq.(4.24)

$$\text{Prob}(H_{1/3} \leq H_{1/3}) = \text{Prob}(H_v \leq H_v) \quad (4.24)$$

This relationship is on the form

$$H_v = AH \cdot H_{1/3}^{BH} \quad (4.25)$$

Common values for the constants AH and BH are

$$AH = 0.5$$
$$BH = 1.33 \quad (4.25a)$$

Substituting Eq. (4.25) into Eq.(4.23) gives the long-term conditional distribution of $H_{1/3}$, $F_{ID,L}(H_{1/3}|T_v,\alpha)$. The conditional probability density function for $H_{1/3}$ is given by

$$f_{ID,L}(H_{1/3}|T_v,\alpha) = \frac{d}{dH_{1/3}}(F_{ID,L}(H_{1/3}|T_v,\alpha)) \quad (4.26)$$

Unfortunately, there is no such simple connection between T_v and $\bar{T}$. On the other hand, it is found that $f_{ID,L}(\bar{T}_3|T_v,\alpha)$ is Gaussian or log-normally distributed.

$\bar{T}_3$ is average apparent period, defined as the mean of T_3 see Fig. 4.2. For the Pierson-Moskowitz spectrum it can be shown that

$$\bar{T} = 1.086\bar{T}_3 \quad (4.27)$$

and hence the distribution of $\bar{T}$, $f_{ID,L}(\bar{T}|T_v,\alpha)$ is Gaussian or log-normally distributed

The expectation of $\bar{T}_3$ is given through

$$E_{ID,L}(\bar{T}_3|T_v,\alpha) = AT\ T_v^{BT} \tag{4.28}$$

where T_v is taken as the class-midpoint and AT and BT are constants.

From Eq. (4.27) and Eq.(4.28) it is seen that

$$E_{ID,L}(\bar{T}|T_v,\alpha) = 1.086\ AT\ T_v^{BT} \tag{4.29}$$

Common values of AT and BT are given in Eqs. (4.30a - 4.30b)

$$\begin{cases} AT = 0.74 \\ BT = 1.00 \end{cases} \tag{4.30a}$$

$$\begin{cases} AT = 2.83 \\ BT = 0.44 \end{cases} \tag{4.30b}$$

The conditional standard deviation $S_c(\bar{T}_3)$ of $\bar{T}_3$ was found to be

$$\sigma_{ID,L}(\bar{T}_3|T_v,\alpha) = S_c(\bar{T}_3) = 1.0 \quad [\text{seconds}] \tag{4.31a}$$

By utilizing Eq.(4.27), Eq.(4.31a) can be written as

$$S_c(\bar{T}) = 1.086 \quad [\text{seconds}] \tag{4.31b}$$

If the Gaussian distribution is assumed, the conditional probability density function of $\bar{T}$ is written as:

$$f_{ID,L}(\bar{T}|T_v,\alpha) = \frac{1}{\sqrt{2\pi}\ S_c(\bar{T})} \exp\{-(\frac{\bar{T}-E_{ID,L}(\bar{T}|T_v,\alpha)}{\sqrt{2}\ S_c(\bar{T})})^2\} \tag{4.32}$$

If the log-normal distribution is assumed, the conditional probability density function is written as:

$$f_{ID,L}(\bar{T}|T_v,\alpha)=\frac{1}{\sqrt{2\pi}\ \bar{T}\ \delta_{ID,L}}\exp\{-(\ln(\frac{\bar{T}}{\beta_{ID,L}})/\sqrt{2}\ \delta_{ID,L})^2\} \tag{4.33}$$

where

$$\beta_{ID,L}=E_{ID,L}(\bar{T}|T_v,\alpha)\ \{1+(\frac{S_c(\bar{T})}{E_{ID,L}(\bar{T}|T_v,\alpha)})^2\}^{-\frac{1}{2}} \tag{4.33a}$$

$$\delta_{ID,L}=\{\ln[1+(\frac{S_c(\bar{T})}{E_{ID,L}(\bar{T}|T_v,\alpha)})^2]\}^{\frac{1}{2}} \tag{4.33b}$$

The joint probability distribution for $H_{1/3}$ and $\bar{T}$ is

$$f_{ID,L}(H_{1/3},\bar{T}|\ T_v,\alpha) = f_{ID,L,J}(\bar{T}|T_v,\alpha,H_{1/3})\cdot f_{ID,L}(H_{1/3}|T_v,\alpha) \tag{4.34}$$

The wave-data available permits only a marginal probability distribution for $\bar{T}$ (with respect to $H_{1/3}$) to be computed, see Eq.(4.32) or Eq.(4.33). Using one of the latter equations in Eq.(4.34) instead of the conditional distribution $f_{ID,L}(\bar{T}|\alpha,T_v,H_{1/3})$ is equivalent with assuming no correlation between $\bar{T}$ and $H_{1/3}$.

The two-dimensional probability distribution of $H_{1/3}$ and $\bar{T}$ then becomes:

$$f_{ID,L}(H_{1/3},\bar{T}|T_v,\alpha)=f_{ID,L}(H_{1/3}|T_v,\alpha)\ f_{ID,L}(\bar{T}|T_v,\alpha) \tag{4.35}$$

Modified Model for Long-term Distribution of Wave Data. Correlation between $H_{1/3}$ and $\bar{T}$ is assumed.

The above assumption seems to be questionable for structures with eigenperiods as low as 2.5 - 6.5 [seconds]. By using the two-dimensional probability density function given in Eq.(4.35), it is found that the probability of exeeding a given response-level has significant contributions from pairs of $H_{1/3}$ and $\bar{T}$ which have no physical meaning.

Walden's data, Ref.(91) on waves in the North-Atlantic, clearly demonstrate that for a given value of T_v there is an upper limit for H_v. It is quite reasonable to assume that a similar situation exists for the parameters $H_{1/3}$ and $\bar{T}$.

The first problem is thus to determine the area of $H_{1/3}$ and $\bar{T}$ where any combination of $H_{1/3}$ and $\bar{T}$ is possible from a physical point of view.
According to Phillips, Refs.(85,86) the wave-spectrum converges towards following for for large values of ω.

$$S_{Eq}(\omega) \simeq \alpha g^2 \omega^{-5} \qquad (4.36)$$

The formula above is known as the equilibrium range spectrum(1)

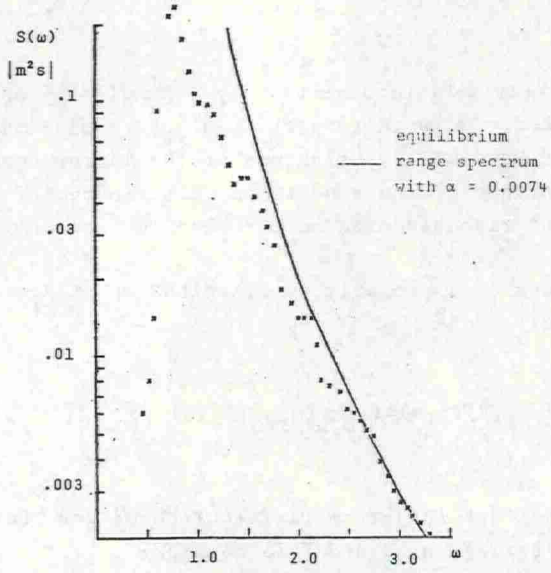

Fig. 4.2 Comparison of observed spectrum (2) and equilibrium range spectrum

(1) The idea of using the equilibrium range spectrum to determine the possible area of $H_{1/3}$ and $\bar{T}$, was proposed by Ragnar Sigbjørnsson, Ref.(108)

(2) S.W.O.P. - Stereo Wave Observation Project 1957

Phillips assumed α to be a universal constant and proposed $\alpha = 0.0074$. In Ref.(86) Phillips compares the actual spectrum with the equilibrium range spectrum for lower values of ω.

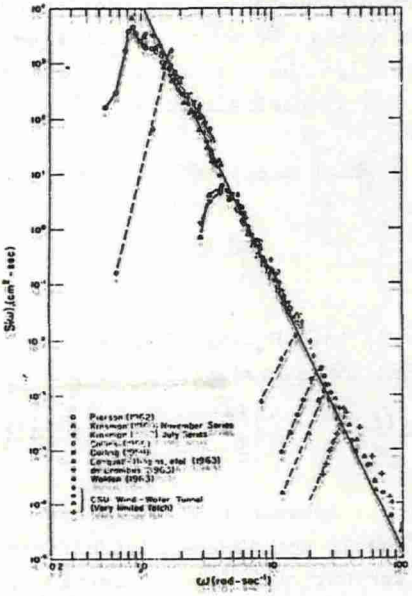

Fig. 4.3 Comparison of observed spectra and the equilibrium range spectrum. From Ref.(87), originally presented in a report of Hess,G.D., Hidy,G.M., Plate,E.S.)

The conclusion was that actual wave spectra are not likely to exeed the equilibrium range spectrum significantly. Fig. 4.2., taken from Ref.(86), shows that the agreement is best for the larger values of ω, but the actual spectrum does not exeed the equilibrium range spectrum. A comparison made by Wiegel in Ref.(87) supports Phillip's conclusion. Fig. 4.3 quoted from Ref.(87) displays an equilibrium range spectrum with $\alpha = 0.0081$.

According to recent wave measurements in the North Sea (JONSWAP), Ref.(88), it is clear that α is not a universal constant. The value of α seems to be a function of the sea-state. For mean wave-periods about 10 seconds, α is typically of the order 0.008, whilst for $\bar{T}$ ~ 3-5 seconds an α equal to 0.02 seems to be more reasonable. This variation of α with the mean wave-period should probably have been accounted for in the modified long-term model. However, as subsequently will be shown by a parameter variation the influence on the results by the actual variation of α is negligible.

Pairs of $H_{1/3}$ and $\bar{T}$ which are possible from a physical point of view, must satisfy

$$S(\omega) \leq \alpha g^2 \omega^{-5} \tag{4.37}$$

Substituting Eq.(4.5) into Eq.(4.37) gives the following inequality to be satisfied for admissibility of pairs ($H_{1/3}$ and $\bar{T}$).

$$\bar{T} \geq 2\pi \left[\frac{0.11}{\alpha g^2}\right]^{1/4} H_{1/3}^{1/2} \quad \text{(admissibility condition)} \tag{4.38}$$

In the foregoing it was assumed that the increase in α for smaller values of $\bar{T}$ would not have any significant influence on the long-term distribution. This assumption is justified by Fig. 4.4. The unbroken line defines the area, R, when α = 0.0081 is assumed for all values of $\bar{T}$. The broken line gives the area, R, when the following values is assumed:

α = 0.0081	$\bar{T}$ > 9 s
α = 0.015	$\bar{T}$ ~ 5 s
α = 0.03	$\bar{T}$ ~ 3 s

It is seen that the difference between the broken and unbroken line is rather small, and would probably have no significant influence on the long-term distribution.

However, it should be noted that the results obtained by assuming α = 0.0081 are non-conservative.

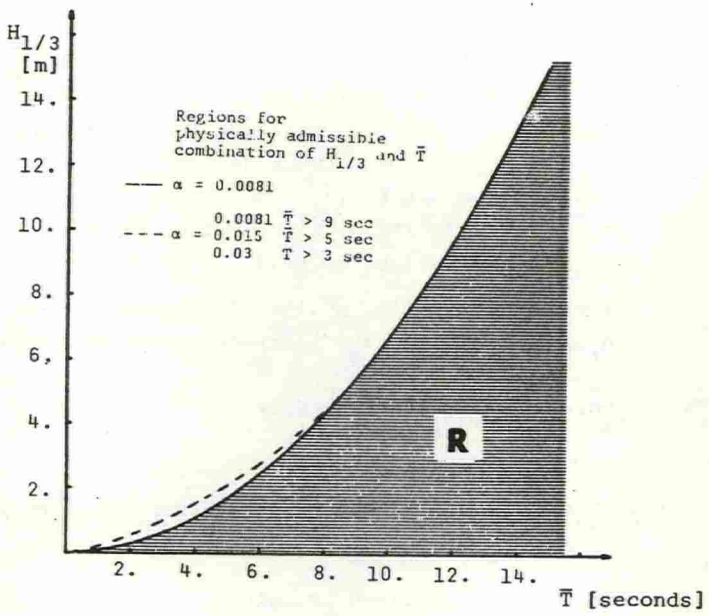

Fig. 4.4 Comparison of physically admissible combinations of $H_{1/3}$ and $\bar{T}$

Using the original assumption of no correlation, and calculating the expected value of $\bar{T}$ by Eq.(4.29) then $E(\bar{T}|T_v,\alpha)$ fall outside the admissible region in Fig. 4.4, especially for small values of T_v. Most of the two-dimensional distribution of $H_{1/3}$, $\bar{T}$ lies outside R for the lowest classes of T_v.

The conventional long-term distribution of $H_{1/3}$ and $\bar{T}$ can be improved by constructing an $f_{ID,L,J}(\bar{T}|T_v,\alpha,H_{1/3})$ in the general equation (4.34) with due consideration of the admissibility criterion (4.38) and the existing observations. The modeling of $f_{ID,L,J}(\bar{T}|T_v,\alpha,H_{1/3})$ is based on the following assumtions:

- for a given $H_{1/3}$ the distribution of $\bar{T}$ $f_{ID,L,J}(\bar{T}|T_v,\alpha,H_{1/3})$ is either a normal or a log-normal distribution, Eqs.(4.32-33).

- the expectation (mean value) of $f_{ID,L,J}$ is assumed to be a function of $H_{1/3}$, (conditional upon $H_{1/3}$). Thus, $E_{ID,L}(\bar{T}|T_v,\alpha)$ in Eqs. (4.32-33) is replaced by $E_{ID,L,J}(\bar{T}|T_v,\alpha,H_{1/3})$ This is the refinement introduced to improve the previous conventional model. To ensure that this modification is in agreement with the known data, the marginal "expectation" (with respect to $H_{1/3}$) of the conditional expectation corresponds to the observed value, Eq.(4.29) (A detailed explanation follows below.)
- the variance of $f_{ID,L,J}(\ )$ is constant, independent of $H_{1/3}$ and equal to the observed value, Eq.(4.31a-b).

The principal assumption regarding the expectation of $\bar{T}$ is:

$$E_{ID,L,J}(\bar{T}|T_v,\alpha,H_{1/3})=TLIM_J(H_{1/3})+FF_{ID,L,J}(\alpha,T_v,H_{1/3}) \quad (4.39)$$

where

$TLIM_J(H_{1/3})$ - is given through Eq.(4.38)

$FF_{ID,L,J}$ - is the distance between the expected value of $\bar{T}$ and the limit of the area R.

To be able to determine $FF_{ID,L,J}$ it is assumed that $FF_{ID,L,J}$ is independent of $H_{1/3}$. In other words it is assumed that for a given direction interval and a given interval of T_v, $FF_{ID,L,J}$ is a constant. Accordingly, Eq.(4.39) is written

$$E_{ID,L,J}(\bar{T}|T_v,\alpha,H_{1/3})=TLIM_J(H_{1/3})+FF_{ID,L}(\alpha,T_v) \quad (4.40)$$

This is illustrated in Fig. 4.5.

From the conditional expectation of $\bar{T}$ given in Eq.(4.40) the "marginal" expectation (marginal with respect to $H_{1/3}$) of $\bar{T}$ may be calculated as follows:

$$EMARG_{ID,L}(\bar{T}|T_v,\alpha)=\int_{H_{1/3}} E_{ID,L,J}(\bar{T}|T_v,\alpha,H_{1/3})$$

$$f_{ID,L}(H_{1/3}|T_v,\alpha)dH_{1/3} \qquad (4.41)$$

where

$f_{ID,L}(H_{1/3}|T_v,\alpha)$ is given in Eq.(4.26)

To ensure that the modified model is "consistent" with the known wave data, it is then required that $EMARG_{ID,L}(\bar{T}|T_v,\alpha)$ is equal to the observed marginal expectation, Eq.(4.29).

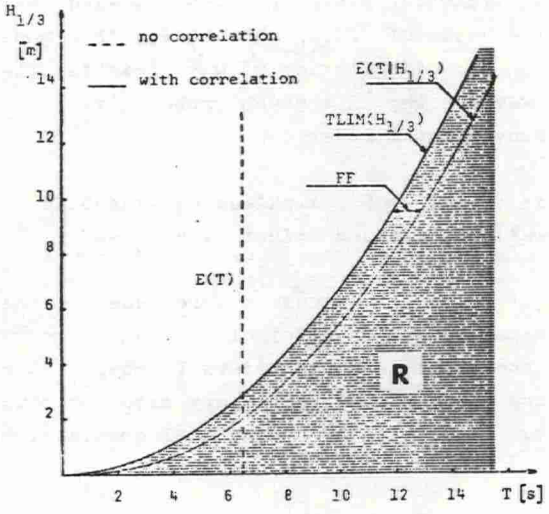

Fig. 4.5 The expectation of $\bar{T}$, with and without correlation between $\bar{T}$ and $H_{1/3}$.

The program "LONTIM" (Part II of Ref. (104)) do automatically calculate $FF_{ID,L}$ such that the following inequality is satisfied

$$|EMARG_{ID,L}(\bar{T}|T_v,\alpha)-E_{ID,L}(\bar{T}|T_v,\alpha)| \leq \varepsilon_o \qquad (4.42)$$

where

$E_{ID,L}(\bar{T}|T_v,\alpha)$ - "marginal" expectation according to Ref. (83) given in Eq.(4.29)

ε_c = a constant, depending on the accuracy that is wanted. In the program LONTIM, $\varepsilon_c = 0.2$ seconds.

This determines the only free variable in Eq.(4.39). Thus, the mean and variance of the normal or lognormal distributions are known and $f_{ID,L}(H_{1/3},\bar{T}|T_v,\alpha)$ is given according to Eq. (4.34) where $f_{ID,L,J}(\bar{T}|H_{1/3},T_v,\alpha)$ is defined by Eq.(4.32) or Eq.(4.33) with mean Eq.(4.39) and variance (as before), Eq.(4.31b).

In this resulting modification a major part of the two-dimensional probability density function given in Eq.(4.34) lies in the area R, depending on the value of $FF_{ID,L}$. Obviously, this modification has no influence on the distribution of wave-heights, The most probable largest wave-height on a given probability level is the same as for the conventional model.

Modified Model for Long-term Distribution of Wave Data based on instrumentally observed values of $H_{1/3}$ and $\bar{T}$

The previous long-term models discussed were based on the visual estimates of wave-period and wave-height. In addition continuous distributions of the short-term parameters $\bar{T}$ and $H_{1/3}$ were assumed. As mentioned before great uncertainties are associated with this long-term model due to potential non-physical combinations of $H_{1/3}$ and $\bar{T}$.

A more reliable long-term model would be a model which was directly based on observed values of $H_{1/3}$ and $\bar{T}$. In this case non-physical combinations of $H_{1/3}$ and $\bar{T}$ would be completely eliminated. However, in this model the most extreme sea-conditions will probably not be included.

Let $H_{1/3}$ be divided into JMAX intervals, and $\bar{T}$ be divided into IMAX intervals. This gives a totally number of IMAX·JMAX different short-term sea-states. Each observed set of $H_{1/3}$ and $\bar{T}$ is associated with one of these blocks.

The probability of occurence of block number (I, J) is assumed to be given as

$$\text{Prob}[((H_{1/3}(J) < H_{1/3} < H_{1/3}(J+1)) \cap (\bar{T}(I) < \bar{T} < \bar{T}(I+1)))|\text{direction}]$$

$$= P_{ID}(H_{1/3}, \bar{T}|\alpha) = \frac{n_{ID}(I,J)}{N_{ID}} \qquad (4.43)$$

where:

$n_{ID}(I,J)$ - number of recordings associated to block (I,J) for direction ID

N_{ID} - total number of recordings for direction ID

$$N_{ID} = \sum_{I=1}^{IMAX} \sum_{J=1}^{JMAX} n_{ID}(I,J)$$

4.5 Long-term Response Statistics

Continuous Distribution for $H_{1/3}$ and $\bar{T}$

The calculation of the long-term distribution of response maxima will be done according to the assumption that the stochastic process consists of a series of stationary processes, characterized by the response spectrum (given by the parameters $\bar{T}$, $H_{1/3}$, α and γ and the parameters characterizing the structural dynamical behaviour):

The conditional long-term probability to exceed a response amplitude for a given interval of visual period and direction may be calculated from Eqs.(4.19) and (4.35) or (4.34) as

$$\text{Prob}(X>x|T_v,\alpha) = Q_{ID,L}(x|T_v,\alpha)$$

$$= \int_{H_{1/3}} \int_{\bar{T}} Q_s(X \geq x|H_{1/3},\bar{T},\alpha)\, f_{ID,L}(H_{1/3},\bar{T}|T_v,\alpha)\, d\bar{T}\, dH_{1/3}$$

(4.44)

The integrals above is evaluated by means of numerical integration, see Ref.(104).

The marginal distribution of response is calculated according to Eq.(4.45)

$$\text{Prob}(X>x) = Q(x) =$$

$$\sum_{ID} PDIR_{ID}(\alpha)\{\sum_{L} PVW_{ID,L}(T_v)\, Q_{ID,L}(x|T_v,\alpha)\} \qquad (4.45)$$

where

$PVW_{ID,L}(T_v)$ - probability that visual wave period T_v fell within interval no. L for direction interval no. ID

$PDIR_{ID}(\alpha)$ - probability that incomming wind fell within direction interval no. ID

Discrete Distribution for $H_{1/3}$ and $\bar{T}$

For each block (i.e stationary sea-state) the probability to exceed a given response-amplitude is given through Eq.(4.22). The long-term distribution is given as

$$P(X>x) = \sum_{ID=1}^{NUDIR} P\,DIR_{ID}(\alpha)\{\sum_{I=1}^{IMAX}\sum_{J=1}^{JMAX} Q_s(X|H_{1/3}, T, \alpha)P_{ID}(I,J)\} \qquad (4.46)$$

The reliability of this model is dependent on that N_{ID} is a great number, for ID = 1, 2, ..., NUDIR. Up to now data has been lacking for this model.

Extreme Value of the Response

Eq.(4.45) can be used in connection with extreme values statistics, Ref.(53), and gives, for instance, the most probable largest value of N maxima, x_N, through:

$$\text{Prob}(X>x_N) \simeq \frac{1}{N} \tag{4.47}$$

Again, the variance of the largest value of N maxima is so small as to justify the use of a single value, x_N, as a design value for ultimate failure modes.

Estimate on the Number of Response Cycles Associated with a Given Amplitude Level

In the design against fatigue the information on the response required is the number of cycles corresponding to each amplitude level.

In the present subsection a simple estimate for this quantity will be given.

It is assumed that the response process is sufficiently narrow-banded so as to justify equivalence between a cycle and a (positive) peak.

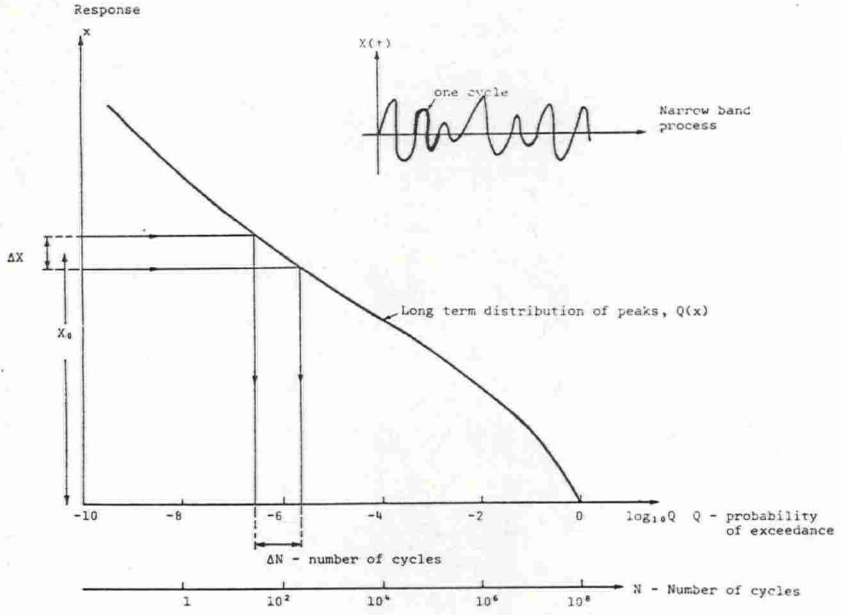

Fig. 4.6 Determination of the number of cycles corresponding to a given amplitude interval. A time interval corresponding to 10^8 cycles is assumed.

The long-term distribution expresses the probability of exceedance for a period of the order of the life-time (20 - 50 years) of the structure. Let the number of cycles in that period be 10^8. One cycle then "corresponds" to a probability 10^{-8}.

The number of cycles, ΔN corresponding to an amplitude level, $(X_0 - \frac{\Delta X}{2}) - (X_0 + \frac{\Delta X}{2})$ then can be obtained from

$$\Delta N = N(X_0 + \frac{\Delta X}{2}) - N(X_0 + \frac{\Delta X}{2}) \qquad (4.48)$$

when the long-term distribution is displayed in a logaritmic scale, Fig. 4.6.

5. NUMERICAL STUDIES

Based on the theory evaluated in Chapters 2 - 4 a computer program was developed. Numerical studies carried out with the computer program are reported in the present section.

5.1 Dynamical Modeling.

5.1.1 Description of Example Platform

Consider the platform shown in the Fig. 5.1 in 146 m of water. The caisson has an equivalent diameter of 90 m and height of 60 m. The total height from the soil to the top of the deck is 175 m. The diameter of the

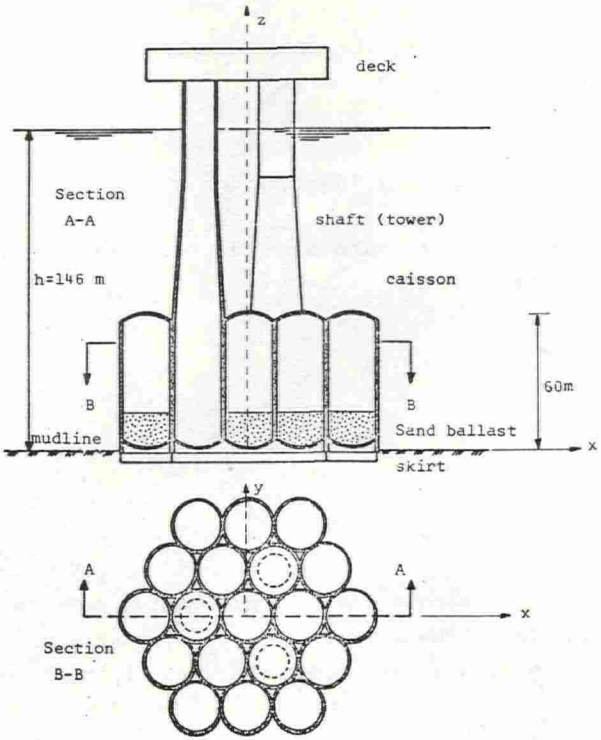

Fig. 5.1 Example gravity platform

shafts is in the range 12 - 20 m.

The platform is assumed to rest on the soil surface with no embedment.

The density and the Poisson ratio of the soil are assumed to be 2000 kg/m^3 and 0.5, respectively. The shear modulus, G_s, is the most important and uncertain of the soil parameters, and a parametric study of G_s in the range $1.0 \cdot 10^7$ N/m^2 to $6.0 \cdot 10^7$ N/m^2 is carried out. In addition, a G_s of $1.0 \cdot 10^9$ is chosen to simulate a fixed base. Equivalent spring and dashpot constants are introduced according to the Chapter 2. The hysteretic damping ratio, $\tilde{D}$, is assumed to be 0.05.

The structural and hydrodynamic damping is represented by a constant damping ratio of 1.5% of the critical for all (interaction) modes of vibration.

5.1.2 Structural Idealization

The actual structure, shown in Fig. 5.1, may be divided into 3 typical parts:

- deck
- shafts
- caisson

Stiffness

The *deck structure* consists of a set of steel girders as shown in Fig. 5.2a, and the idealization is shown in Fig. 5.2b.

Since the deck mainly exhibits horizontal motions, the model in Fig. 5.2b is justified. Stiffness relations are obtained by flexibility considerations of the actual deck.

The mass is lumped in the nodal points, and the elements in the deck is modelled as three-dimensional beams with cross-sectional properties as given in the Table 5.1.

Material properties for *steel*:

Modulus of elasticity $E = 2.1 \cdot 10^{11}$ [N/m^2]

Poisson's ratio $\mu = 0.3$

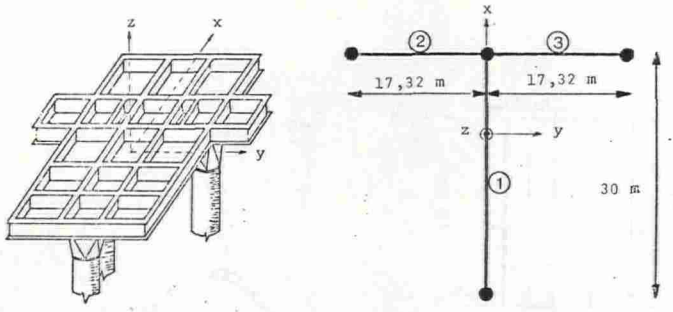

a) Main girders in the deck structure

b) Equivalent deck system

Fig. 5.2 Deck model

Table 5.1 Cross-sectional properties of the deck structure, (unit [m])

Element no.	A	$A_{sx(y)}$	A_{sz}	$I_{x(y)}$	I_z	I_t
1	.82	.13	.32	6.92	4.25	$1.5 \cdot 10^{-4}$
2 , 3	1.94	.56	1.09	16.4	10.75	$6.3 \cdot 10^{-4}$

Remarks: In reality the stiffness I_z is fictious since the bottom of the deck provides "infinite" stiffness in its plane.

x(y) - horizontal; z - vertical; s - shear; t- torsion.

Fig. 5.3 shows one of the *concrete shafts* and its idealization. The model consists of 4 beams with constant cross-sectional properties within each element.

Material properties of *concrete*:

Youngs modulus E = $2.45 \cdot 10^{10}$

Poisson's ratio μ = 0.25

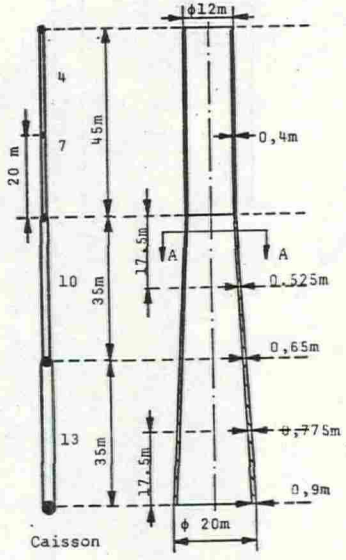

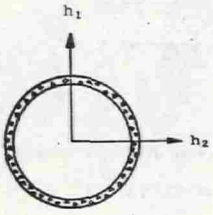

Section A-A

Fig. 5.3 Shaft Model

The mass is lumped in the nodal points. Since the lower order modes predominate this approximation is justified.

Table 5.2 Cross sectional properties of the shafts (Unit [m])

Element no.	A	A_s	$I_{x(y)}$	I_t
4,5,6,7,8,9	16.0	8.0	274.	548.
10,11,12	40	23.6	576.	1010.
13,14,15	45.7	32.	1740.	3230.

The *caisson* consists of 19 cylinders, each with a diameter of 20 m, see Fig. 5.1. This part of the structure is very stiff as compared to the stiffness of the other components of the structure. Thus,it is modelled by 6 beam elements, and the cross sectional properties are choosen equal to 50 times the value at the lowest shaft element. The masses are lumped to the nodal points, see Fig. 5.4.

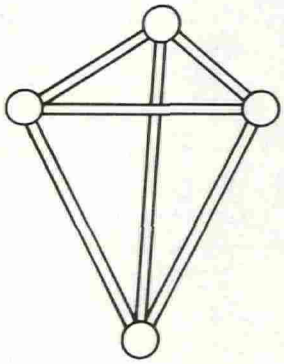

Fig. 5.4 Model of the caisson

Mass

The mass includes the mass of the structure itself, the mass of equipment on the deck, possible water in the columns and the caisson and the added mass of the environmental water.

The mass of *the deck* itself and maximum functional equipment on the deck is 25000 tons.

The dimensions of the *concrete columns* are shown in Fig. 5.3. The density of the concrete is put equal to 2.4 t/m^3. All three columns are assumed to be filled with water up to 20 m below still water level (Sloshing effects in the water are neglected).

The added (hydrodynamic mass) of the columns is put equal to the displaced water.

The *caisson* consists of 19 equal cylinders. The dimension of one of them is shown in Fig. 5.5. Each cylinder is assumed to contain sand up to a level 4.2 m over the bottom. In addition, it is conservatively assumed that all cells are filled with water.

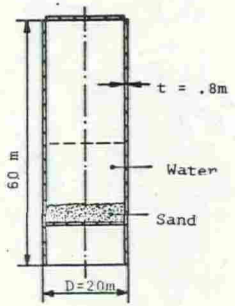

Fig. 5.5 A typical cylinder in the caisson

The hydrodynamical mass of the caisson is calculated by applying diffraction theory, Refs.(45-46) and considering the caisson to be equivalent to a cylinder of height 60 m and diameter 90 m. The masses associated with the lower node (no. 17) of the model are given in Fig. 5.6b.

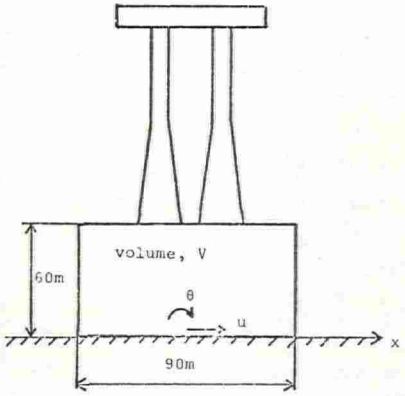

a)

Mass matrix:

$$\underline{\underline{M}}_{sub} = \rho_f V \begin{bmatrix} M_{xx} & M_{x\theta} \\ M_{\theta x} & M_{\theta\theta} \end{bmatrix} \cdot \begin{bmatrix} u \\ \theta \end{bmatrix}$$

$$= \rho_f V \begin{bmatrix} 2.5 & -1.5 \\ -1.5 & 1.5 \end{bmatrix} \begin{bmatrix} u \\ \theta \end{bmatrix}$$

b) Hydrodynamical masses associated with the caisson

Fig. 5.6 Hydrodynamical mass for coupled horizontal and rotational motion

The added mass for vertical translation is put equal to the volume of a hemisphere with diameter 90 m minus the displaced volume of the three columns within this hemisphere.

For rotation about the vertical axis, the added mass is obtained by assuming that it is equivalent to a water layer with a thickness of 4 m surrounding the caisson. The corresponding inertia moment is then computed.

The resulting lumped masses are (index refers to nodal point number, see Fig. 5.8):

$$
\begin{aligned}
m_1 &= 10.3 \cdot 10^6 \text{ kg} \\
m_2 &= 6.5 \cdot 10^6 \text{ kg} \quad \text{all directions} \\
m_3 = m_4 &= 5.5 \cdot 10^6 \text{ kg} \\
m_5 = m_6 = m_7 &= 3.2 \cdot 10^6 \text{ kg} \quad \text{x\&y dir.} \\
&= 2.0 \cdot 10^6 \text{ kg} \quad \text{z dir.} \\
m_8 = m_9 = m_{10} &= 7.2 \cdot 10^6 \text{ kg} \quad \text{x\&y dir.} \\
&= 3.4 \cdot 10^6 \text{ kg} \quad \text{z dir.} \\
m_{11} = m_{12} = m_{13} &= 13.3 \cdot 10^6 \text{ kg} \quad \text{x\&y dir.} \\
&= 6.1 \cdot 10^6 \text{ kg} \quad \text{z dir.} \\
m_{14} = m_{15} = m_{16} &= 122.5 \cdot 10^6 \text{ kg} \quad \text{x\&y dir.} \\
&= 135.3 \cdot 10^6 \text{ kg} \quad \text{z dir.} \\
m_{17} &= 393. \cdot 10^6 \text{ kg} \quad \text{x\&y dir.} \\
&= 268. \cdot 10^6 \text{ kg} \quad \text{z dir.}
\end{aligned}
$$

Rotational mass inertia moment in node 17

$$
\begin{aligned}
I_x = I_y &= 27.5 \cdot 10^{10} \text{ kgm}^2 \\
I_z &= 53.4 \cdot 10^{10} \text{ kgm}^2
\end{aligned}
$$

Damping

The structural damping and hydrodynamical damping are combined, and assumed to be of 1.5 percent of the critical.

5.1.3 Representation of Boundary Conditions of Surrounding Media

The platform structure is bordered by 3 media. The appropriate boundary conditions for the platform may be obtained by considering these media .

- The air
  The wind effect is neglected in the present case
- The water
  For the dynamic behaviour of the structure, the effect of the environmental water is included in the lumped masses represented by the added mass components as outlined in Chapter 2, and 5.1.2. Excitation forces are considered in Chapters 2.5 and 5.3.

- The soil
  The interaction between the platform and the soil is of great importance for the dynamic behaviour, see Chapter 2.

It is assumed that the effect of the soil on the interaction system may be described by equivalent soil stiffness and damping coefficients, see Fig. 5.7. The selection of coefficients are made according to Section 2.4.

Soil Stiffness

The soil stiffness is a function of the shear modulus, G_s, and the circular frequency, ω. In Table 5.3 the equivalent stiffness coefficients of the soil are given for various shear moduli and one frequency (eigenfrequency of lower order modes of the interaction system). In the actual case the soil stiffness is practically independent of the frequency.

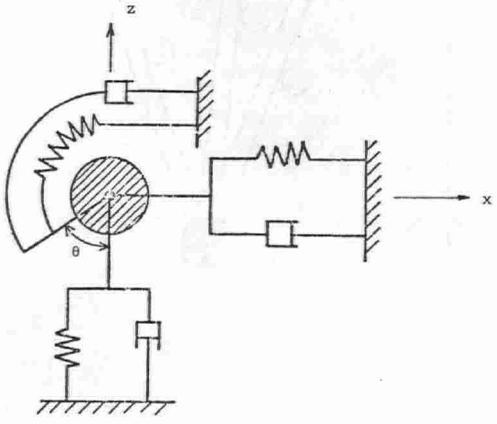

Fig.5.7 Soil stiffness and damping (in x-z plane)

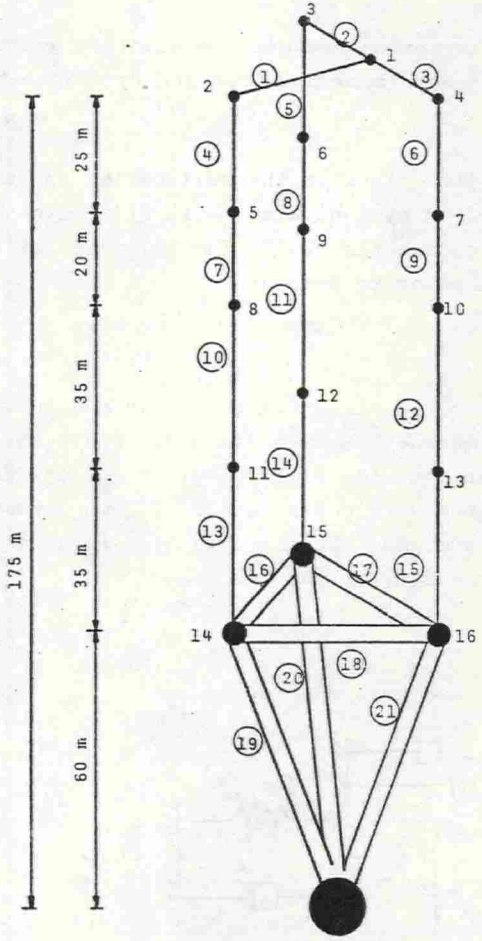

Fig. 5.8 Model of the entire platform structure

Density for soil - ρ_s = 2000 kg/m^3
Poisson's ratio - μ_s = 0.5

Table 5.3 Equivalent stiffness of the soil for various shear moduli. Unit k_x -[N/m] , k_θ-[Nm]

G_s[N/m^2]	ω	k_x, k_y	k_θ, k_ψ	k_z	k_ϕ
$1.65 \cdot 10^7$	1.12	$4.00 \cdot 10^9$	$8.1 \cdot 10^{12}$	$6.14 \cdot 10^9$	$8.85 \cdot 10^{12}$
$3.00 \cdot 10^7$	1.43	$7.20 \cdot 10^9$	$15.2 \cdot 10^{12}$	$11.20 \cdot 10^9$	$15.40 \cdot 10^{12}$
$6.00 \cdot 10^7$	1.76	$14.65 \cdot 10^9$	$30.4 \cdot 10^{12}$	$22.3 \cdot 10^9$	$32.17 \cdot 10^{12}$
10^9	2.04	$2.47 \cdot 10^{11}$	$5.3 \cdot 10^{14}$	$3.72 \cdot 10^{11}$	$5.36 \cdot 10^{14}$

Soil Damping

The damping in the soil is assumed to be viscous and represented by dashpots for each degree of freedom. For the actual frequency range only the rocking damping is really frequency dependent. In the actual frequency range the damping varies nearly proportionally with frequency and is zero at zero frequency.

Table 5.4 displays the values of equivalent damping coefficients for various shear moduli and the frequency corresponding to the lowest eigenfrequency of the interaction system.

Table 5.4 Equivalent damping in the soil at resonance frequency for various shear moduli. Unit c_x -[Ns/m], c_θ -[Nms]

G_s [N/m]	$\omega[\frac{rad}{s}]$	c_x, c_y	c_θ, c_ψ	c_z	c_ϕ
$1.65 \cdot 10^7$	1.12	$1.18 \cdot 10^9$	$29.5 \cdot 10^{10}$	$2.87 \cdot 10^9$	$8.51 \cdot 10^{10}$
$3.0 \cdot 10^7$	1.43	$1.50 \cdot 10^9$	$28.3 \cdot 10^{10}$	$3.37 \cdot 10^9$	$11.23 \cdot 10^{10}$
$6.0 \cdot 10^7$	1.76	$2.24 \cdot 10^9$	$40.0 \cdot 10^{10}$	$5.09 \cdot 10^9$	$16.24 \cdot 10^{10}$
10^9	2.04	$9.01 \cdot 10^9$	$10.4 \cdot 10^{10}$	$20.79 \cdot 10^9$	$66.3 \cdot 10^{10}$

5.2 Determination of Eigenfrequencies and Eigenmodes

The resulting dynamical model was a system governed by 102 equations with a half bandwidth of the stiffness matrix of 24. The eigenvalue problem

$$K\phi = M\phi\omega^2 \qquad (5.1)$$

is solved by the use of a subspace iteration algorithm. 10 eigenvalues and eigenmodes were determined. With a convergence tolerance of 10^{-5} 27 secs. CPU time was required for the solution of Eq.(5.1).

The eigenvalues were determined for 5 different shear moduli of the soil, see Table 5.5 The lowest eigenfrequencies were remarkably sensitive to the magnitude of the shear modulus. Higher eigenfrequencies were rather independent of the shear modulus. Fig. 5.9 displays the variation of the lowest eigenfrequency with shear modulus. The highest shear modulus, $G_s = 10^9 [N/m^2]$ simulates a fixed platform structure. The value 10^9 is chosen to avoid numerical ill-conditioning of the eigenvalue problem. In Figs. 5.10a - d the four lowest eigenmodes are shown for a shear modulus of $6 \cdot 10^7 [N/m^2]$.

Table 5.5 The 10 lowest eigenfrequencies for various shear moduli

Eigen freq. no. i	$G_s=1.0\cdot10^7$		$G_s=1.65\cdot10^7$		$G_s=3.0\cdot10^7$		$G_s=6.0\cdot10^7$		$G_s=1.0\cdot10^9$	
	ω_i	T_i	ω_i	T_i	ω_i	T_i	ω_i	T_i	ω	T_i
1	0.758	8.294	1.104	5.690	1.392	4.515	1.761	3.568	2.041	3.079
2	0.762	8.247	1.121	5.606	1.436	4.376	1.906	3.296	2.357	2.665
3	1.902	3.303	2.426	2.590	2.670	2.335	3.242	1.938	4.289	1.446
4	1.920	3.273	2.589	2.427	3.003	2.093	3.487	1.802	6.491	0.968
5	2.243	2.801	2.878	2.183	3.869	1.624	4.253	1.477	8.422	0.746
6	2.612	2.405	3.001	2.093	3.931	1.598	5.438	1.156	8.772	0.716
7	2.707	2.321	3.234	1.943	3.931	1.598	5.556	1.131	9.056	0.694
8	3.025	2.077	3.424	1.835	4.110	1.529	5.584	1.125	9.160	0.686
9	4.408	1.425	4.479	1.403	5.018	1.252	6.470	0.971	9.903	0.634
10	6.509	0.965	6.510	0.965	6.514	0.965	6.863	0.916	10.650	0.590

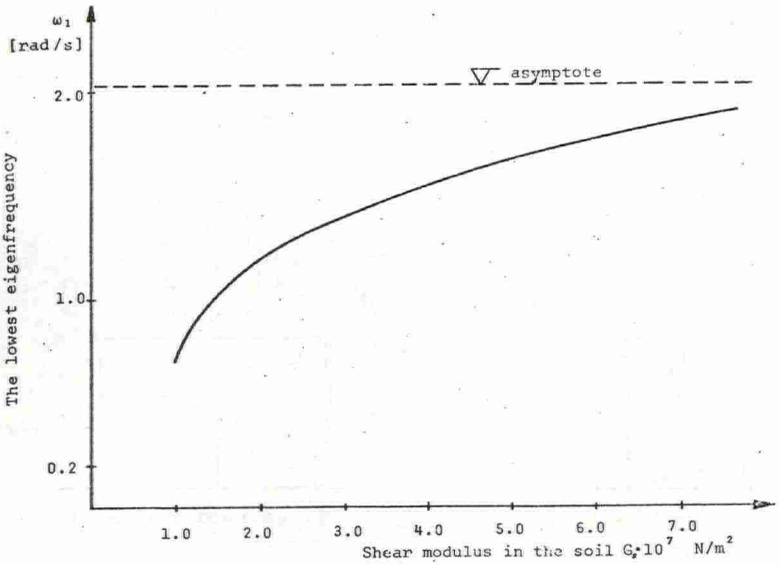

Fig. 5.9 The variation of the lowest eigenfrequency with the shear modulus in the soil.

5.3 Response to Harmonic Wave Excitation

5.3.1 Hydrodynamical Excitation Forces

General Remarks

When the eigenvalues and eigenmodes are determined, the next step is to determine the response of the structure in the form of transfer-functions due to wave forces. Wave forces are calculated on the basis of Airy's first order wave theory, see Chapter 2. Equivalent nodal forces are determined for a harmonic wave with a height of 1 m. One load vector is calculated for each wave frequency. Waves having circular frequencies in the range 0.314 to 3.14 are considered, and calculation is performed for 20 intermediate frequencies. In particular, three excitation frequencies

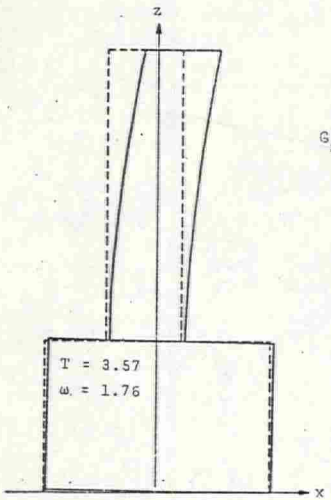

1. vibration mode

$G_s = 6{,}0 \cdot 10^7 [N/m^2]$

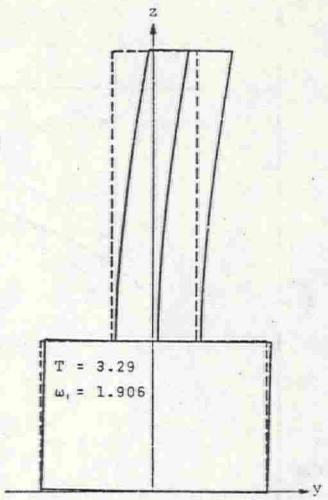

2. vibration mode

a) First and second eigenmode

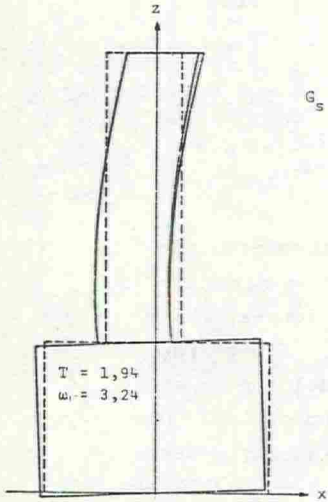

3. vibration mode

$G_s = 6{,}0 \cdot 10^7 [N/m^2]$

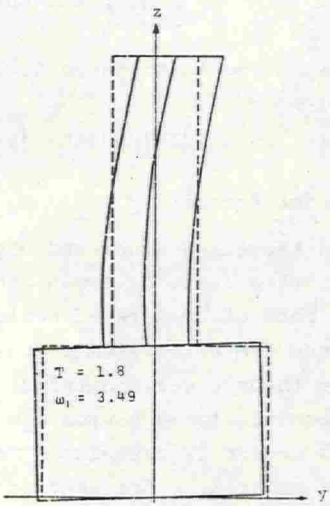

4. vibration mode

b) Third and fourth eigenmode

Fig. 5.10 Eigenmodes for a shear modulus of $G_s = 6.0 \cdot 10^7$ N/m²

corresponding to the eigenfrequencies of the three lower order modes are included. The forces are calculated separately for the caisson and the shafts. For wave periods less than 9 secs, the loading on the caisson is negligible, see Fig.(5.11a). The difference in phase angle between the nodal forces on the caisson and the different shafts is duely accounted for. The center of the caisson is chosen as the reference position for the wave loading, see Fig. 5.11a.

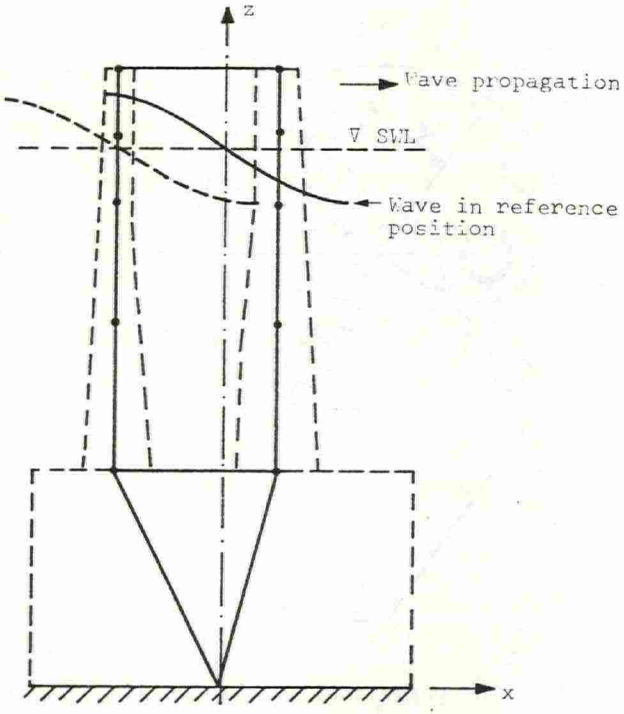

Fig. 5.11a Maximum wave load for wave in reference position. Dotted line corresponds to maximum loading on Shaft 1.

Assuming a long-crested wave with a wave length equal to λ and a direction of propagation with an inclination α with the x-axis, the phase angle between load on the caisson and the shafts will be:

$$\delta_1 = 2\pi\, \ell_1/\lambda \quad \text{for Shaft 1}$$
$$\delta_2 = 2\pi\, \ell_2/\lambda \quad \text{for Shaft 2}$$
$$\delta_3 = 2\pi\, \ell_3/\lambda \quad \text{for Shaft 3}$$

where ℓ_1 and ℓ_3 are negative and ℓ_2 is positive, see Fig. 5.11b.

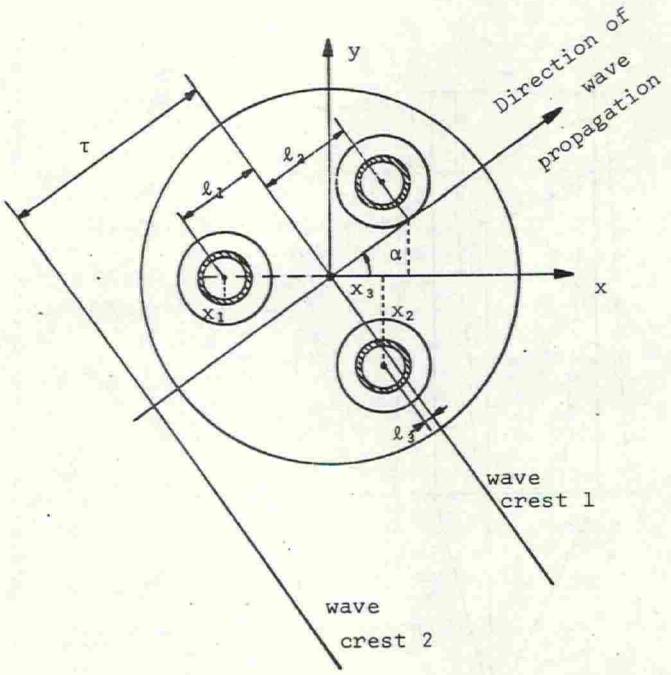

Fig. 5.11b The phase angle between maximum loads on the shafts. Wave propagating at an angle in a direction forming an angle α with the x-axis.

Forces on the Shafts

The distributed inertial wave loading on a typical shaft is shown in Fig. 5.13 for four wave periods. The distributed loading is transformed into equivalent nodal forces and moments by application of the virtual work concept. The variable stiffness along the beam elements is accounted for. The calculation of nodal forces is done automatically in the computer program for a shaft with specified orientation in a wave and with given nodal points. The corresponding nodal forces for four wave periods are listed in Table 5.6.

Table 5.6 Nodal point forces. Wave height 1 m. Units are [ton] for force and [ton·m] for moment.

Node	T=17 sec		T=11 sec		T= 7 sec		T = 4 sec	
Number	Force	Moment	Force	Moment	Force	Moment	Force	Moment
5	8.4	-42.1	23.6	-96.8	47.3	-177.6	38.7	-113.4
8	37.4	-52.5	56.0	-17.9	64.0	117.5	20.4	105.1
11	50.9	89.1	46.7	182.0	14.5	126.2	0.16	2.4
14	26.4	196.3	15.2	117.0	1.0	10.1	0	0

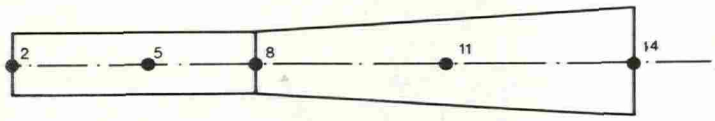

Fig. 5.12 Nodal points along a shaft

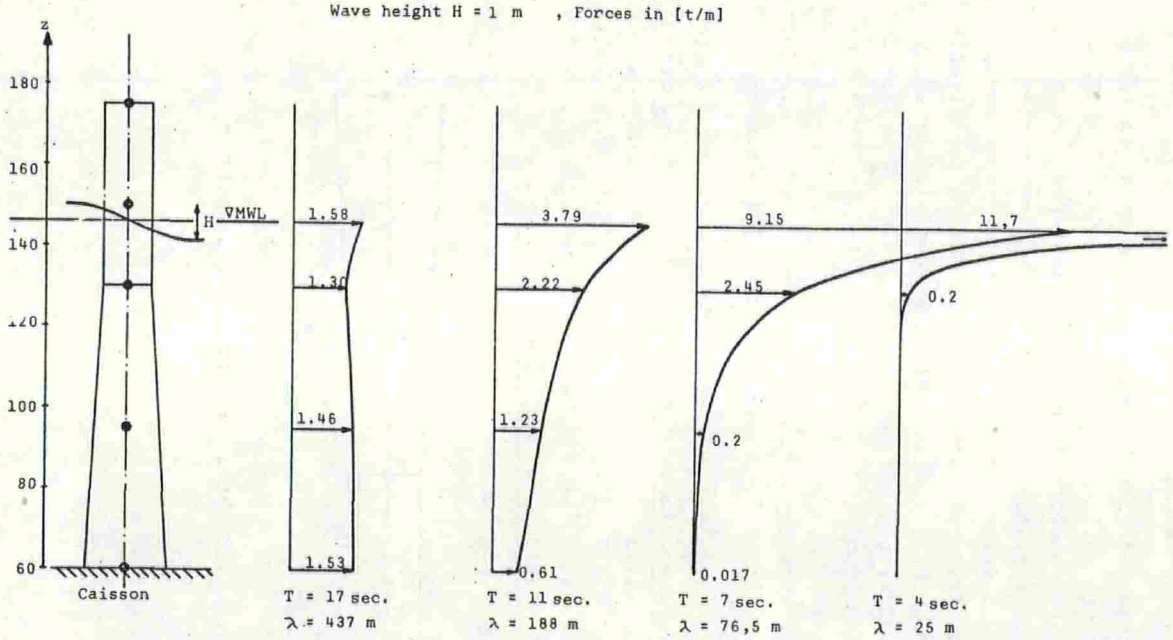

Fig. 5.13 Distributed inertial wave forces on a single shaft for various wave periods.

Forces on the Caisson

The inertial wave loading on the caisson is evaluated by assuming the caisson to be equivalent to a cylinder with the following dimensions:

Height	s_1	= 60 m
Radius	r_0	= 90 m
Cross-sectional area	A	= 6360 m^2
Volume	V	= $3.815 \cdot 10^5$ m^3

Fig. 2.17 and Fig. 2.18 show the idealized structure.

The forces on the caisson are calculated according to Eqs. 2.31 and 2.32. Maximum load on the caisson appears when the wave is in reference posistion, see Fig. 5.11a. Interaction effects between the slender shafts and the caisson are neglected. In the present case pressure under the bottom of the structure is assumed to be equivalent to the pressure corresponding to free water in the soil.

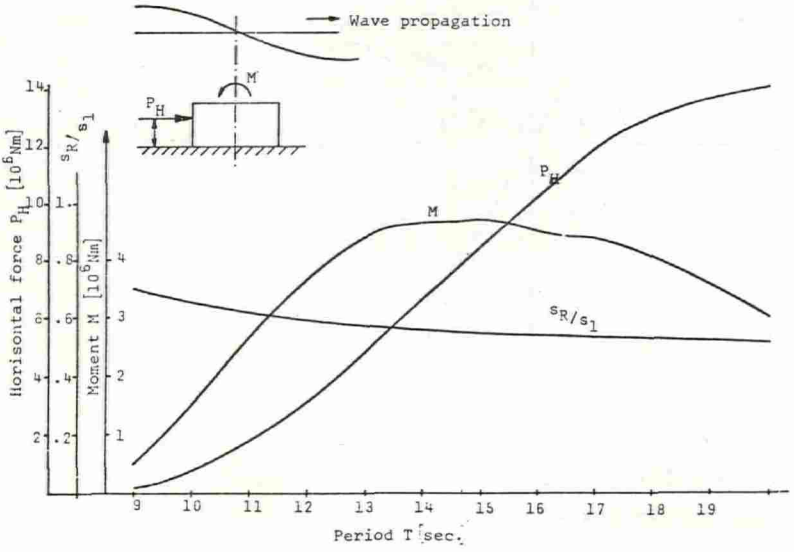

Fig. 5.14 Variation of horizontal force, overturning moment and eccentricity of the horizontal force resultant with wave period T.

The resultant horizontal force and moment computed for the caisson are shown in Fig. 5.14.

The vertical force resultant is neglected, as it is assumed to have insignificant influence on the behaviour of the structure.

The horizontal force resultant is applied as nodal forces. These forces act in the three nodal points on the top of the caisson and the node at the soil - caisson interface. The moment from the pressure distribution on top and bottom of the caisson is applied in the node at the soil-caisson interface.

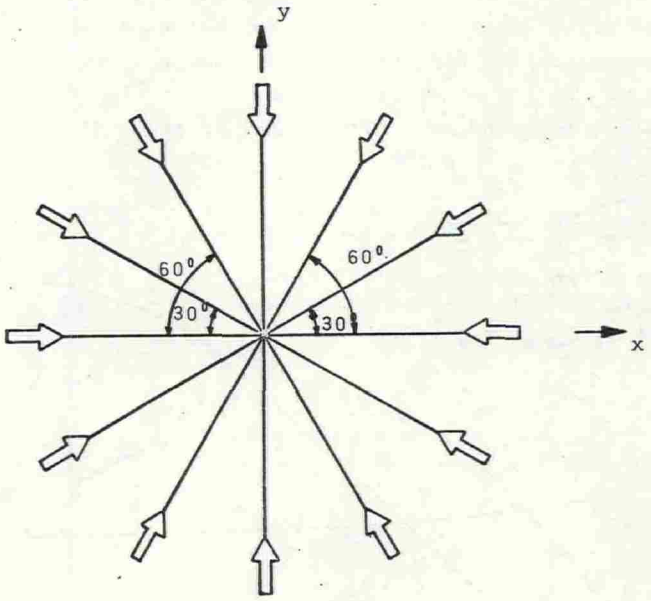

Fig. 5.15 Directions for which the hydrodynamical loading are calculated

Table 5.7 Typical load vectors for wave frequency 0.48 [rad/sec]. Wave propagation in x and y direction, respectively. Wave height H = 1 m.

Direction of load	Node no	Local degree of freedom	Force [N] Moment [Nm]	Phase angle [°]
	5	2	132847.	
	6	2	132847.	26.6
	7	2	132847.	-26.6
	5	4	651200.	
	6	4	651200.	26.6
	7	4	651200.	-26.6
	8	2	466587.	
	9	2	466587.	26.6
	10	2	466587.	-26.6
	8	4	467400.	
	9	4	467400.	26.6
	10	4	467400.	-26.6
y	11	2	522455.	
	12	2	522455.	26.6
	13	2	522455.	-26.6
	11	4	-1497200.	
	12	4	-1497200.	26.6
	13	4	-1497200.	-26.6
	14	2	1137162.	
	15	2	1113162.	5.1
	16	2	1113162.	-5.1
	14	4	-1607800.	
	15	4	-1607800.	26.6
	16	4	-1607800.	-26.6
	17	2	2031160.	
	17	4	4389000.	
	5	1	132847.	-27.
	6	1	132847.	13.
	7	1	132847.	13.
	5	5	-651200.	-27.
	6	5	-651200.	13.
	7	5	-651200.	13.
	8	1	466587.	-27.
	9	1	466587.	13.
	10	1	466587.	13.
	8	5	-467400.	-27.
	9	5	-467400.	13.
	10	5	-467400.	13.
x	11	1	522455.	-27.
	12	1	522455.	13.
	13	1	522455.	13.
	11	5	1497200.	-27.
	12	5	1497200.	13.
	13	5	1497200.	13.
	14	1	1112592.	- 5.2
	15	1	1127590.	2.5
	16	1	1127590.	2.5
	14	5	1607800.	-27.
	15	5	1607800.	13.
	16	5	1607800.	13.
	17	1	2031160.	
	17	5	4389000.	180.

Resulting Hydrodynamical Loading on the Platform

The resulting environmental hydrodynamic loading consists of the load on the shafts and the caisson. A load vector is established for 20 separate wave frequencies in the range 0.314 to 3.14 [rad/sec] and 12 directions of wave propagation. However, due to symmetry about a plane only 6 directions were actually calculated. The 12 directions for wave propagation is shown in Fig. 5.15.

When the load, applied as nodal forces, is combined, the difference in phase between the load components is accounted for. The loadvectors for waves progressing in the x and y direction are listed in Table 5.7 for a typical frequency. The reference point for zero phase angle is the center of the caisson. The local degrees of freedom are defined in Fig. 5.16.

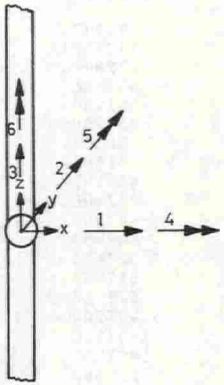

Fig. 5.16 Definition of local degrees of freedom in a nodal point.

5.3.2 Transfer-functions

General Remarks

The transfer-functions are determined both with a dynamic and static model. The harmonic response of the structure is calculated according to the procedure outlined in Chapter 3. The harmonic response for nodal displacements is found by modal superposition. Input to the analysis are eigenvectors, eigenfrequeicies, the mass-matrix and the load vector amplitude and corresponding phase angles. 8 eigenvectors were used in the computations.
As previously mentioned the computation was accomplished for 20 wave frequencies and 6 directions of wave propagation.

In the subsequent part of this section, calculated transfer-functions for displacement and internal forces in the structure will be reported and discussed. The results are presented in the following sequence:

- transfer-functions for displacement of the deck. Various shear moduli of the soil. Wave propagating in x- and y-direction.
- transfer-functions for moments in top and bottom of the shafts. Various shear moduli in the soil. Wave propagating in x- and y-direction.
- transfer-functions for moments in top and bottom of shaft no. 2. Shear modulus of the soil equals $3.0 \cdot 10^7$ [N/m^2]. 12 directions of wave propagation.

Transfer-functions for Displacement of the Deck.

The transfer-functions for the deck displacement are shown in Fig. 5.17-18. Dynamic and static transfer-functions are displayed for waves propagating in x- and y-directions.

The curves in Fig. 5.17 display the effect of the shear modulus of the soil on the dynamic response.

The soil-structure interaction has two principal effects:

- the resonant frequency of the system decreases to a value below that applicable to the fixed-base structure
- it modifies the magnitude of the peak response, decreasing the value for short, quatty structures and increasing the value for tall slender structures.

The first effect is easy to understand. The second effect, which appears to be contradictory at first glance requires some explanation. The change in magnitude of the peak response is the result of two opposing mechanisms. Because of the energy which is dissipated by radiation into the supporting medium, the effective damping of the flexibly mounted structure is greater than that of the fixed-base structure, and this tends to *decrease* the response of the interacting system. However, the rocking of the foundation increases the acceleration inertia force, and the corresponding whipping effect leads to a corresponding *increase* in response. The first factor is predominate for short structures, whereas the second factor is predominate for tall structures.

The peaks and throughs in the transfer-functions are associated with "resonances" and phase differences in the loading on different shafts.

A remarkable difference in both the shape and the magnitude of the transfer-functions are observed for circular frequencies of the waves higher than 1.0. This is a result of the difference in phase angle between maximum load on the shafts as illustrated in Fig. 5.19. For small frequencies this difference in phase angle is insignificant. Thus, the transfer-functions show only a small difference at low frequencies.

It is observed from Fig. 5.18 that the transfer-functions for waves propagating in the x- and y-direction are quite different. This is principally due to the difference in phase angles.

By comparing the response for dynamic and quasistatic analysis it is observed that the dynamic amplification is of great importance for the frequency range $\omega = 0.7 - 1.7$. The amplification decreases with decreasing frequency when the frequency is below the lowest eigenfrequency of the structure.

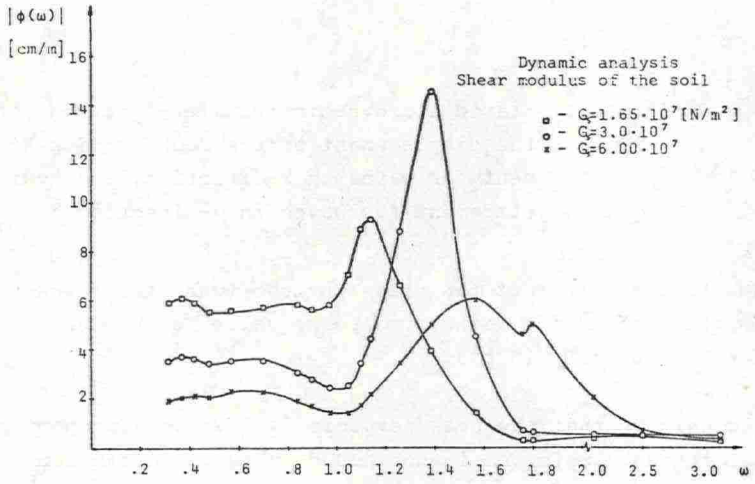

Fig. 5.17 Dynamic transfer-function for the displacement of the deck in x-direction for waves in x-direction. Three values of the shear modulus in the soil were used

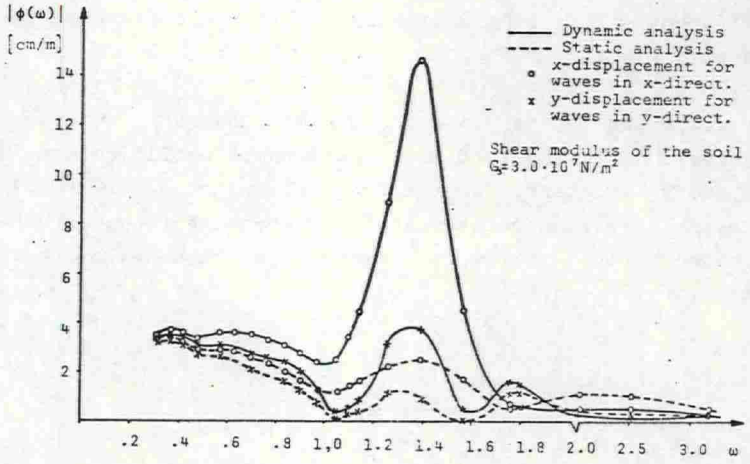

Fig. 5.18 Static and dynamic transfer-function for the displacement of the deck. x-displacement for waves in x-direction, and y-displacement for waves in y-direction

Due to the effect of the phase angle between the forces on the shafts, the highest response value is obtained for $G_s = 3.0 \cdot 10^7$ [N/m^2].

Recognizing that the peak response is inversely proportional to the damping ratio in a 1DOF-system, the maximum dynamic amplification obviously must be sensitive to the choice of damping in the system.

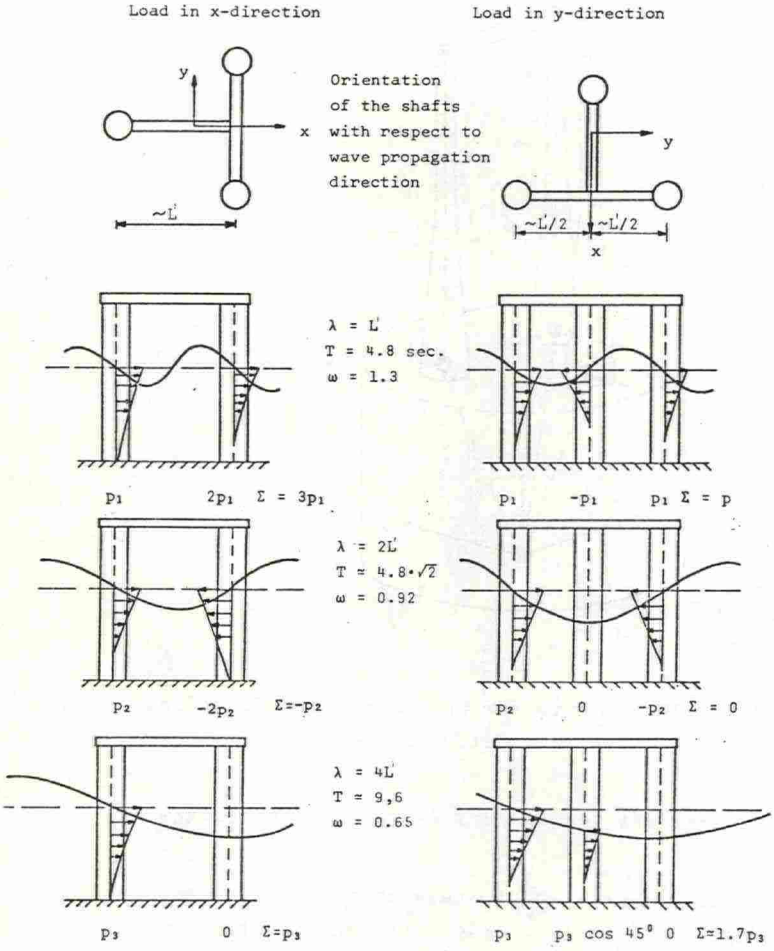

a) Wave propagating in x direction.

b) Wave propagating in y direction.

Fig. 5.19 Effect of phase differences of the loading on various shafts on the total loading for various wave lengths (-periods). Only inertial forces on shafts are considered. (Σ denotes the resulting wave force on the shafts).

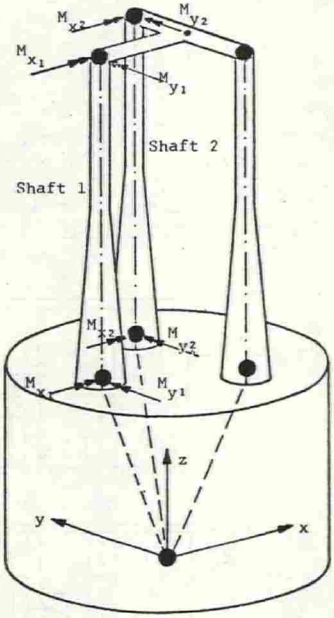

Fig. 5.20 Moments for which transfer-functions are calculated.

Transfer-functions for Moments in the Top and Bottom of the Shafts

The internal moments (and forces) at the top and the bottom of the shafts are particularly important in the structural design.

Transfer-functions for moments in Shaft no. 1 and 2 were determined for waves propagating in the x- and y-direction, respectively. In addition, the transfer-functions for the moments, M_x and M_y at the bottom of Shaft no. 2 and moment M_x

at the top of Shaft no. 2 were computed for waves propagating in a series of directions in steps of 30°.

Static and dynamic analyses were accomplished. Various shear moduli of the soil were utilized.

Comparison between the transfer-functions for the moment in the top of the shafts is made in Figs. 5.21-22. The principal characteristics of the moment transfer-functions are quite similar to the displacement transfer-functions.

While the displacement transfer-functions tend to increase by decreasing frequency, the moments transfer-functions do not. The increase in the displacement transfer-functions is primarily due to the fact that forces on the caisson are activated by lower frequencies (large wave lengths); thereby introducing significant rigid body motions. In Figs. 5.23-24 the transfer-function for the moment at the bottom of Shafts 1 and 2 are shown for waves propagating in the x- and y directions, respectively. The transfer-function for the bottom moment is quite similar to the moment at the top of the corresponding shaft.

To investigate into more detail the effect of the directionality of the wave progress on the response, the moments about x- and y-axis in top and bottom of Shaft 2 were considered. The shear modulus of the soil was choosen to be $G_s = 3.0 \cdot 10^7$ [N/m^2] for all cases. Fig. 5.27 displays the transfer-functions for the moment at the top of Shaft 2 for the 12 wave directions. The response is very sensitive to wave direction. This observation may be explained by the fact that the phase angle between maximum load on each shaft is highly influenced by the direction of incoming waves. Furthermore, the unsymmetric deck-structure indicates directional dependency of the moments in the top of the shaft. This effect is not that much pronounced in the moment at the bottom of the shaft, see Figs. 5.25-26.

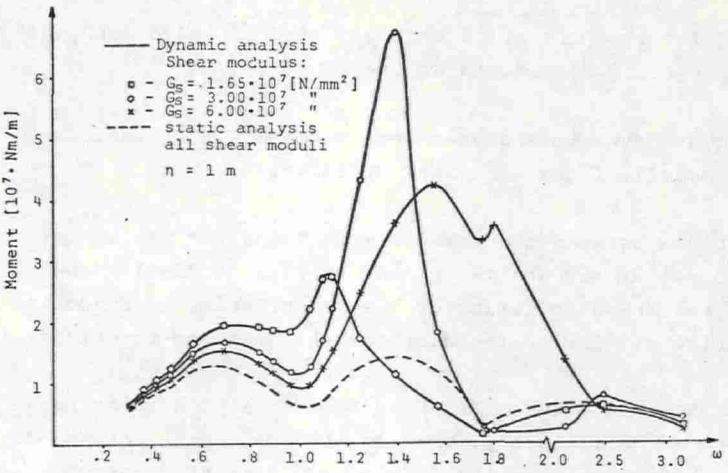

Fig. 5.21 Transfer-function for the moment M_y at the top of Shaft no. 1. Wave progressing in the x-direction.

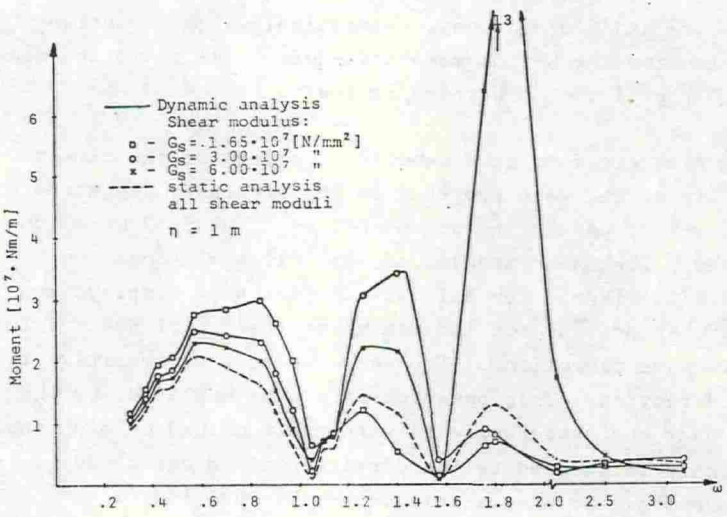

Fig. 5.22 Transfer-function for the moment M_x at the top of Shaft no. 2. Wave progressing in the y-direction.

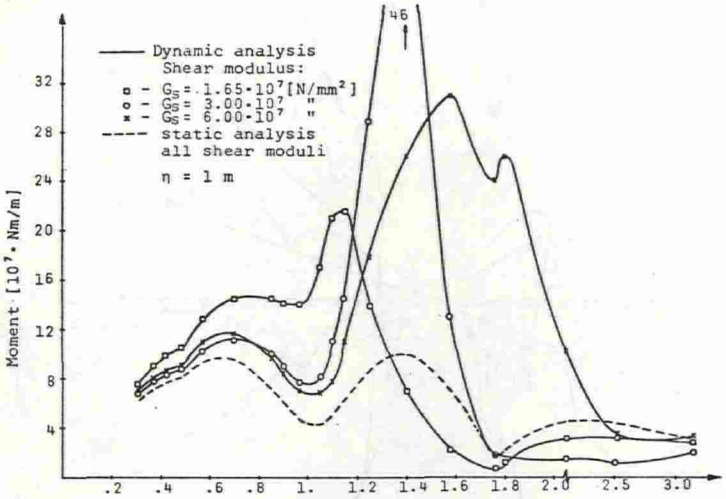

Fig. 5.23 Transfer-function for the moment M_y at the bottom of Shaft no. 1. Wave propagating in the x-direction.

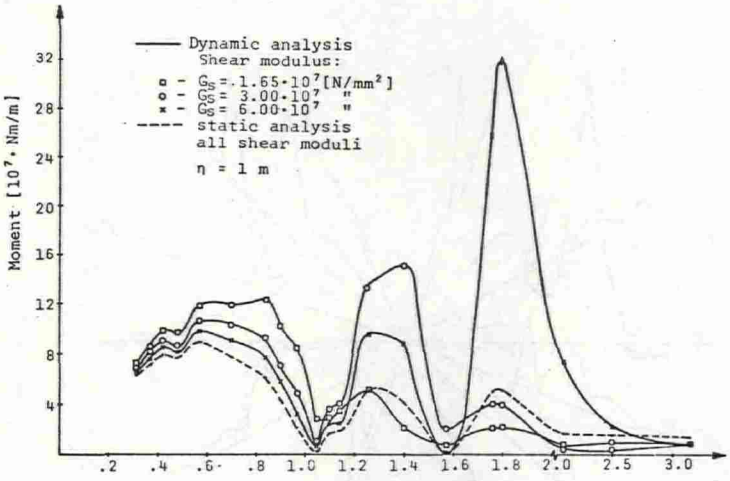

Fig. 5.24 Transfer-function for the moment M_x at the bottom of Shaft no. 2. Wave propagating in the y-direction.

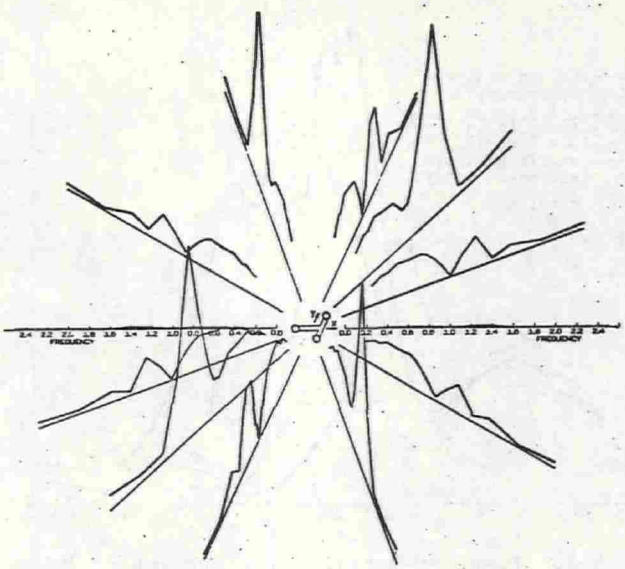

Fig. 5.25 Transfer-functions for moment about x-axis at the bottom of Shaft no. 2 for 12 directions of wave propagation. $G_s = 3.0 \cdot 10^7$ [N/m²]

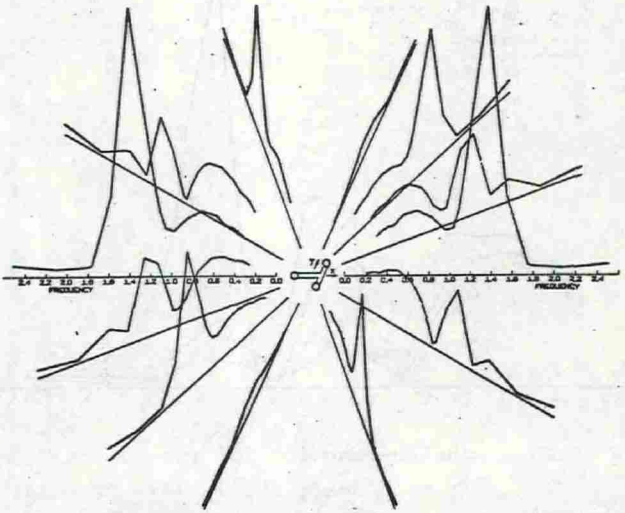

Fig. 5.26 Transfer-functions for moment about y-axis at bottom of Shaft no. 2 for 12 directions wave propagation. $G_s = 3.0 \cdot 10^7$ [N/m²]

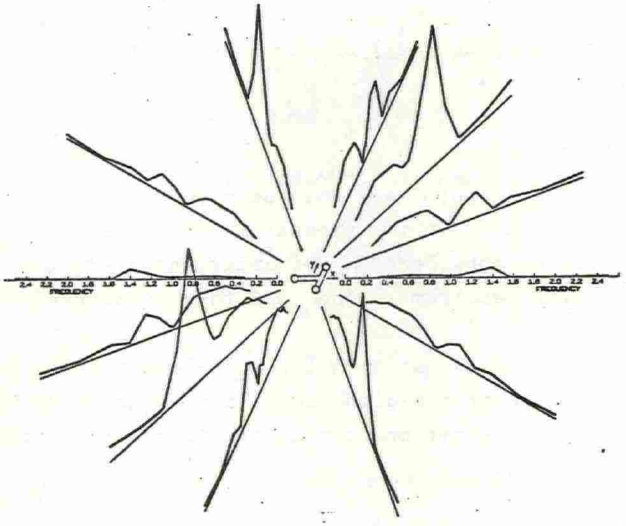

Fig. 5.27 Transfer-functions for moment about the x-axis at the top of Shaft no. 2 for 12 directions of wave propagation. The angle between each direction is 30^{o}

5.4 Statistical Analysis

5.4.1 Short- and Long-term Description of the Sea

The statistical response analysis is based on the methods outlined in Chapter 4.

Short-term Sea-state

In the short-term state, the sea is assumed to be described by the wave-spectrum. In the present analysis several types of spectra will be considered. Primarily, however, the Pierson-Moskowitz sepctrum on the ISSC form is adopted.

The analysis is carried out both for long- and short-crested waves. In the case of two-dimensional spectra both Mark's and Pierson's representation of the directionality function $f(\theta)$ are considered.

Long-term Sea-state

The long-term description of the sea is given through the long-term distribution of the parameter $H_{1/3}$, $\bar{T}$ and α describing the short-term states. Three alternative long-term models were discussed in Chapter 4.

Only the *conventional* model together with the *modification* incorporating correlation between $H_{1/3}$ and $\bar{T}$ will be pursued in the present context.

In the conventional model the two-dimensional probability function of $H_{1/3}$, $\bar{T}$ is determined from the distribution of the visual parameters H_v and T_v and no correlation between $H_{1/3}$ and $\bar{T}$ is assumed. The relationship between the visual and instrumental parameters used in the present analysis is given below.

$$H_v = 0.5.H_{1/3}^{1.33}$$

$$E(\bar{T}) = 1.086.AT.T_v^{BT} \qquad (5.2\,a\text{-}b)$$

Two different sets of values were used for AT and BT in the analysis. The values are given below.

AT	2.83	0.74	(5.3)
BT	0.44	1.00	

The two sets were proposed by Nordenstrøm, in Ref.(81).

The standard deviation is assumed to have a constant value, given as

$$S_C(\bar{T}) = 1.086 \text{ [seconds]} \qquad (5.4)$$

according to Ref.(81).

The long-term wave data used in this analysis are grouped in 6 intervals of visual period.

The midpoints of each interval of visual period are listed in Table 5.9. In addition, the expected value of the average mean period, $\bar{T}$, is given for the two sets of AT,BT. It is seen that there is a rather great discrepancy in the expected value for the two sets . Both the normal- and the log-normal-distribution are considered for the average mean period,$\bar{T}$. The distribution of $H_{1/3}$ was assumed to follow a Weibull-distribution.

Obviously, the sea-state is dependent upon the location. Even in the North Sea region the weather conditions vary.

The long-term weather data used in this analysis are given in Tables 5.9-10. The Table 5.9 is quoted from Ref.(97) and it is based on wave observations on the weather ship "Famita".

The observations have been accomplished over a period of 10 years from 1959 to 1969, and only in the period from october to march.

Table 5.9 Parameters of Weibull distribution of visual wave heights on the North Sea, data from "Famita" ($57^{o}30'N$, $3^{o}E$)

T_v	H_o	H_c	γ_o	$P(T_v)$
4.5	1.2	1.3	0.62	.3764
6.5	1.2	1.83	1.04	.3425
8.5	2.0	2.80	0.99	.1989
10.5	2.0	3.30	1.32	.0626
12.5	1.5	3.95	1.20	.0164
14.5	.0	4.50	3.15	.0032

Throughout the same 10-years period observations of visual wave parameters were recorded for 12 separate directions, Ref.(90). In spite of a rather long observation period the data are rather insufficient to establish a long-term distribution of the visual wave heights for each direction. However, a separate Weibull distribution for each direction is estimated from the given data. Parameters obtained for these distributions are given in the Table 5.10. The distributions are normed so that the average distribution by integration over all directions gives the same long-term distribution of wave height as for the marginal distribution displayed in Table 5.9.

Unfortunately, these distributions are not very reliable, due to a limited amount of basic data and should be used with care. In the present report the directional distribution are applied to obtain some guidance regarding directionality effects.

Table 5.10 Parameters in the Weibull-distributions for 12 directional sectors

Direction no.	T_v	H_o	H_c	γ_o	$P(T_v)$
1	4.500	.900	1.250	.960	.33710
	6.500	1.450	2.150	1.020	.34600
	8.500	.000	2.800	2.300	.21340
	10.500	.000	3.800	2.500	.07450
	12.500	.000	2.800	2.100	.02780
	14.500	.000	3.600	2.600	.00130
2	4.500	.000	1.250	2.630	.55140
	6.500	.000	1.900	2.750	.26870
	8.500	.000	2.650	1.630	.12620
	10.500	.000	1.950	2.100	.04210
	12.500	.000	4.100	3.430	.00930
	14.500	.000	3.000	1.750	.00230
3	4.500	.800	1.200	1.040	.44750
	6.500	.000	2.000	2.500	.35930
	8.500	.000	2.600	2.300	.16100
	10.500	.000	3.250	1.340	.01190
	12.500	.000	3.100	2.000	.01690
	14.500	.000	4.600	3.100	.00340
4	4.500	.000	1.300	1.900	.28090
	6.500	.000	1.300	1.280	.33520
	8.500	1.450	2.450	.930	.27770
	10.500	1.250	2.950	1.080	.08500
	12.500	.000	3.400	1.360	.01890
	14.500	.000	9.500	10.100	.00240
5	4.500	.650	1.250	1.100	.26910
	6.500	.900	1.800	1.270	.35250
	8.500	1.400	2.770	1.470	.26370
	10.500	1.700	3.800	1.400	.09200
	12.500	.000	5.200	3.200	.02150
	14.500	.000	5.000	3.600	.00110
6	4.500	.650	1.220	1.200	.36670
	6.500	1.000	2.000	1.400	.33890
	8.500	.000	3.030	2.680	.20770
	10.500	2.000	4.300	1.500	.06140
	12.500	.000	5.000	3.880	.02190
	14.500	.000	5.700	3.800	.00340

Table 5.10 Parameters in the Weibull-distributions for 12 directional sectors (continued).

Direction no.	T_v	H_o	H_c	γ_o	$P(T_v)$
7	4.500	.450	1.290	1.660	.39630
	6.500	1.300	1.750	.840	.31780
	8.500	1.000	2.500	1.440	.22010
	10.500	.000	3.000	2.230	.05520
	12.500	1.000	4.000	1.200	.00990
	14.500	.000	3.000	1.750	.00070
8	4.500	.650	1.400	1.340	.41090
	6.500	.800	1.750	1.440	.34980
	8.500	.000	2.770	2.600	.18780
	10.500	.000	3.200	2.430	.04400
	12.500	.000	4.800	2.260	.00700
	14.500	.000	3.000	1.750	.00050
9	4.500	.550	1.350	1.600	.43140
	6.500	1.000	1.850	1.100	.34450
	8.500	1.000	2.600	1.400	.17300
	10.500	1.400	2.600	1.150	.04230
	12.500	.000	3.600	2.000	.00440
	14.500	.000	5.200	3.400	.00440
10	4.500	1.300	1.400	.550	.51790
	6.500	.000	1.700	1.750	.32910
	8.500	.750	2.800	1.940	.09860
	10.500	.000	2.700	3.170	.02980
	12.500	.000	4.300	1.600	.01620
	14.500	.000	4.200	8.200	.00850
11	4.500	1.400	1.530	.650	.39530
	6.500	.000	2.000	1.750	.33290
	8.500	.000	2.750	1.880	.15980
	10.500	.000	3.500	2.450	.08250
	12.500	.000	4.500	2.970	.02310
	14.500	.000	4.000	7.000	.00630
12	4.500	.000	1.300	1.700	.28190
	6.500	1.200	1.830	1.040	.37190
	8.500	.000	3.200	2.740	.22330
	10.500	.000	4.100	2.280	.09080
	12.500	.000	4.800	3.000	.02410
	14.500	.000	3.400	3.250	.00800

However, the return period for given extreme wave heights derived from the distributions for each direction compare fairly well with published data., in Ref.(89).

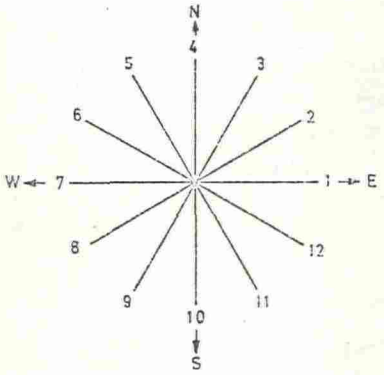

Fig. 5.29 Identification of directions in which the Weibull-distributions are determined.

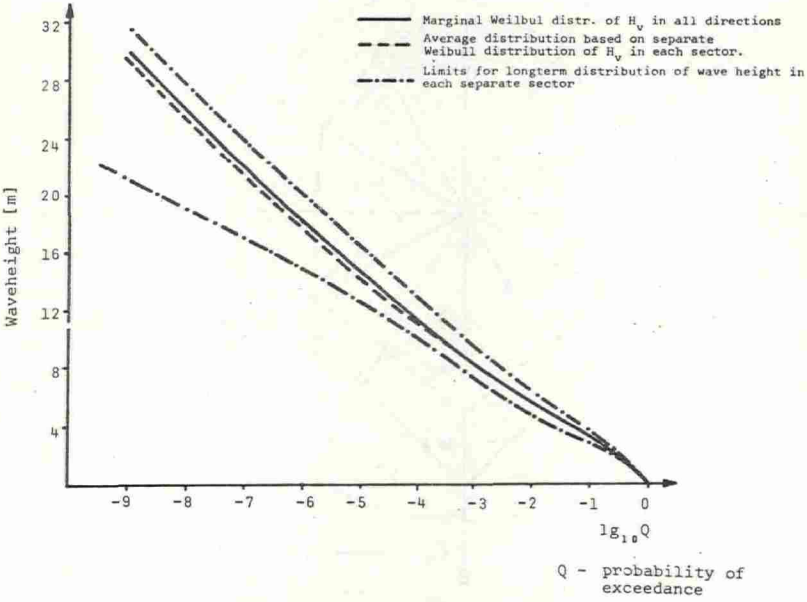

Fig. 5.30 Long-term distribution of wave height.

In Fig. 5.30 the long-term distribution of visual wave heights is displayed. It is seen that the discrepancy between the original marginal distribution, Table 5.9, and the marginal distribution calculated from the directional distributions in Table 5.10, is insignificant. The various distributions for the directional sectors deviate considerably from the marginal distribution. A more illustrative display of the directional distribution is presented in Fig. 5.31. From South East to North East rather small waves should be expected, whilst North, South and West give the largest waves at a given probability level.

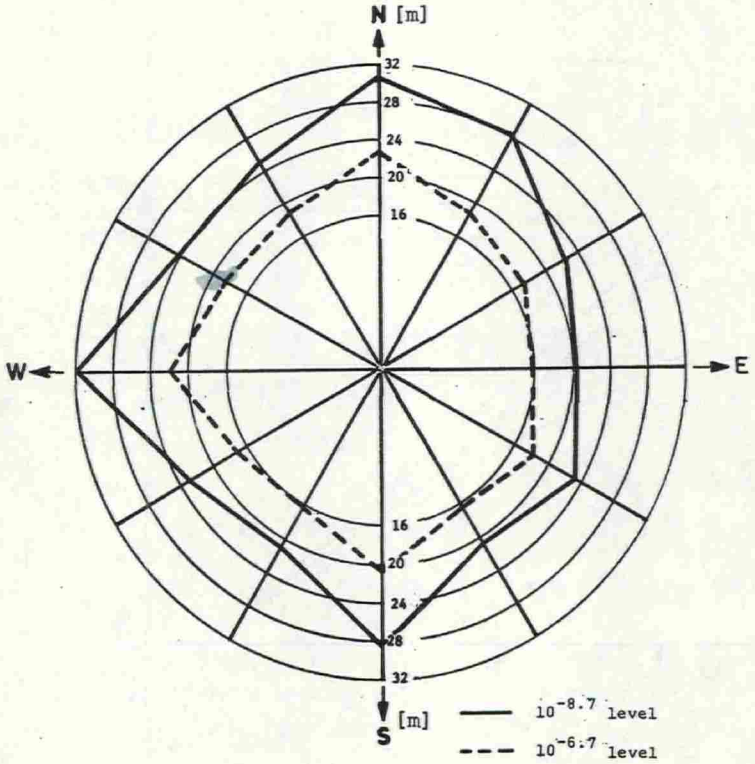

Fig. 5.31 Most probable largest wave height at probability level $10^{-8.7}$ and $10^{-6.7}$

At last the probability density function of the principal direction of incoming waves must be determined.

From the weather ship "Famita" information are given both for the wave- and wind-distribution.
According to Eq.(4.23) the point probability of each direction section of weather state is required in the long-term model. From the weather ship "Famita" information are given both for the wave- and wind-distribution. In Fig. 5.32 both wind and wave point probabilities are quoted. The analysis to follow is based on the wave data.

It is expected that using wind data will give nearly the same distributions.

Modified Long-term Model based on Correlation between $H_{1/3}$ *and* $\bar{T}$

The conventional long-term model is modified so as to avoid un-physical combinations of $H_{1/3}$ and $\bar{T}$, see Chapter 4.3.

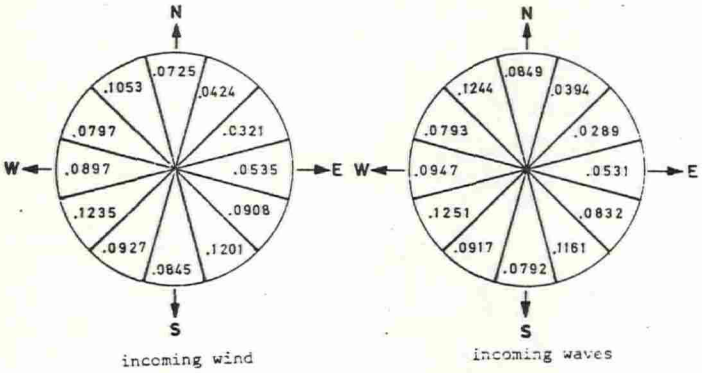

Fig. 5.32 Long-term probabilities of the principal direction of incoming wind and waves.

5.4.2 Long-term Distribution of the Response of the Platform

General Remarks

The long-term distribution of the response is calculated, using the program "LONTIM" (part II of Ref.(104)), with the following data as input:

- transfer-functions as calculated in Section 5.3.3
- weather distribution as given in Section 5.4.1

The following long-term distributions are given in terms of the *response-amplitude*:

Long-term Distribution of the Deck Displacement. Conventional Long-term Model with all Waves Propagating in one Direction.

The transfer-functions are given in Figs. 5.17-18. Static and dynamic responses were considered. Long-crested waves described by a Pierson-Moskowitz spectrum is assumed. Further, the conventional long-term model is assumed implying no correlations between $H_{1/3}$ and $\bar{T}$.

The parameters in the H_v-$H_{1/3}$ and T_v-$\bar{T}$ relationships are:

$$\begin{aligned} AH &= 0.5 \\ BH &= 1.33 \\ AT &= 2.83 \\ BT &= 0.44 \end{aligned} \qquad (5.5)$$

and the standard deviation of $\bar{T}$ is $S_c(\bar{T}) = 1.086$.
Normal distribution of $\bar{T}$ is assumed.

All incoming waves are assumed to come from the same direction. The weather data is therefore given by Table 5.9. In the first place the waves were assumed to propagate paralell with x-axis, and then they were assumed to propagate paralell with the y-axis.

The resulting long-term distributions of the displacement are given in Figs. 5.33-35.

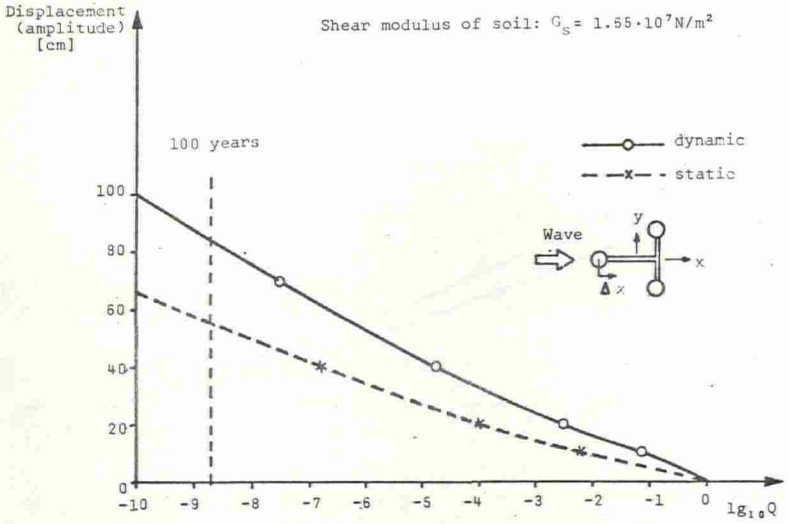

Fig. 5.33 Long-term distribution of the displacement of the deck in the x-direction. Transfer-function is given in Fig. 5.17. Pierson-Moskowitz spectrum and conventional long-term model. Weather date from Table 5.9.

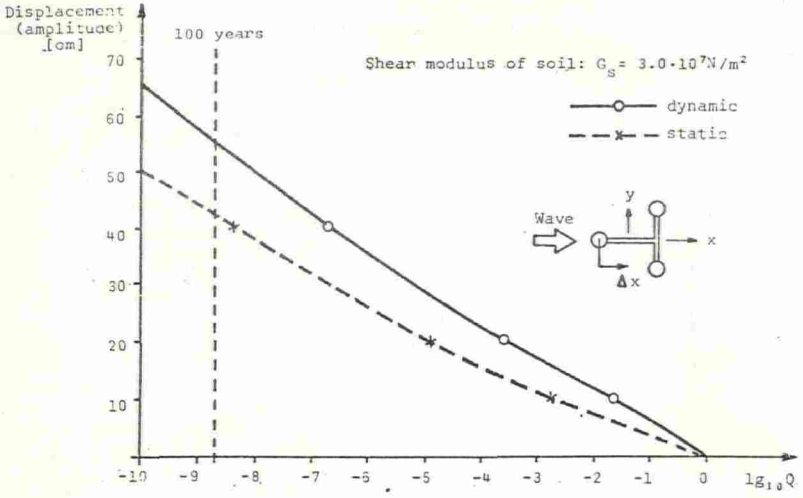

Fig. 5.34 Long-term distribution of the displacement in the x-direction. Transfer-function is given in Fig.5.17. Pierson-Moskowitz spectrum and conventional long-term model. Weather data from Table 5.9.

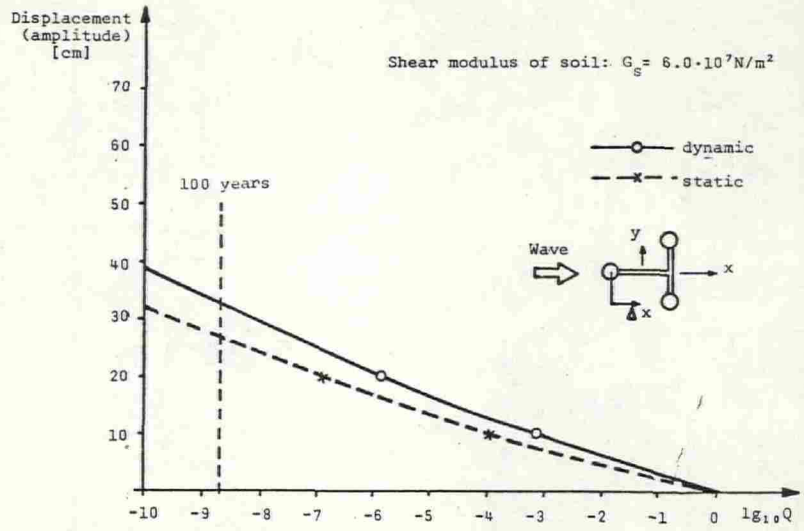

Fig. 5.35 Long-term distribution of the displacement of the deck in x-direction. Transfer-function is given in Fig. 5.17. Pierson-Moskowitz spectrum and conventional long-term model. Weather data from Table 5.9.

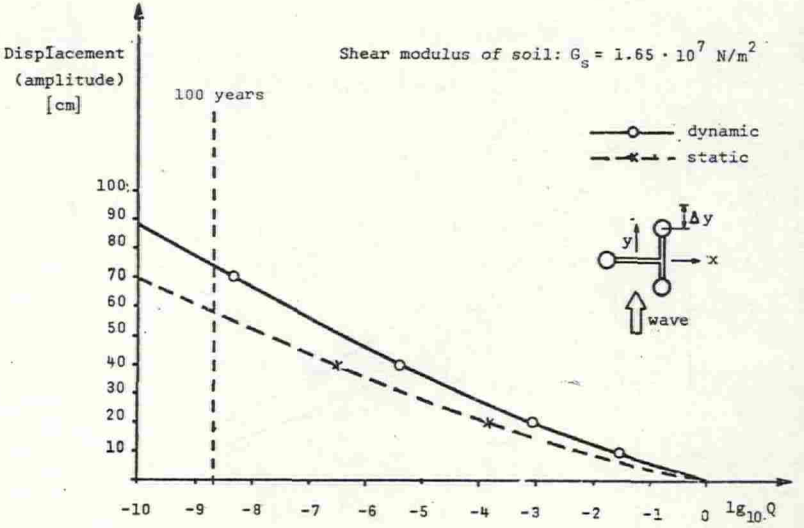

Fig. 5.36 Long-term distribution of the displacement of the deck in y-direction. Pierson-Moskowitz spectrum and conventional long-term model. Weather data from Table 5.9.

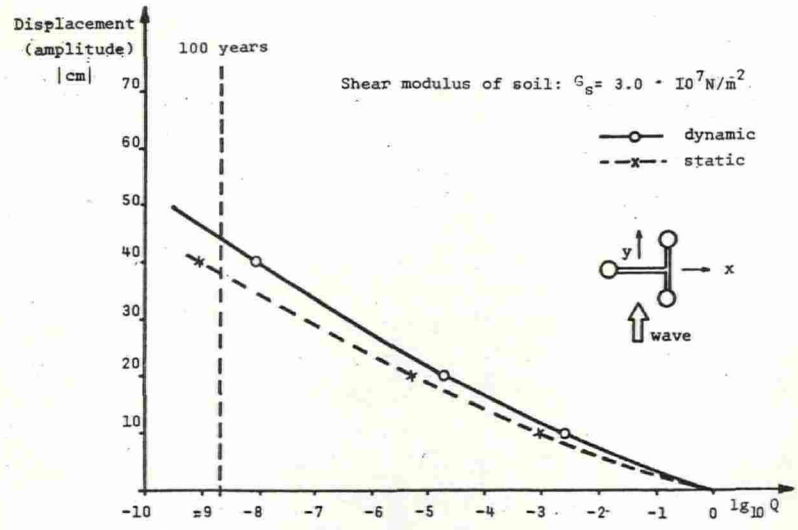

Fig. 5.37 Long-term distribution of the displacement of the deck in y-direction. Transfer-function is given in Fig. 5.18. Pierson-Moskowitz spectrum and conventional long-term model. Weather data from Table 5.9.

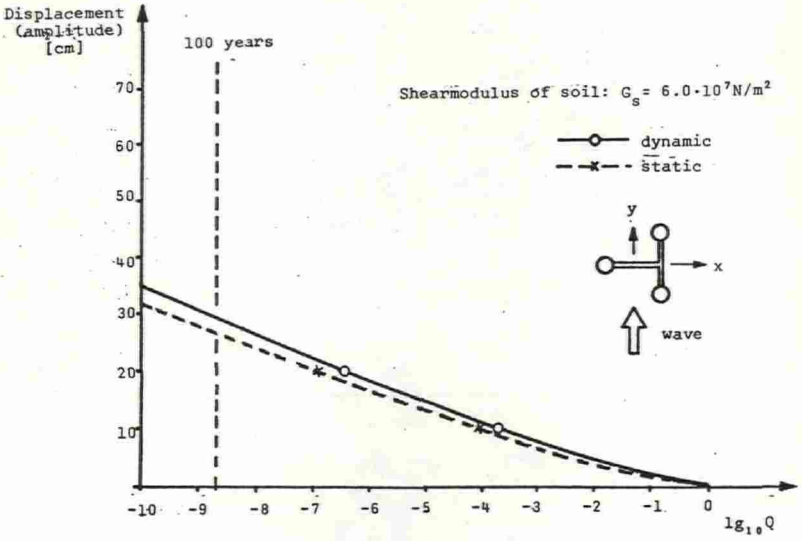

Fig. 5.38 Long-term distribution of the displacement of the deck in y-direction. Pierson-Moskowitz spectrum and conventional long-term model. Weather data from Table 5.9.

The response at a probability level of $10^{-8.7}$ corresponding to a return period of about 100 years is displayed in Fig. 5.39. The "dynamic amplification" varies from about 10% for load in the y-direction and a shear modulus $G_s = 6.0 \cdot 10^7$ [N/m^2] and up to more than 50% amplification for a load in the x-direction and a shear modulus of $1.65 \cdot 10^7$[N/m^2]. As might be expected the displacement of the deck corresponding to a given probability of occurence decreases towards a limit for increasing shear modulus of the soil. This limit represents the fixed base platform.

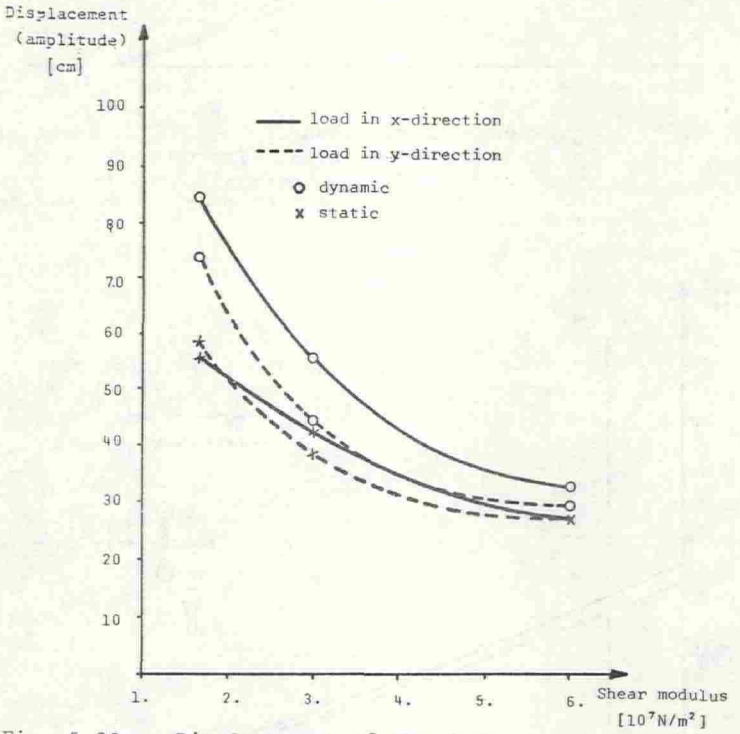

Fig. 5.39 Displacement of the deck at the probability level $10^{-8.7}$, as a function of the shear modulus of the soil.

Long-term Distribution of the Moments in the Shafts. Conventional Long-term Model with all Waves Propagating in one Direction.

The statistical treatment is based on the same assumption utilized by evaluating the displacement response in the previous section.

Figs. 5.40-41 display the long-term distributions of the moments in the shafts.

The effect of a variation of the shear modulus in the soil is displayed in Fig. 5.42. The moments are less sensitive to the variation of the shear modulus than the displacement. This is due to the rigid body rotation of the platform which gives rather large contributions to the displacement, but introduces no internal forces in the structure. It is interesting to note that the maximum response does not necessarily occur for the minimum shear modulus in the actual range of variation. This fact may be explained by examining the differences in the corresponding transfer-functions.
When loaded in the x-direction, the maximum dynamic amplification is about 82% for the moment in the top of Shaft no. 1, and about 52% in the bottom of the Shaft, see Fig. 5.42.

Fig. 5.43-44 display the long-term distribution of the moment at the top and bottom of Shaft no. 2. A constant shear modulus in soil $G_s = 3.0 \cdot 10^7$ [N/m^2] is used.

There is a remarkable difference in the dynamic amplification for the case with waves progressing in the y-direction as compared to the x-direction. From Figs. 5.43-44 it is seen that the dynamic amplification for waves in y-direction is 34 % and 22% for the moment in the top and the bottom of Shaft no. 2 respectively, as expressed on probability level $10^{-8,7}$.

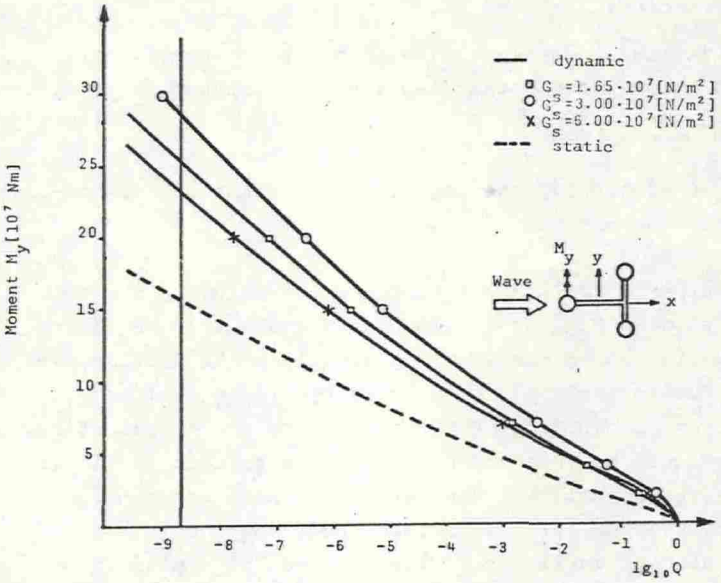

Fig. 5.40 Long-term distribution of the moment M_y at the top of the Shaft no. 1. Transfer-functions are given in Fig. 5.21. Pierson-Moskowitz spectrum and conventional long-term model. Weather data from Table 5.9.

Again, this of course must be explained on the basis of the transfer functions. As previously emphasized, a major source for the difference is differences in the phase angles between maximum wave loads on the shafts.

If the transfer-functions for the moments are more carefully examined, it might be seen that maximum response probably should be expected when the shear modulus in the soil is in the range $1.5 - 3.0 \cdot 10^7$ [N/m²]

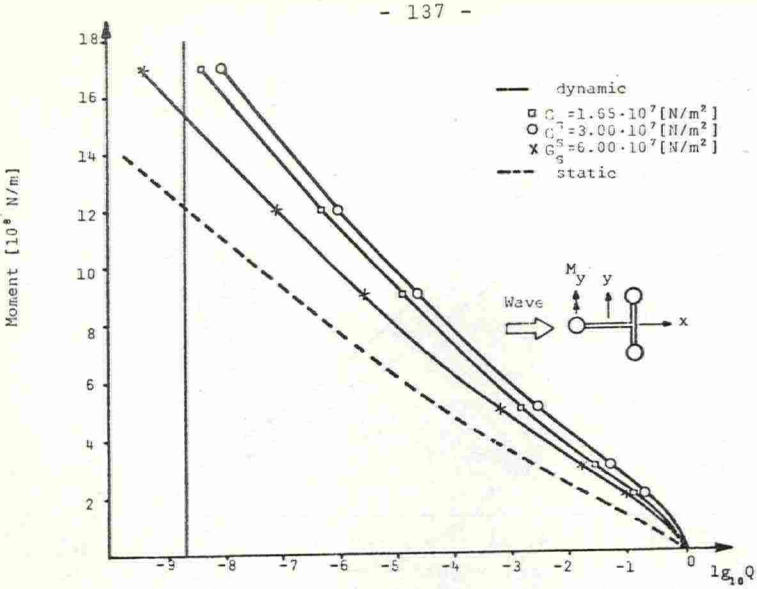

Fig. 5.41 Long-term distribution of the moment M_y at the bottom of the Shaft no.1. Transfer-functions are given in Fig. 5.23. Pierson-Moskowitz spectrum and conventional long-term model. Weather data from Table 5.9.

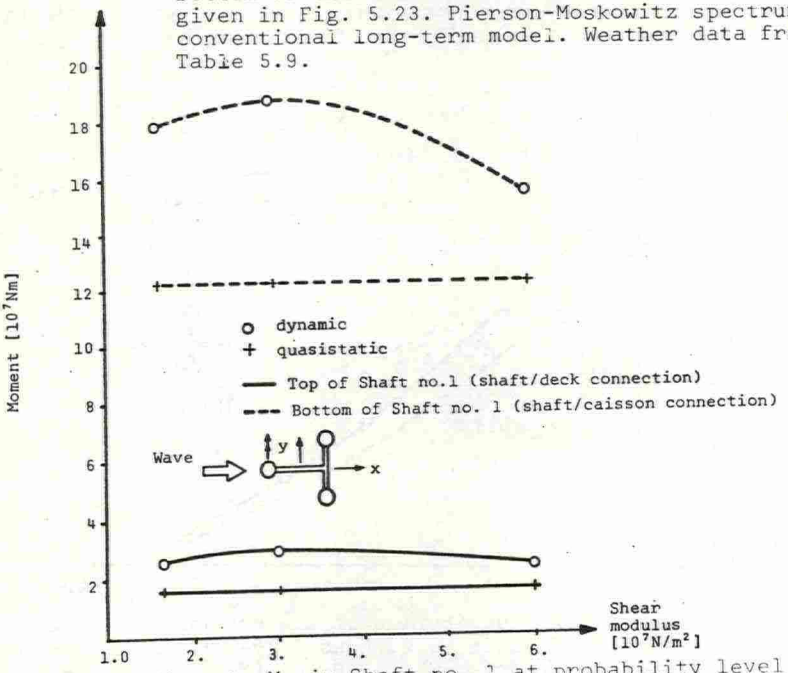

Fig. 5.42 Moments M_y in Shaft no. 1 at probability level $10^{-8.7}$, as a function of the shear modulus in soil. Wave propagating in x-direction.

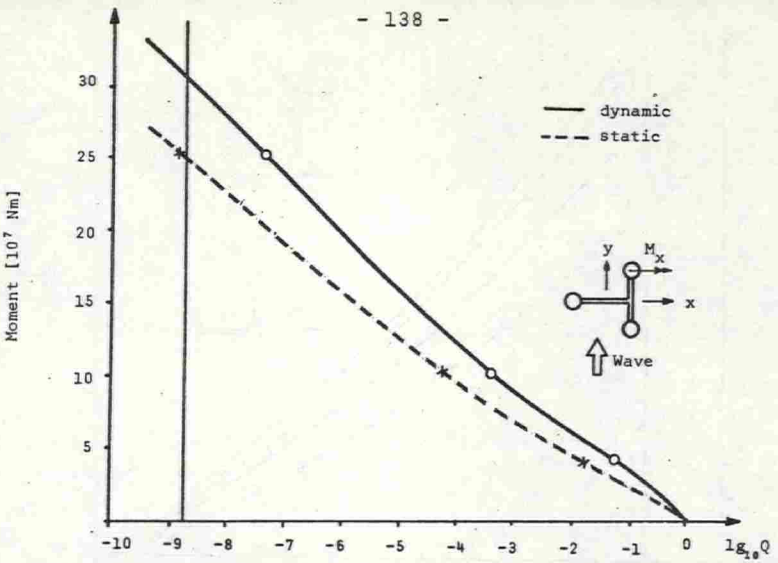

Fig. 5.43 Long-term distribution of the moment M_x at the top of Shaft no.2. Load in y-direction. Shear modulus in soil, $G_s = 3.0 \cdot 10^7$ [N/m^2]. Transfer-function is given in Fig. 5.22. Pierson-Moskowitz spectrum and conventional long-term model. Weather data from Table 5.9.

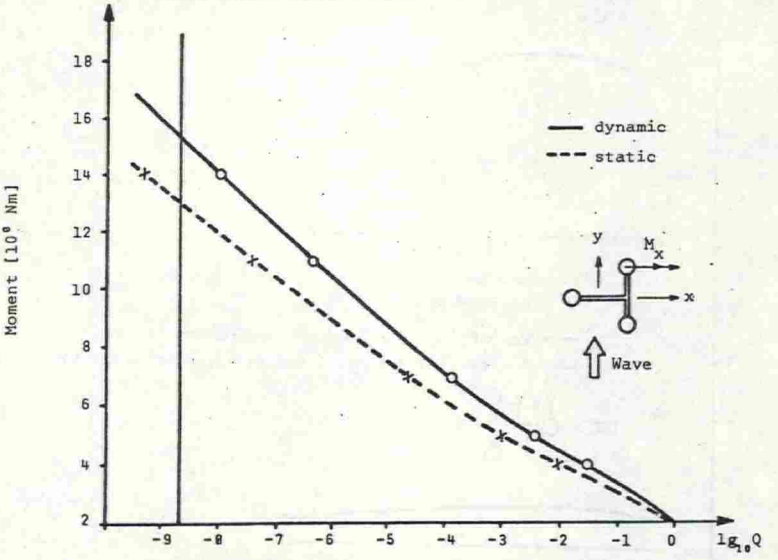

Fig. 5.44 Long-term distribution of the moment M_x at the bottom of Shaft no.2. Load in y-direction. Shear modulus in soil, $G_s = 3.0 \cdot 10^7$ [N/m^2]. Transfer-function is given in Fig. 5.24. Pierson-Moskowitz spectrum and conventional long-term model. Weather data from Table 5.9.

Long-term Distributions of the Response for Different Directions. Conventional Long-term Model with all Waves propagating in one Direction.

In this part of the study, the platform is, as before located with the x-axis in East direction and the y-axis in North direction. The shear modulus in soil is fixed, $G_s = 3.0 \cdot 10^7$ [N/m^2].

Only long-crested waves are considered and it is assumed that there is no correlation between $H_{1/3}$ and $\bar{T}$.

Parameters in H_v-$H_{1/3}$ and T_v-$\bar{T}$ relationship are given by Eq.(5.5) and the standard deviation of the mean wave period $S_c(\bar{T})$ is 1.086. Normal distribution of $\bar{T}$ is assumed.

For a given response quantity the maximum response at a given probability level can be determined by assuming all weather to be uni-directional, but vary the direction of the weather progress to obtain the maximum response.

Consider the moment M_x at the top of Shaft no. 2 and assume a long-term sea-state as given by Table 5.9. The actual directions of wave progress are identified in Fig. 5.45.

The resulting long-term distributions are displayed in Fig. 5.46

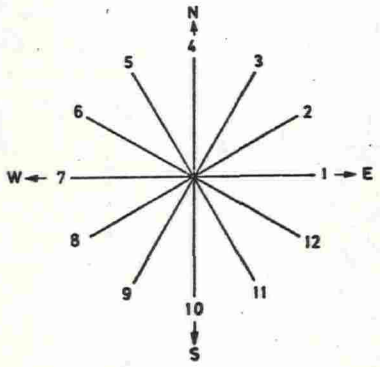

Fig. 5.45 Identification of direction.

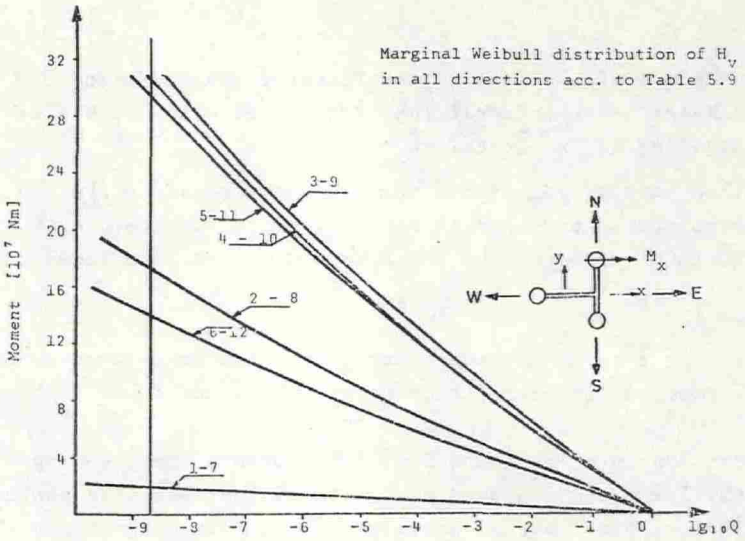

Fig. 5.46 Long-term distribution of the moment M_x at the top of Shaft nr. 2. Pierson-Moskowitz spectrum and conventional long-term model. The marginal distribution of wave heights (Table 5.9) is utilized for each of the directions.

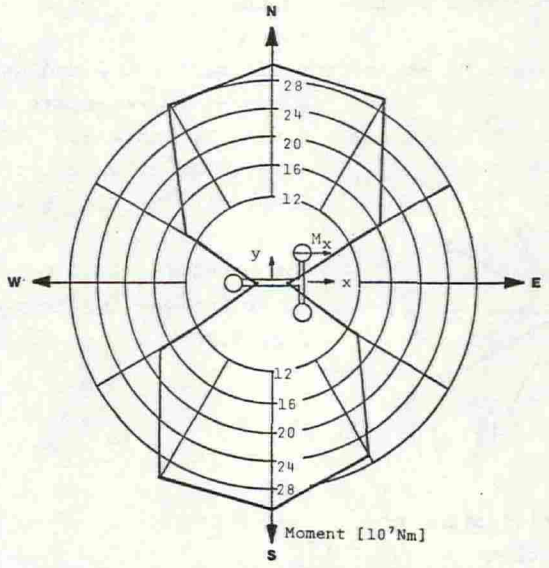

Fig. 5.47 Most probable largest moment M_x at the top of Shaft no.2, at a probability level $10^{-8.7}$. Pierson-Moskowitz spectrum and conventional long-term model. Weather conditions according to Table 5.9 for each of the directions.

The long-term distributions in Fig. 5.46 clearly express the effect og directionality on the response. Furthermore, it should be noted that maximum long-term response is obtained for incoming weather in the Direction no. 3 and not normal to the x-axis. Again the worst direction depends on a combined effect of resonance conditions and phase difference between loadings on the shafts. Fig. 5.47 displays the most probable moment amplitude at probability level $10^{-8.7}$ as depending on the wave direction.

Rather than letting all weather come from one direction, a more consistent method would be to account for the directionality (α) of the long-term variation of the weather. By utilizing the conventional long-term model, the directionality can be described by establishing "long-term" distribution for a discrete number of directions. In Table 5.10 a Weibull dirtribution for the visual wave height for some directions is established for a region surrounding the location $57^{\circ}30'N$ and $3^{\circ}E$ in the North Sea.

Firstly, the long-term distribution of the moment M_x at the top of Shaft no. 2 is determined by applying the actual distributions of wave heights associated with each direction separately. The distributions for the response are shown in Fig. 5.48. Note that the response for waves progressing for instance southwards and northwards are determined separately to illustrate the effect of the difference in weather coming from North and South, respectively. However, since transfer-functions are identical for these "two directions", it is necessary to consider 6 rather than 12 directions in the statistical treatment.
Table 5.10 contains directions with both "worse" and "milder" wave height distributions than the "average" marginal distribution in Table 5.9. Therefore, the response, M_x, at the top of Shaft no. 2 is about 20 percent greater by applying the "actual" distribution for Direction no. 4 as compared to applying the "average" distribution (obtained by combining the wave height distribution for all directions). Even if the percentage of 20 is unreliable due to the lack of information by preparing the directional distribution in Fig. 5.10, it ex-

presses a correct trend.

Secondly, the long-term distribution of the response is determined when accounting for the actual directionality of the long-term sea-state, see Table 5.10. The probability that the incoming weather fall within a given directional sector is then given in Fig. 5.32.

The result thus obtained may be compared with the long-term distribution obtained by using the marginal long-term data in Table 5.9. By the consistent method the most probable largest response amplitude on probability level $10^{-8.7}$ was found to be $29.0 \cdot 10^7$, while the other approach resulted in 30.5 (see Fig. 5.43).

Due to lack of reliable data for the directional distribution of wave heights all weather is oftenly assumed to come from one direction, using Table 5.9. Furthermore, it is natural to let the wave propagate in the most adverse direction for the actual response quantity of current interest. It might be expected that the most probable largest response amplitude

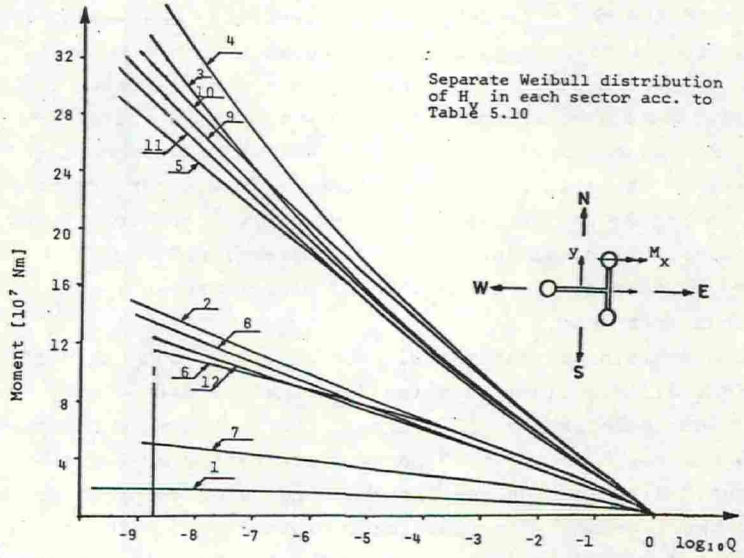

Fig. 5.48 Long-term distribution of moment M_x in top of Shaft no. 2. Pierson-Moskowitz spectrum and conventional long-term model. The actual long-term distribution of wave heights for each direction is utilized (Table 5.10).

found by this analysis would be very conservative. Assuming all weather to come from direction no. 3 the most probable moment-amplitude is found to be about $32 \cdot 10^7$ Nm (probability level $10^{-8.7}$). From the conditional distributions given in Fig. 5.48 the marginal long-term distribution is found, and the most probable largest moment-amplitude is about $29.5 \cdot 10^7$ Nm (probability level $10^{-8.7}$), in other words about 8% less than the value found by assuming all weather to come from one direction. What is said here is valid when the structure is orientated with the x-axis towards East. In the next part, it will be shown that the orientation of the structure seems to be of great importance.

Looking at Fig. 5.48 one would possibly expect the marginal distribution to give a lower value than given above, but recognizing that the marginal distribution is given as

$$Q(x) = \sum_{ID} Q_{ID}(x|\alpha) \cdot PDIR_{ID}$$

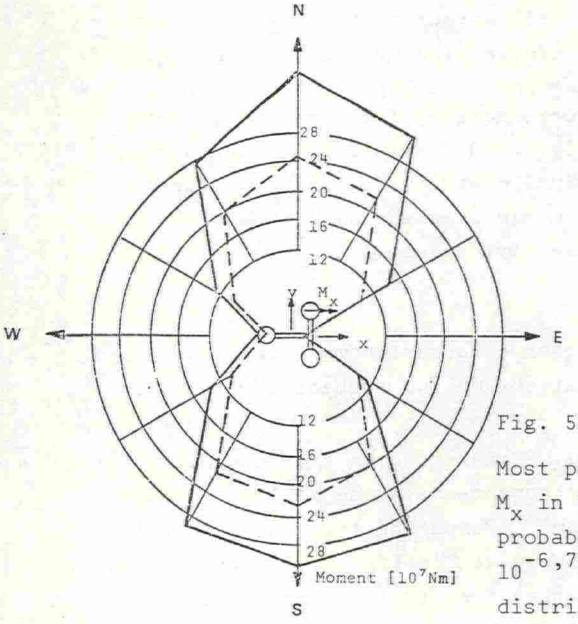

Fig. 5.49

Most probable largest moment, M_x in top of Shaft no. 2 at probability level $10^{-8,7}$ and $10^{-6,7}$. Separate Weibull-distribution of H_v in each sector.

one will see that the marginal distribution is dominated of the "highest" conditional distributions, specially for greater response-amplitudes.

The marginal Long-term Distribution of Response for Various Orientations of the Platform. Conventional Long-term Model.

The marginal long-term distribution of the moment at top of Shaft no. 2 is calculated for 6 various orientations of the platform. The statistical treatment is similar to that outlined in the previous sections.

Two cases of weather data is applied, namely:

- uni-directional,("marginal"), Table 5.9 and Fig. 5.32
- directional data according to Table 5.10 and Fig.5.32.

In the first case, the long-term distribution is nearly independent of the orientation since the wave height distribution is the same for all directions. A negligible difference is found since the direction-probability in Fig. 5.32 is varying with the directions, see Fig. 5.50.
In the second case, the orientation of the platform have a significant effect. Fig. 5.50 displays the upper and lower bound for the marginal distribution. The difference between maximum and minimum moment-amplitude is approximately 15% on a probability level of $10^{-8.7}$ for this case.

In Fig. 5.51 the most probable largest moment amplitude is given for each orientation at two probability levels.

Furthermore, assuming all weather to come from one direction, the most probable largest moment-amplitude at $10^{-8.7}$ level was found to be $32 \cdot 10^7$ [Nm]. Comparing this value with the most probable largest value given in Fig. 5.51, probability level $10^{-8.7}$, it is seen that for $\gamma \sim 150^{\circ}$ the above value is *less* than the marginal value.

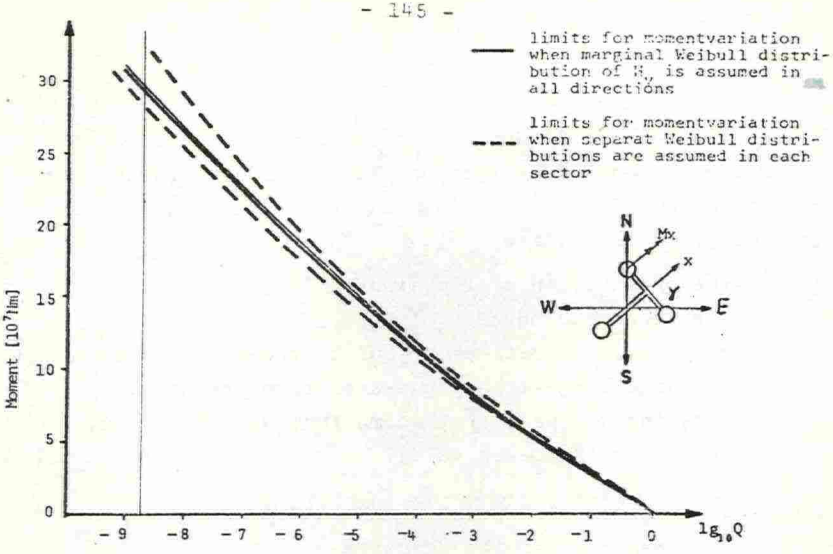

Fig. 5.50 Upper and lower limit for the long-term distribution of the moment M_x at the top of Shaft no. 2 for various orientations of the platform. The platform is turned 180° in steps of 30°.

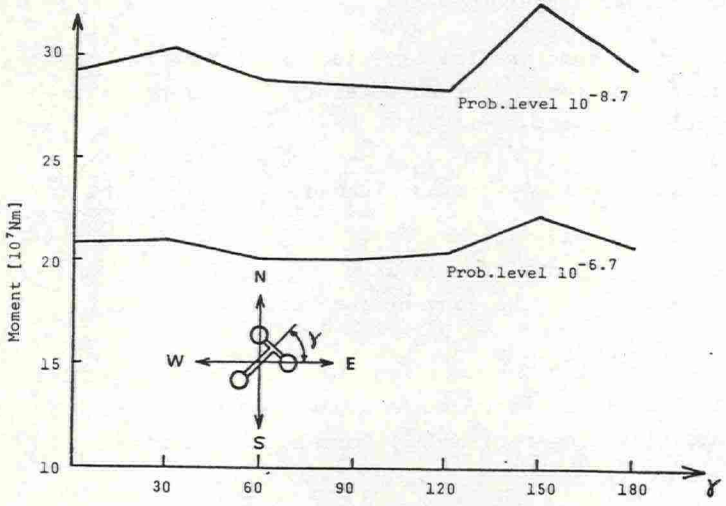

Fig. 5.51 Variation in the most probable largest moment, M_x, in Shaft no. 2 by varying the orientation of the platform in steps of 30°. Long-term analysis based on "actual" directional data, Table 5.10 and Fig. 5.32.

Since the actual directional distributions constructed for the present investigation (Table 5.10) is rather uncertain, no final conclusions can be made. However, the results indicate that:

- the orientation of the structure, γ, is an important parameter
- one should be rather careful to treat the most probable largest response-amplitude, found by assuming all weather to come from one direction, as an overestimated value.

5.4.3 Parametric Studies on the Statistical Treatment of the Response

General Remarks

Thusfare, Chapter 5.4 has been devoted to the statistical treatment of the response by means of a version of the conventional long-term model.

In this section some preliminary studies will be reported on the investigation on the uncertainties inherent in the statistical modeling.

The following items will be considered:

- choice of wave spectrum
- effect of short-crested waves
- parameters in the conventional long-term distribution
  In particular the empirical relation between visual and absolute (instrumental) wave-period and -height
- modified long-term model, Correlation between $H_{1/3}$ and $\bar{T}$.

In this study a single dynamic model will be considered for the platform in Fig. 5.1. The shear modulus of the

soil is assumed to be $G_s = 3.0 \cdot 10^7$ [N/m^2].

The transfer-functions for the moment M_y at the top of Shaft no. 1 and the moment M_x at the top of Shaft no. 2 will be considered.

Long-term Distributions of the Response for Different Wave Spectra, Conventional and Modified Long-term Model with Unidirectional Long-term Wave Propagation.

The following spectra were considered

Pierson-Moskowitz
Jonswap (with various peakedness factors)
Derbyshire-Scott
Modified Derbyshire Scott

Only long-crested waves were taken into account.

The conventional long-term model is applied with the data in Eq.(5.5)

The modified model is applied assuming a correlation between $\bar{T}$ and $H_{1/3}$ as expressed by Eqs. (4.41 - 4.44). The numerical value on the equilibrium parameter α is here assumed to be

$$\alpha = 0.0081 \qquad (5.6)$$

The uni-directional long-term wave data in Table 5.9 were utilized.

The results are displayed in Figs. 5.52- 53. It is observed that the discrepancy between the results of the conventional and modified long-term model is significant. The conventional and modified long-term model will be discussed in a subsequent parameter study. Also, the choice of wave spectrum has a definite influence on the distribution of response amplitudes. In particular it is observed that the upper bounds on the long-term response is obtained by different spectrum models, depending upon the response quantity considered.

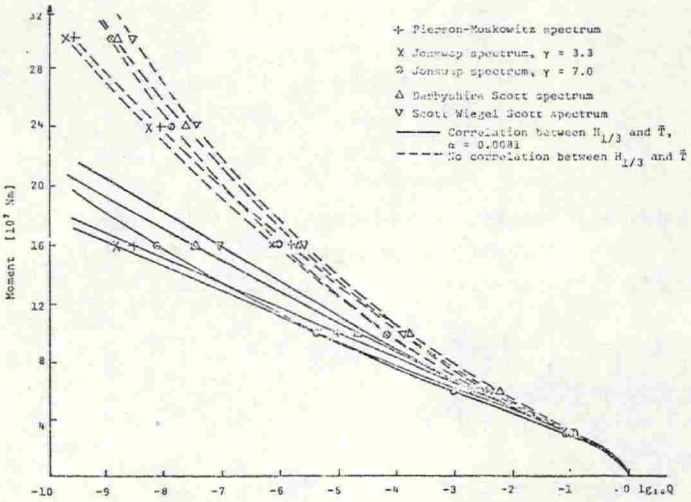

Fig. 5.52 Long-term distribution of moment ,M_y, at the top of Shaft no. 1. Dynamic analysis. Unidirectional wave data, Table 5.9.

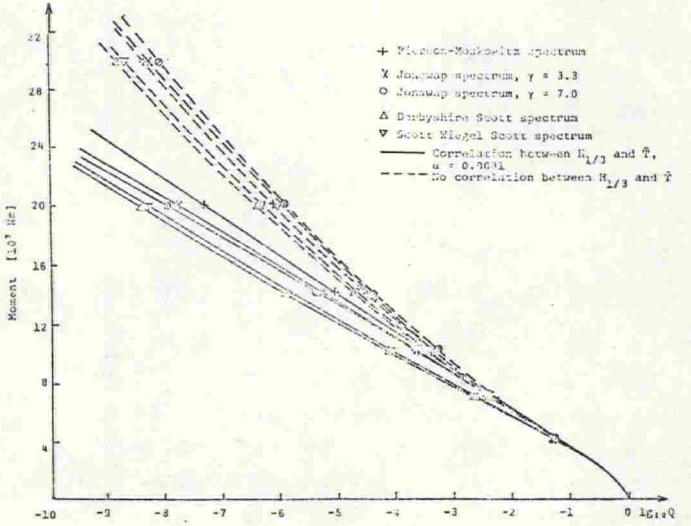

Fig. 5.53 Long-term distribution of moment, M_x at the top of Shaft no. 2. Dynamic analysis. Unidirectional wave data, Table 5.9.

Long-term Distribution of the Response for Different Directional Wave Spectra. Conventional Long-term Model with Unidirectional and Directional Long-term wave Propagation.

The platform is orientated with the x-axis in East direction. The moment response, M_x at the top of Shaft no. 2 is considered.

Up to now long-crested waves have been assumed in the determination of long-term distributions. A more realistic representation of the sea is to assume short-crested waves, using a two-dimensional wave-spectrum, given in Eq. (4.1). Appropriate directional functions are given in Eqs. (4.9 - 10). The present investigation is accomplished with Pierson's and Mark's representations.

Parameters in the relationships between H_v-$H_{1/3}$ and T_v-$\bar{T}$ in the conventional long-term model are

$$\begin{aligned} AH &= 0.5 \\ BH &= 1.33 \\ AT &= 2.83 \\ BT &= 0.44 \end{aligned} \qquad (5.7)$$

Two alternative long-term wave-height distributions were applied

- unidirectional long-term wave propagation, using Table 5.9. The two directions 3 and 4 in Fig. 5.45 were considered.
- directional long-term distribution assuming a separate Weibull-distribution of H_v for each direction, Table 5.10.

The resulting long-term distributions for the response are given in Figs. 5.54-55.

In the unidirectional long-term model a strong reduction in the most probable largest moment amplitude was found for Direction no. 3. For this direction, which is the most adverse for the actual response when long-crested waves

are assumed, a reduction of about 17% was found, when using Pierson's directionality function.

For Direction no. 4, which is close to the most adverse direction, the corresponding reduction was only about 7%. Therefore, as can be observed in Fig. 5.54 the Direction no. 4 (of nos. 3 and 4) is the most adverse direction for the actual response quantity when short-crestedness is accounted for.
The reason for the significant reduction found for Direction no. 3 is that the transfer-functions in the neighbourhood of Direction no. 3 are considerably smaller than the transfer-function for Direction no. 3, see Fig. 5.47. For short-crested waves a part of the energy is put in transfer functions which have a small response level. Hence the total response is reduced.

When Direction no. 4 is the principal direction, the neighbouring directions do not represent a much lower response level than Direction no. 4 itself, Direction no. 3 do even represent a higher response level. Hence the reduction is less significant than for Direction no. 3.

If the principal direction is chosen to be a direction corresponding to a small level of the transfer-function, the use of short-crested waves instead of long-crested waves will increase the response.

For the second case, Fig. 5.55, the most probable largest moment on probability level $10^{-8.7}$, is found to decrease with about 7%, using Pierson's directionality function.

The sensitivity of the modified model with respect to the choice of directional spectrum is expected to be of the same order as for the conventional model.

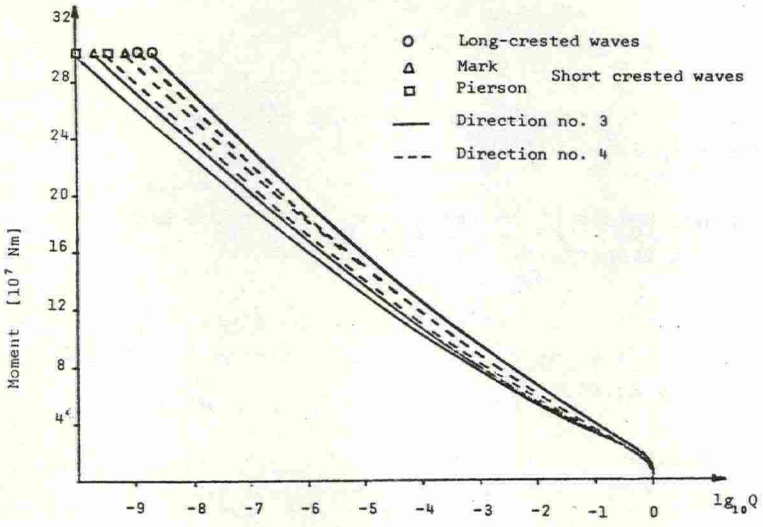

Fig. 5.54 Long-term distribution of moment M_x in the top of Shaft no. 2. Pierson-Moskowitz spectrum with long- and short-crested waves is considered. Conventional long-term model with unidirectional waves, Table 5.9 is assumed.

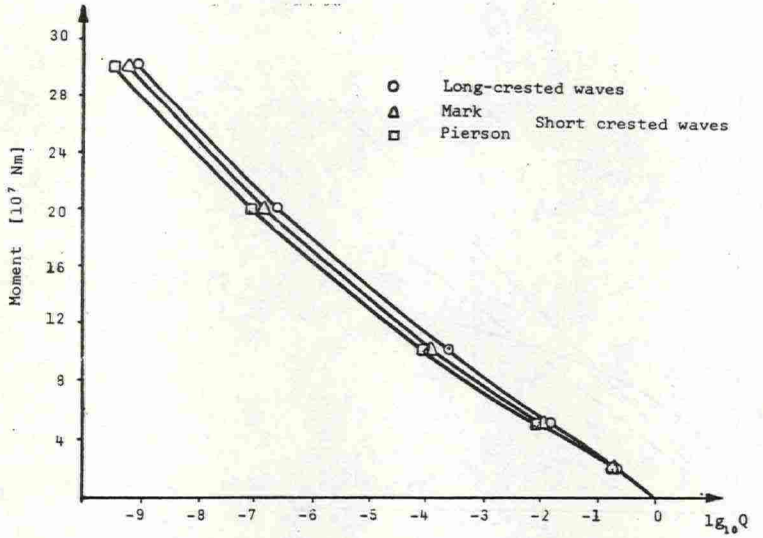

Fig. 5.55 Long-term distribution of moment M_x in the top of Shaft no. 2. Pierson-Moskowitz spectrum with long- and short-crested waves is considered. Conventional long-term model is assumed. Separate Weibull-distribution of H_v in each sector, Table 5.10.

Long-term Distribution of the Response by varying the Relationship between $\bar{T}$ and T_v

The moments M_y and M_x in the top of Shaft no. 1 and Shaft no. 2 respectively are considered.

The statistical analysis is based on the Pierson-Moskowitz spectrum and the alternative parameter sets for (AT, BT) given by Eq.(5.8)

$$\begin{aligned} AT &= 2.83 \qquad BT = 0.44 \\ AT &= 0.74 \qquad BT = 1.00 \end{aligned} \tag{5.8}$$

These sets were proposed by Nordenstrøm, Ref.(81). The parameters relating $H_{1/3}$ and H_v are given by Eq.(5.2)

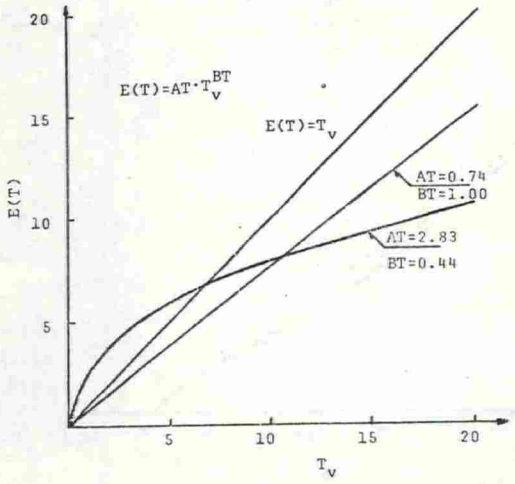

Fig. 5.56 The relations between T_v and $E(\bar{T})$

The long-term wave data given in the Table 5.9 are utilized.

Figs. 5.57 and 5.58 display the effect of the choice of parameters on the long-term distribution of the moment.

The variation of the long-term distribution of the moments with the different parameter sets are rather small.

The long-term distribution for both response quantities obtained by quasistatic analysis is particularily insensitive to the parameter variation.

The results displayed show that the parameters in the relation between T_v and $E(\bar{T})$ might be of great importance for problems where highly peaked resonance top exists. When the transfer-function do not have this typical resonance top the choice of parameters seems to be of less importance with respect to the result.

The two parameter sets recommended by Nordenstrøm represents two different interpretations of existing data from weather stations in the North Atlantic. The difference in the result between these two sets is rather small, - 3 - 4 % in Fig. 5.57. However, it is not quite sure that the relations above are valid for the North Sea.
It is, of course, possible that an actual relation found for the North Sea might have a greater influence on the results.

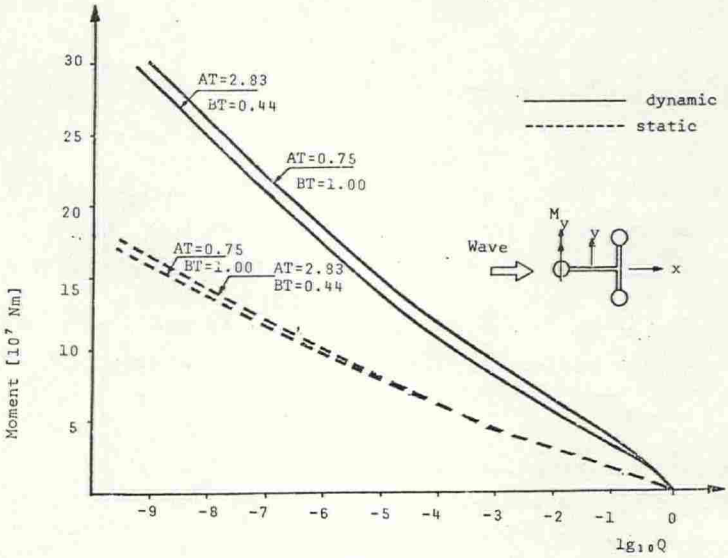

Fig. 5.57 Long-term distribution of moment M_y in top of Shaft no. 1. Pierson-Moskowitz spectrum and conventional long-term model. Long-term wave data from Table 5.9. Variation of parameters relating $\bar{T}$ and T_v

Long-term Distribution of the Response by assuming Correlation between $H_{1/3}$ and $\bar{T}$ (Modified Long-term Model)

The response for the moment M_y at the top of Shaft no. 1 is considered. The Pierson-Moskowitz spectrum is applied with no directional spectrum. Parameter sets relating $H_{1/3}$-H_v and $\bar{T}$-T_v are given by Eq.(5.5), and $\bar{T}$ is assumed to be normal distributed. Unidirectional wave data according to Table 5.9 are assumed.

The effect of introducing a correlation between $H_{1/3}$ and $\bar{T}$ in their join" probability distribution is investigated, see Chapter 4.3.

Besides the uncertainty by assuming an equilibrium spectrum itself, the constant α in Eq.(4.37) may vary. Two values for α, namely $\alpha = 0.0081$ and $\alpha = 0.02$ are therefore utilized.

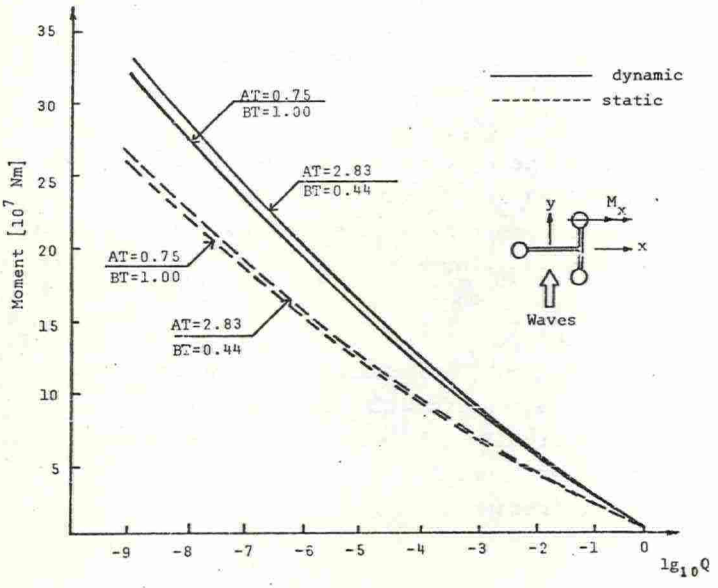

Fig. 5.58 Long-term distribution of moment in top of Shaft no.2. Pierson-Moskowitz spectrum and conventional long-term model. Long-term wave data from Table 5.9. Variation of parameters relating $\bar{T}$ and T_v.

The result of the analysis is given in Fig. 5.59 and Figs. 5.52-53. The discrepancy between the conventional and modified model is rather great, in particular for the dynamic response. Originally, the dynamic amplification was calculated to about 80% at a probability level of $10^{-8.7}$. With the assumption of correlation between $H_{1/3}$ and $\bar{T}$, the dynamic amplification is reduced to about 40%. The discrepancy between the results for $\alpha = 0.02$ and $\alpha = 0.0081$ is about 5%, as is seen in Fig. 5.59. In the reality α will probably vary from 0.008 for $\bar{T} > 10$s to $\alpha \sim 0.03$ for $\bar{T} \sim 3$ and the most realistic result will probably lie between the results for $\alpha = 0.02$ and $\alpha = 0.0081$. Obviously this modified model is associated with uncertainties since the long-term joint distribution for $H_{1/3}$ and $\bar{T}$

is constructed based on certain assumptions rather than measured data. The most important incertainties are

- the determination of the area R, see Fig. 4.
- the assumption of $FF_{I,L,J}$ independent of $H_{1/3}$

As will be shown in the next sections, the modified model seems to give more realistic "extreme values" than the original model when comparing with the results from a short-term analysis. However, further research is necessary before final conclusions can be made.

Using long-term model on the response of ships and semisubmersibles, the results will probably not be influenced by this problem. This is due to the fact that ships and semisubmersibles have their eigenfrequencies in a very low frequency range.

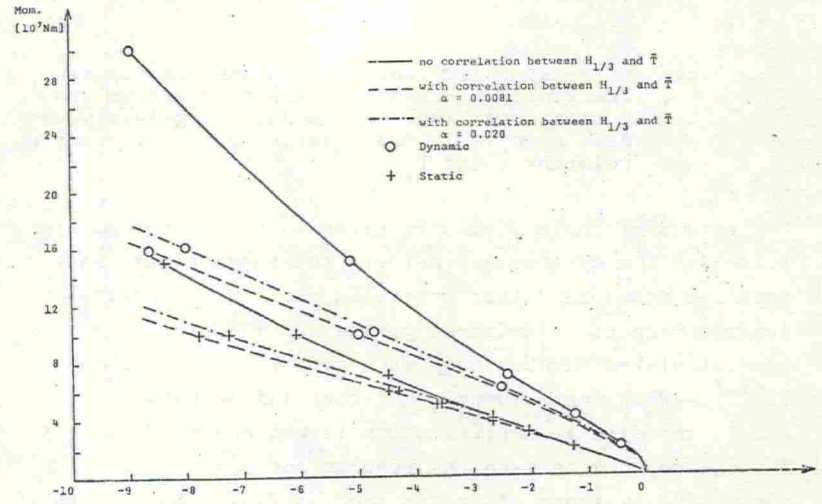

Fig. 5.59 Long-term distribution of dynamic and static Moment M_y at the top of Shaft no. 1. Pierson-Moskowitz spectrum and conventional long-term model, and modified model with correlation assumed. Unidirectional wave propagation, see Table 5.9.

Long-term Distribution of the Response. Normal versus Log-normal Distribution of Average Mean Period.

The moment M_y in the top of the Shaft no. 1 is considered, the transfer-function obtained by the dynamic analysis is utilized.

The conventional parameter set in the relationship between H_v-$H_{1/3}$ and between T_v-$\bar{T}$ are utilized, see Eq.(5.5)

The conventional and modified long-term models are applied.

The long-term distributions are displayed in Fig. 5.60. The effect by the choice of distribution for the average mean period is greatest for the conventional long-term model. Using the log-normal distribution the most probable largest moment-amplitude, on probability level $10^{-8.7}$, is reduced with about 10%, for the original long-term model. Principally this difference is originated in the lowest classes of visual wave period, and is due to the skewness of the log-normal probability density function, and to the fact that the highest eigen-period is lying in the area where this skewness is causing a rather great difference between the normal- and the log-normal probability density functions.

The actual transfer-function is highly peaked for the lowest eigenfrequency. For responses with less peaked transfer-functions, the discrepancy will probably be less than for the example given here.

Using the modified long-term model the difference in the most probable largest moment-amplitude on probability level $10^{-8.7}$ is less than 3%, and of rather little interest.

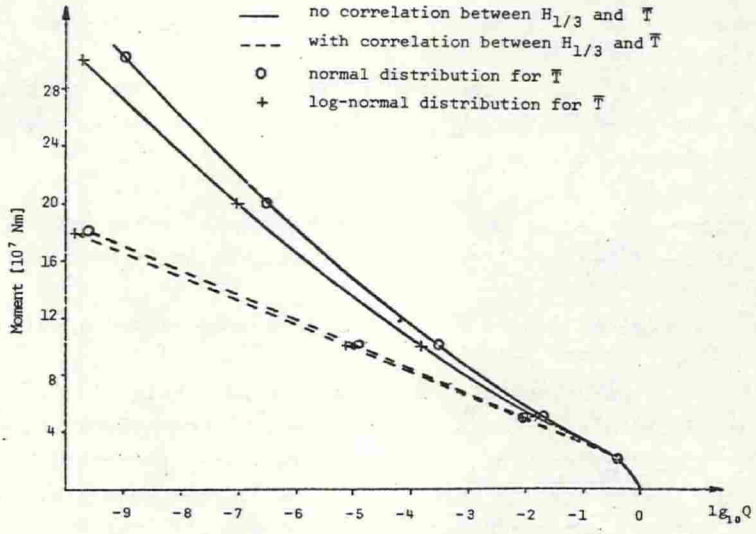

Fig. 5.60 Long-term distribution of moment M_V in the top of Shaft no. 1. Pierson-Moskowitz spectrum with conventional and modified long-term model. Effect of choice of distribution for average mean period.

5.4.4 Remarks on the Design Wave Approach and Short-term Stochastic Response Analysis

General remarks

As mentioned in the introduction the design is in general concerned with

- a single excursion failure (excessive yielding, or cracking, collapse,..)

or,

- failure by cumulative damage (fatigue)

In the first case an extreme value of the response (at a low probability level) is required. In the second case the number of cycles for each amplitude (and mean stress level) is required.

In this section extreme response values obtained by the design wave, short-term and long-term approach will be compared.

Design Wave Approach

According to Ref. (2) a platform may be designed by determining the extreme response by placing the structure in a sinusoidal long-crested wave with height corresponding to an extreme wave. The return period is in general chosen to be 100 years. The wave height is determined by application of long-term statistics on wave height data.

In the design against a single excursion failure the wave period and the location of the structure with respect to the wave is varied so as to obtain the maximum response value. In this case dynamic effects can be accounted by using a dynamic load factor (DLF)- which for the present platform is in the range 1.05 to 1.25 depending on the soil conditions. The lower bound of the wave period to be chosen depends on the limit for wave breaking.

The moments M_y and M_x at the top of Shaft no. 1 and 2, respectively, are considered. The shear modulus of the soil is $G_s = 3.0 \cdot 10^7$ [N/m^2].

The wave height is taken to be 29 m, see Fig. 5.30, corresponding to the data in Table 5.9.

The moment-amplitudes for waves with wave-amplitude 1 m is taken from the transfer-functions, Figs. 5.21 -5.24.The response for waves with height 29 m is then found by

multiplying the values from the transfer-function by 14,5.

Table 5.11 Deterministic response. Design loads

Wave period [seconds]	Moment, M_y, in Shaft no. 1 [10^7 Nm]		Moment, M_x in Shaft no. 2 [10^7 Nm]	
	Dynamic	Static	Dynamic	Static
16	12.8	11.0	21.5	19.7
14	15.1	12.5	26.1	22.6
12	18.7	15.9	31.9	27.2

Short-term Response Analysis

The long-term state consists of a series of short-term states. The short-term state (a single stationary storm state) may be utilized to estimate the extreme response value.

The stationary sea-state is then defined by for instance the two parameters $H_{1/3}$ and $\bar{T}$. The important decisions by the short-term response analysis is the choice of type of spectrum, (including directionality function), $H_{1/3}$ and $\bar{T}$.

Now, there exists a relation between the extreme wave height H_{max} in the storm and the $H_{1/3}$ and the mean period $\bar{T}$ in the sea-state.

Assuming a (stasionary) storm of duration 12 hours, corresponding to about $3.6 \cdot 10^3$ maxima with an average mean period $\bar{T}$ = 12 seconds. The most probable largest maxima ,x, is found from Eq.(4.20) inserting the Rayleigh parameter $r=\sqrt{2m_o}$

$$\tilde{x} = E(x) = r\{\sqrt{\log_e N} + \frac{0.5772}{2\sqrt{\log_e N}}\} \qquad (5.8a)$$

with $N = 3.60 \cdot 10^3$ $\tilde{x}$ is found to be

$$\tilde{x} = 2.96 \cdot r \qquad (5.8b)$$

The Rayleigh-parameter r for the two sea-states is taken from the output of LONTIM, and $\tilde{x}$ is given in Table 5.12.

Thus, the sea-state $(H_{1/3}, \bar{T})$ may be chosen so as to yield the same extreme wave height as mentioned in connection with the design wave approach.

A storm duration of 12 hours, $H_{1/3} = 13.8$ m, $\bar{T} = 12$ secs. corresponds to $H_{max} \simeq 29$ m.

Table 5.12 Design response values by short-term approach. Pierson-Moskowitz wave spectrum with significant wave height 13.8 [m]. Storm duration 12 hours

Average wave period, $\bar{T}$ [seconds]	Moment M_y in top of Shaft no.1 [10^7 Nm]		Moment M_x in top of Shaft no. 2 [10^7 Nm]	
	Dynamic	Static	Dynamic	Static
16	14.2	10.4	22.5	19.1
14	16.2	11.5	25.4	22.0
12	18.9	13.3	28.0	24.4

Fig. 5.61 illustrates the influence of storm duration on the peak response.

Short term respons for different wave spectra.

A study on the effect the choice of wave spectrum has on the short term respons was performed. Figs. 5.62 and 5.63 display the results obtained by applying 5 different wave spectra. Calculation was performed assuming

- significant wave height $H_{1/3} = 15$[m]
- storm duration L = 12 hours

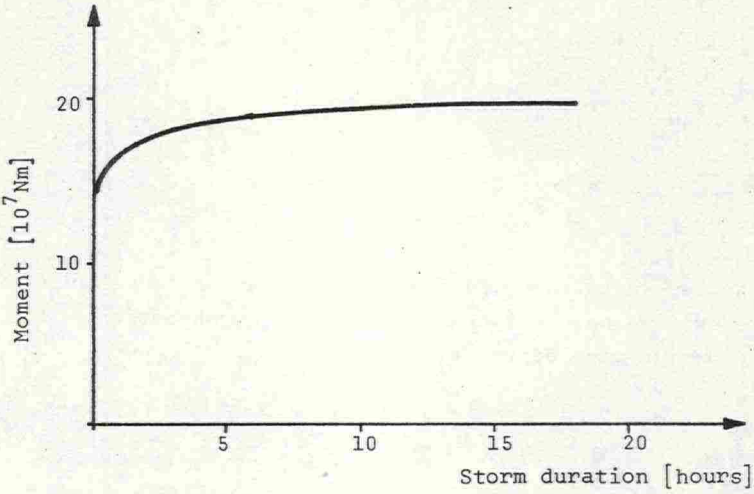

Fig. 5.61 Expected peak moment in top of Shaft no. 1, versus storm duration. $\bar{T}$ = 12 seconds, $H_{1/3}$ = 13.8 meters.

The mean period in the wave spectra was varied between 10 and 18 seconds. The dynamic peak response in top of Shaft No. 1 and 2 are considered. As displayed the variation in the results are significant. The difference between maximum and minimum peak response varies between 18 and 77 percents of the minimum peak response. Only parts of the region where respons is calculated should be regarded as significant. According to the admissibility condition, Eq. (4.38), only spectra where $\bar{T}$ is greater or equal 14 seconds are physically allowable when the equilibrium constant is assumed to be 0.01 and $H_{1/3}$ = 15[m].

The results states that care must be taken in choise of wave spectrum when short term respons is calculated.

Comparison between Deterministic, Short-term and Long-term Response Analysis

The response, for which comparison is made, is the moment in the top of shafts no. 1 and 2.

Table 5.11 give the deterministic response. Compared to the short-term peak response given in Table 5.12 no signi-

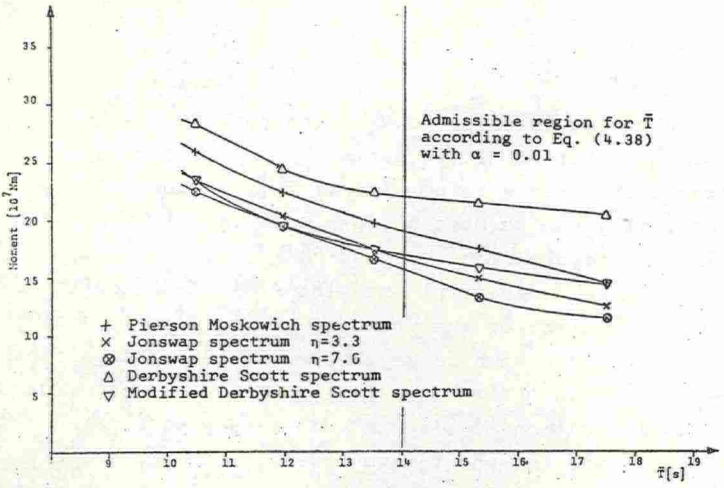

Fig. 5.62 Short-term distribution of peak moment - response in top of Shaft no. 1. $H_{1/3}$ = 15 meters, Storm duration is 12 hours.

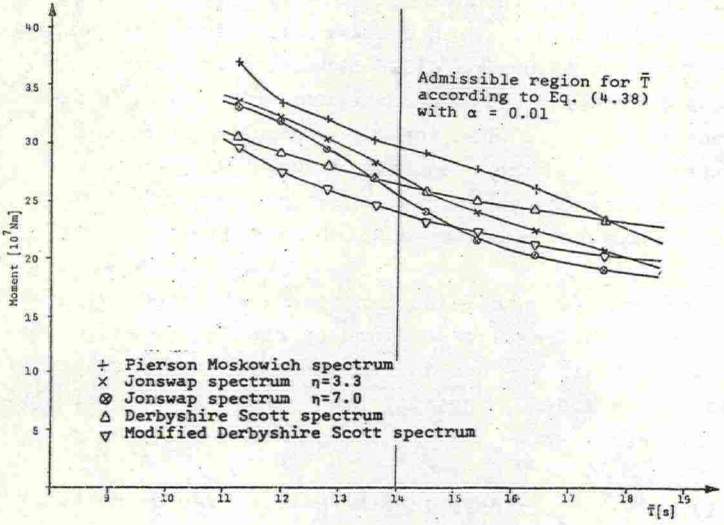

Fig. 5.63 Short-term distribution of peak moment-response in top of Shaft no. 2. $H_{1/3}$ = 15 meters, Storm duration is 12 hours.

ficant difference is observed when the periods are 14 and 16 seconds. At a deterministic period T = 12 seconds a significant difference is obtained. This is probably due to a physically not permissible period/wave-height ratio. Accordingly, the deterministic and short-term analysis is in reasonably good agreement when the Pierson-Moskowitz spectrum is applied for the present structure/soil/ocean system. Other wave spectra may, however, give a significant difference between these two calculation procedures. The dynamic amplification is also in good agreement for the deterministic and the short-term model.
A slightly higher amplification is observed in the short-term model. This should be expected as the short-term model includes parts of the transfer-function where the dynamic amplification is high. In the actual analysis the damping for the fundamental mode is about 10 % of the critical damping. With a lower value for this damping the dynamic amplification will increase when short-term response is considered. The deterministic model, however, will not be affected when the eigenfrequencies in the structure is in a high frequency range. Thus greater difference between deterministic and short-term response should be expected when the damping is reduced.

The long-term response is as mentioned, affected by several parameters. The results obtained by short-term and deterministic analysis are herein compared by three variants of the long-term model. The response in the top of Shaft no. 1 is considered.

Firstly, the conventional long-term with Pierson-Moskowitz spectrum, with no directional wave spectrum is assumed. Directional wave height data and a normal-distribution for $\bar{T}$ are assumed. The most probable largest moment amplitude on probability level $10^{-8.7}$ was found to be

Dynamic: $28.4 \cdot 10^7$ Nm
Static: $16.0 \cdot 10^7$ Nm
"Dynamic lodafactor": 1.78

Secondly, let $\bar{T}$ follow a log-normal distribution rather than a normal one. The corresponding values is then found to be

Dynamic: $25.8 \cdot 10^7$ Nm
Static: $16.0 \cdot 10^7$ Nm
Dynamic loadfactor: 1.61

Comparing these values with the values from the deterministic- and short-term model, the following seems to be clear:

The original long-term model overestimates the extreme values, and in particular by application of dynamic analysis. The reason for this is discussed in Section 4.

Thirdly, using the modified long-term model instead of the conventional one, (and assuming $\bar{T}$ to be normal) the most probable largest moment amplitude on probability level $10^{-8.7}$ was found to be:

Dynamic: $16.6 \cdot 10^7$ Nm
Static: $12.0 \cdot 10^7$ Nm
Dynamic loadfactor: 1.38

This is of the same order as predicted by the deterministic- and short-term model. According to the discussion in Section 4 the modified long-term model is expected to be more realistic for estimating long-term extreme values.

6. CONCLUSIONS AND RECOMMENDATIONS FOR FURTHER WORK

Fixed base gravity platforms in water depth up to 150 m have fundamental eigenperiods ranging up to 5.0 seconds. Dynamic amplification of the response to wave loading occurs if eigenperiods are increased towards the band of periods of ocean waves where large energy concentration is present. This increase of eigenperiods may be due to extra flexibility provided by the soil foundation and/or increased water depth. In particular, the sensitivity analysis of the effect of the shear modulus of the soil showed that the variation of this parameter has a considerable influence on the structural response, due to its effect on the stiffness (and then eigenfrequency) of the system.

Besides the magnitude of the lowest eigenfrequencies and the phase differences of forces on different shafts are found to have a major influence on the response.

For tall platforms on soft soils it is not sufficient to design the platform on the basis of static response analysis.

The determination of design values of the response and the dynamic analysis may basically be obtained either by a deterministic design wave, a stochastic short-term, or a stochastic long-term approach. In this report emphasizes has been placed on the latter approach. However, the three approaches are compared. Parameter studies have been carried out to investigate the effect of:

- choice of wave spectrum
- short-crested - versus long-crested waves
- assuming all weather to come from one direction versus assuming a long-term directionality distribution of incoming weather
- the orientation of the structure for a given long-term directionality distribution of weather

- the relation between visual wave-period and expected value of average mean period
- the joint long-term distribution of the spectrum parameters (significant wave height and average mean wave period):
    - marginal distribution of average mean period.
    - dependence between the parameters or not.

In the parameter studies on the statistical model, the same dynamical model was utilized. The shear modulus of the soil was $G_s = 3.0 \cdot 10^7$ N/m^2.

The highest eigenperiod was 4.5 seconds and the modal damping for the first two modes was about 10% of the critical damping.

The effect of the type of wave spectrum applied in the statistical treatment was investigated both through short- and long-term analyses. In the short-term analysis an extreme storm situation was considered with significant wave height of 15 m and various average mean periods. Discrepancies of the order 25 - 60% in the extreme responses were observed, depending the choice of spectrum (Pierson-Moskowitz, Jonswap, Derbyshire-Scott, Modified Derbyshire-Scott. The effect of the choice of wave spectrum is, as expected, less as expressed by the extreme values (at a certain probatility level $10^{-8.7}$) obtained through a long-term analysis. The discrepansies are in the order of 10 - 25%.

The difference between the use of the more realistic short-crested waves instead of long-crested waves was investigated by two alternative long-term analyses:

- In the first place all waves were assumed to come from one direction. Two directions were considered. The reductions of the response values due to short-crested waves were 13 and 3 percent, respectively.

- In the second place it was assumed that the estimated directionality distribution were describing the weather conditions. The reduction was found to be about 10 %. However, the size of the reduction is dependent of the directionality distribution and the orientation of the structure, and due to the uncertainity in the distribution it is hard to make any final conclusions for this part.

Reliable data on the long-term directionality is yet not available. A common procedure for calculating the long-term distribution of response have been to assume all weather to come from one direction. The direction is normally chosen to be the most adverse direction for the actual response. To investigate the adequacy of the above assumption a reasonable long-term directionality distribution was estimated, and the result of this analysis was compared to the results obtained under the first assumption. The most probable largest response amplitude, at probability level $10^{-8.7}$ corresponding to a return period of about 100 years, was found to be of the same order for the two analyses.

In the foregoing analysis the orientation of the structure was fixed with all weather coming from the most adverse direction. However, it is also interesting fo examine the effect of the orientation of the structure taking the long-term directionality distribution into account. The orientation of the structure was changed in steps of 30°. For all orientations the most probable largest response amplitude on probability level $10^{-8.7}$ was calculated. The difference between the highest and lowest response-amplitude was found to be about 15%; the maximum being approximately 10 % larger than the value obtained by letting all waves come from the most adverse direction for the actual response quantity. Although the used directionality distribution is not quite reliable, it seems to be clear that the orientation of the structure is an important parameter.

Investigation on the relation between visual wave-period and expected average mean period shows that the two relations recommended of Nordenstrøm, Ref.(81), gives no significant difference in the results.

A primary concept in the long-term approach is the joint long-term distribution of the wave spectrum parameters (significant wave height $H_{1/3}$ and mean average wave period, $\bar{T}$) which completely describe each short-term state. In the conventional long-term model $H_{1/3}$ and $\bar{T}$ are assumed independent. In the modified formulation the expectation of $\bar{T}$ is assumed to depend on $H_{1/3}$ while the standard deviation of $\bar{T}$ is a constant. The relationship between the expectation of $\bar{T}$ and $H_{1/3}$ is determined so as to avoid physically non-admissible combinations of $\bar{T}$ and $H_{1/3}$ (according to Phillips' equilibrium concepts). Using this modified long-term model, the most probable largest response amplitude was reduced with up to about 50% compared with the corresponding values for the original long-term model.

Comparison between a log-normal- and a normal distribution for $\bar{T}$ revealed that the most probable largest moment-amplitude (probability level $10^{-8.7}$) was reduced with up to 10% for the original long-term model using the log-normal distribution, whilst for the modified long-term model the difference was negligible.

At last a comparison between the deterministic response, the short-term response and the long-term response was made for an actual response quantity. The following conclusions were reached:

- the deterministic model probably underestimates the dynamic amplification. Using the deterministic model is only recommended if the results are calibrated to the results from a more accurate method

method.

- the short-term model can be utilized to estimate extreme loads. But care must be excercised when chosing the wave spectrum.
- the original long-term model overestimate the most probable largest response-amplitude as compared to the modified long-term model, which is physically a more realistic model, and gives results of the same order as obtained by a short-term model.

A long-term model is the only consistent probabilistic method to obtain response quantities for design against yielding and fatigue failure. However, up to now it suffers from lack of appropriate environmental data, i.e. data for the joint long-term distribution of wave parameters (significant wave height and average mean wave period. In particular instrumental data on:

- the distributions of the average mean period
- the correlations between significant wave-height and average mean period

are lacking.

For design against yielding a short-term model may be utilized. But in this method deterministic decisions regarding the weather conditions have to be made. When it comes to fatigue design, a long-term model is the only consistent method. The modified long-term model represents a possibility both for fatigue design and design against yielding. However, due to the lack of data, further work is necessary before final conclusions on the modified model can be made.

In the future efforts must be directed towards improved modelling of dynamic soil behaviour. More instrumental information- and in particular on directionality - on the statistical distribution of wave-spectrum parameters is required.

A fully reliable long-term model will probably not be found until one is independent of the visual observations.

The effect of scatter in basic data describing the soil, structure and sea behaviour, together with uncertainties inherent in the analysis technique can be transformed into scatter in response values. This information then may serve as a basis for a consistent reliability analysis.

REFERENCES

1. Martinsen, I.O.R. "Concrete Platforms", Paper presented at *Offshore North Sea Technology conference and Exhibition* Stavanger 1974.

2. Det norske Veritas: *Rules for the Design Construction and Inspection of Fixed Offshore Structures*, Det norske Veritas, Oslo 1974.

3. Fédération Internationale de la Précontrainte (FIP)(ed), *Recommendations for the Design of Concrete Sea Structures*, Cement and Concrete Association, London, 1973.

4. *Report of ISSC Committee 10- Design procedure* Proc. Fifth Int. Ship Structures Congress, Hamburg 1973.

5. The Task Committee on Structural Safety Adm. Committee on Analysis and Design of the Structural Division. (ed) "Structural Safety - A Literature Review". *J. Structural Division ASCE*, Vol. 98, 1972, No. 4, pp. 845 - 884.

6. Kanazawa, T.: *Recent Studies on Fatigue and Brittle Fracture in Japan*, Division of Ship Structures, The Norwegian Institute of Technology, Sept. 24-25th 1973.

7. Hanson, J.M. et al.: "Considerations for Design of Concrete Structures Subjected to Fatigue Loading", *ACI-journal*, March 1974, pp. 97-121.

8. Dowling, N.E.:"Fatigue Fracture Predictions for Complicated Stress-Strain Histories", *Journal of Materials*, Vol. 7. 1972, pp. 71 - 87.

9. Granholm, H.: *Reinforced Concrete*, John Wiley & Sons, New York, 1965.

10. Holand, I. and Hjort-Hansen, E.: *Damping of Vibrations in Cantilevered Prestressed Concrete Beams*, Division of Structural Mechanics, The Norwegian Institute of Technology, Trondheim, 1964.

11. Brøndum-Nielsen, T.: "Effect of prestress on the damping of concrete", *IABSE Symposium, Resistance and Ultimate Deformability of Structures Acted on by Well Defined Sepeated Loads*, Lisbon, 1973.

12. Ragget, J.D.: "Estimating Damping of Real Structures", *J. Structural Division, ASCE*, to appear.

13. Lazan, B.J. and Goodman, L.E.: "Material and Interface Damping", *Shock and Vibration Handbook*, Vol.11, Harris C.M. and Crede, C.E. (eds) McGraw Hill, New York, 1961.

14. Hurty, W.C. and Rubinstein, M.F.: *Dynamics of Structures*, Pentice Hall, 1964.

15. Zienkiewicz, O.C.: *The Finite Element Method in Engineering Science*, McGraw Hill, New York, 1971

16. Clough, R.W. and Penzien, J.: *Dynamics of Structures*, McGraw Hill, New York, 1975

17. Hsieh, T.K.: "Foundation Vibrations", *Proc.Inst. Civ. Engrg.* Vol. 22, 1962, pp. 211 - 226.

18. Hall, J.R.: "Coupled Rocking and Sliding Oscillations of Rigid Circular Footings", *Proceedings of the International Symposium on Wave Propagation and Dynamic Properties of Earth Materials*, Albuquerque, New Mexico, 1967.

19. Richart, F.E., Hall, J.R. and Woods, R.D.: *Vibrations of Soil and Foundations*, Pentice-Hall, Englewood Cliffs, New Jersey, 1970.

20. Veletsos, A.S., and Wei, Y.T.: "Lateral and Rocking Vibration of Footing". *J.Soil Mechanics and Foundations Division, ASCE*, Vol. 97, 1971, SM 9, pp. 1227 - 1248.

21a. Hardin, B.O. and Drnevich, V.P.:"Shear Modulus and Damping in Soils; I. Measurements and Parameter effects"*J.Soil Mechanics and Foundations Division, ASCE*, Vol. 98, 1972, SM 6, pp. 603 - 624

21b. Hardin, B.O. and Drnevich, V.P.: "Shear Modulus and Damping in Soils: "Design Equations and Curves"*J.Soil Mechanics and Foundations Division, ASCE*, Vol. 98, 1972, SM 7, pp. 667 - 692.,

22. Tajimi, H.: "Dynamic Analysis of a Structure Embedded in an Elastic Stratum", *Proc, 4th World Conference, Earthq. Engng.* Santiago, 1969.

23. Sarrazin, M, Roesset, J.M. and Whitman, R.V.:"Dynamic Soil-structure Interaction", *J. Structural Division, ASCE*, Vol. 98, 1972, pp. 1525 - 1544

24. Krizak, R.J., Gupta, D.C. and Parmelee, K.A.:"Coupled Sliding and Rocking of Embedded Foundations", *J. Soil Mechanics and Foundations Division, ASCE*, Vol. 98, 1972, SM. 12, pp. 1347 - 1358.

25. Roesset, J.M., Whitman, R.V. and Dobry, R.:"Modal analysis for structures with foundation interaction". *J. Structural Division ASCE*, Vol. 99, 1973, pp. 399 - 416.

26. Luco, J.E. and Westmann, R.A.:" Dynamic Response of a Rigid Footing Bonded to an Elastic Half-space". *J. Appl. Mech. ASME* 39, June 1972, pp. 527 - 534.

27. Awojobi, A.O.:"Estimation of the Dynamic Surface Modulus of a Generalized Gibson Soil from the Rocking Frequency of Rectangular Footings". *Geotechnique*, Vol. 23, 1973, No. 1. pp. 23 - 31.

28. Kobori, T., Minai, R., Suzuhi, T. and Kusahabe:"Dynamical Ground Compliance of Rectangular Foundation", *Proc, of the 16th Japan Nat. Congr. for Applied Mechanics*, 1966

29. Sarrazin, M.A.: *Soil-structure Interaction in Earthquake Resistant Design*, Research Report R70-59, Dept. of Civil Engng., Mass.Institute of Technology, Sept. 1970

30. Luco, J.E.:"Impedance Functions for a Rigid Foundation on a Layered Medium", *Nucl. Engng. and Design*, Vol. 31, 1974, pp. 204 - 217.

31. Veletsos, A.S. and Verbic, B.:"Basic Response Functions For Elastic Foundations", *J. Engineering Mechanics Division ASCE*, Vol. 100, 1974, . EM2, pp. 189 - 201.

32. Novak, M. and Beredugo, Y.O.:" The Effect of Embedment on Footing Vibration", *Proc. 1.st Can. Conf. on Earthquake. Eng. Res.*, University of British Columbia, Vancouver, B.C. May 1973, pp. 111 - 125.

33. Urlich, C.M. and Kuhlemeyer,R.L.:"Coupled Rocking and Lateral Vibration of Embedded Footings". *Canadian Geotechnical Journal*, Vol. 10, 1973, pp. 145 - 160.

34. Anandakrishnan, M. and Krishnaswamy, N.K.: "Response of Embedded Footings", *J.Soil Mechanics and Foundation Division, ASCE*, Vol. 99, 1973, pp. 863 - 883.

35. Bielak, J.: *Dynamic Behaviour of Structures with embedded foundations*, Research Report E8, Institute de Ingenieria Universidad Nacional Autonoma de Mexico, 1974.

36. Novak, M.:"Effect of Soil on Structural Response to Wind and Earthquake", *Earthq. Engng. and Structural Dynamics*, Vol. 3. 1974, pp. 76 - 96

37. Veletsos, A.S. and Meek, J.W.:"Dynamic Behaviour of Building-foundation systems" *Earthq. Engng. and Structural Dynamics*, Vol. 3, 1974, pp. 121 - 138.

38. Lee, T.M."Surface Vibration of a Semi-infinite Visco-elastic medium". *Proc. Int. Symp. on Wave Propagation and Dynamic Properties of Earth Materials.*

39. Velestos, A.S. and Verbic, B."Vibration of Viscoelastic Foundations", *Earthq. Engng. and Structural Dynamics*, Vol. 2, 1973, pp. 87- 102.

40. Öner, M. and Janbu, N.: "Dynamic Soil-Structure Interaction in Offshore Storage Tanks", *Proc. Int. Conf. on Soil Mechanics and Foundation Engng. Istanbul*, March 1975.

41. Lamb, Sir Horace, "*Hydrodynamics*" 6th ed. New York: Dover Publications, Inc. 1945

41b. Havelock, T.H. "The Pressure of Water Waves upon a Fixed Obstacle", *Proceedings of the Royal Society of London* A 175, 1940

42. Morrison, J.R., O'Brien, M.P., Johnson, J.W. and Scaaf, S.A.: "The Force Exerted by Surface Waves on Piles", *Petroleum Trans.*, 189, TP 2846, (1950), pp. 149 - 154.

43. Kinsman, B.: *Wind Waves*, Prentice Hall Inc. Englewood Cliffs, New Jersey, 1965.

44. McCamy, R.C. and Fuchs, R.A.:"Wave Forces on Piles, a Diffraction Theory", *Beach Erosion Board*, Tech. Memo, Vol. 69, 1954.

45. Faltinsen, O, and Michelsen, F.C.:"Motions of Large Structures in Wave at Zero Froude Number", *International Symposium on The Dynamics of Marine Vehicles and Structures in Waves*, University College, London, 1974.

46. Garrison, C.J. et al.:"Wave Forces on Large Volume Structures - A Comparison Between Theory and Model Tests." Preprints *Offshore Technology Conference*,OTC paper No. 2137, 1974.

47. Hafskjold, P.S., Tørum, A, and Eie, J.:"Submerged Offshore Concrete Tanks," *Proc. XIII International Navigation Congress of PIANC*, Ottawa, Canada, July 1973.

48. Garrison, C.J. and Chow, P.T. "Wave Forces on Submerged Bodies", *J. Waterways, Harbours and Coastral Engng. Div. ASCE*, Vol. 98, 1972, pp. 375 - 389.

48b. Larsen P.K.:" Dynamiskerespons av plattformer." (in Norwegian) Symposium on : Strøm,bølge og vindkrefter på marine konstruksjoner, NIF , Geilo 1975

49. Hogben, N. and Standing, R.G.:"Wave Loads on Large Bodies." *International Symposium on the Dynamics of Marine Vehicles and Structures in Waves*, University College, London, 1974.

50. Dalton, L. and Helferstine,L.A.:"Potential Flow Past a Croup of Circular Cylinders", *ASME paper*, 71-FE-18 1971.

51. Bretschneider, C.L.:"Overwater Wind and Wave Forces", in *"Handbook of Ocean and Underwater Engineering"*, Myers J.J., Hohn, C.L, and McAllister, R.F.(eds) McGraw Hill, 1969.

52. Moan, T. and Giske, K.: *WACUFO - Automated Calculation of Wave- and Current-forces on Three-dimensional Structures Composed of Cone Members*. Users Manual SK/P19, Division of Ship Structures, The Norwegian Institute of Technology, Aug. 1973.

53. Clough, R.W.:"Application of the Finite Element Method to Problems of Structural Dynamics" , *NATO Advanced Study Institute on Finite Element Methods in Continuum Mechanics*, LNEC, Lisbon, 1971.

54. Lin, S.C. and Fager, L.W.:"Earthquake Interaction by Fast Fourier Transform", *J. Engineering Mechanics Division ASCE*, Vol. 197, No.EM 4, Proc.Paper 8324, Aug. 1971, pp. 1223 - 1237.

55. Foss , K.A.:"Co-ordinates which Uncouple the Equations of Motion of Damped Linear Dynamic Systems".*J. Appl. Mechanics*, Vol. 25, 1958, pp. 361 - 364.

56. Whitman, R.V.:"Soil-Structure Interaction" in "*Seismic Design for Nuclear Power Plants*", R.J. Hansen, (ed) MIT Press, Cambridge, Mass., pp. 241 - 269.

57. Johnson, T.E. and McCaffery, R.J.:"Current Techniques for Analyzing Structures and Equipment for Seismic Effects", presented at the February 3 - 7, 1969, *ASCE National Meeting on Water Resources*, held at New Orleans, La.

58. Nien-Chien Tsai.:"Modal Damping for Soil Structure Interaction", *J. Engineering Mechanics Division, ASCE*, Vol. 100, 1974, No.ST 4, pp. 324 - 341.

59. Thomson, W.T., Calkins, T. and Caravani, P.:"A Numerical Study of Damping", *Earthq. Engng. and Structural Dymanics*, Vol. 3, 1974, pp. 97 - 103.

60. Caughey, T.K.:"Classical Normal Modes in Damped Linear Dynamic Systems", *J. Appl.Mechanics*, Vol. 27, 1960, pp. 269 - 271.

61. Wilson, E.L. and Penzien, J.:"Evaluation of Orthogonal Damping Matrices", *Int. J. Num. Meth. Engng.* Vol. 4, 1972, pp. 5 - 10.

62. Richtmyer, R.O. and Morton, K.W.: *Difference Methods for Initial-value Problems*, 2nd.ed. John Wiley, New York, 1967

63. Argyris, J.H., Dunne, P.C. and Angelopoulos, T.:"Non-linear Oscillations Using the Finite Element Technique," *Comp. Meth. Appl. Mech. Engng.2*, 1973, pp. 203 - 250.

64. Bathe, K.J. and Wilson, E.L.:"Stability and Accuracy of Direct Integration Methods",*Earthq, Engng. Structural and Dynamics*, Vol. 1, 1973, pp. 283 - 291.

65. Nickell, R.E.:"Direct Integration Methods in Structural Dynamics", *J. Engineering Mechanics Division, ASCE*, Vol.99, EM 2, 1973, pp. 303 - 317.

66. Dean, R.G. and Harleman, D.R.F.:"Interaction of Structures and Waves", Ch. 8 of *Estuary and Coastline Hydrodynamics* A.T. Ippen, (ed) , McGraw Hill 1966.

67. Nath, J.H. and Harleman, D.F.R.:"Dynamics of Fixed Towers in Deep-Water Random Waves", *J. Waterways , Harbours and Coastal Engineering Division, ASCE*, Vol. 95, WW 4, Nov. 1969.

68. Wilson, J.F. and Muga, B.J.: *Dynamic Analysis of Ocean Structures*, Plenum Press 1970.

69. Malhotra, A.K. and Penzien, J.:"Non-deterministic Analysis of Offshore Tower Structures", *J. Engineering Mechanics Division, ASCE*, Vol. 96, 1970, No. EM 6, pp. 985 - 1003, Discussion by S.K. Chakrebarti, in Vol. 97, 1971, EM 3 pp. 1028 - 1029.

70. Foster, E.T. "Model for Non-linear Dynamics of Offshore Tower", *J. Engineering Mechanics Division, ASCE*, Vol. 96, . EM 1, February 1970, pp. 41 - 67.

71 Selna, L. and Cho,D. :"Resonant Response of Offshore Structures", *J. Waterways, Harbours and Coastal Engineering Division, ASCE*, Vol. 98, . WW 1, February 1972, pp. 15 - 24.

72. Berge, B.: *Three-dimensional Stochastic Response of Offshore Towers to Wave Action*, Ph.D.thesis, University of California, Berkeley, Nov. 1973.

73. Lin. Y.K. *Probabilistic Theory of Structural Dynamics*, McGraw Hill, N.Y. 1967.

74. Gumbel, E.J.: *Statistics of Extremes*, Columbia University Press, New York, 1958.

75. Lonquet-Higgens M.S.:"On the Statistical Distributions of Heights of Sea Waves", *J.Mar.Res.* Vol. 11, No.3. 1953.

76. Cartwright, D.E. and Lonquet-Higgens, M.S.: "Statistical Distribution on the Maxima of a Random Function", *Proceedings Royal Society of London, Series A*, Vol.237,pp.212 - 232.

77. St. Denis, M. and Pierson, W.J.:"On the Motions of Ships in Confused Seas", *SNAME, Trans.* Vol. 61, 1953.

78. Jasper, N.H.:"Statistical Distribution, Patterns of Ocean Waves and Wave Induced Ship Stresses and Motions with Engng. Applications", *SNAME, Trans*, Vol. 64, 1956.

79. Bennet.R.:"*Stresses and Motion Measurements on Ship at Sea*" Swedish Shipbuild. Res. Found. Rep. No. 13 - 15 1958-59.

80. Band, E.G.U.:"*Long-Term Trends of Hull Bending Moments*" Amer.Bureau of Shipping 1966.

81. Nordenstrøm, N.:"*Methods for Predicting Long-term Distribution of Wave Loads and Probability of Failure for Ships*", Det norske Veritas, report 71-2-S.

82. Ochi, M.K. and Bolton, W.E."Statistics for Prediction of Ship Performance in a Seaway", *Int. Shipbuilding Progress*, Part I: No. 222, Febr. 1973, Part II: No.224, April 1973, Part III: No. 229, Sept. 1973.

83. Price, W.G. and Bishop, R.E.D.: *Probabilistic Theory of Ship Dynamics*, Chapman and Hall, London, 1974.

84. Borgmann, L.E.:"Spectral Analysis of Ocean Wave Forces on Piling", *J. Waterways, Harbours and Coastral Engng. Division, ASCE*, Vol. 93, WW 2, May 1967.

85. Phillips, O.M.:"On Some Properties of the Spectrum of Wind- generated Ocean Waves", *Journal of Marine Research*, Vol. 16, 1958, No. 3, pp. 231 - 245.

86. Phillips, O.M.:"The Equilibrium Range in the Spectrum of Wind-generated Waves", *Journal of fluid mechanics*, Vol. 4 1958, No. 4, pp. 426 - 434.

87. Wiegel, R.L.:"Ocean Wave Spectra, Eddies and Structural Response", *Flow-Induced Structural Vibrations*, Symposium Karlsruhe, 1972, Springer-Verlag 1974.

88. Hasselmann, K. et.al.:"Measurements of Wind-wave Growth and Swell Decay During the Joint North Sea Wave Project.(J.O.N. S.W.A.O) *Dt. Hydrogr. Z*, 1973, Vol. A8, pp. 1 - 95.

89. Houmb, O.G. and Rye, H.:"Analysis of Wave Data From the Norwegian Continental Shelf," *Proc. Sec. POAC, Conf.* Trondheim, 1972.

90. Haaland, L.:"Private communication", The Norwegian Meterological Institute, Oslo.

91. Walden, H.: "Die Eigenschaften der Meerswellen im Nordatlantischen Ozean", Deutscher Wetterdienst, Seewetteramt, Einzelveröffentlichungen, No. 41, Hamburg, 1964.

92. *Report of ISSC Committees No. 1,2 and 3,* Proc. Fifth Int. Ship Structures Congress Hamburg, 1973.

93. Amin, M, and Ang. N.H.S.:"Non-stationary Stochastic Model of Earthquake Motions", *J. Engineering Mechanics Division, ASCE,* Vol. 94, EM 2 1968, pp. 559 - 583.

94. Shinozuka, M.S.:"Monte Carlo Solution of Structural Dynamics", *Computers and Structures,*Vol.2,1972 pp 855-874.

95. Borgmann, L.E.:"Ocean Wave Simulation for Engineering Design", *Proc. Conf. Civil Engrg. in the Oceans,* 1968.

96. Burke, B.G. and Tighe, J.T.:"A Time Series Model for Dynamic Behaviour of Offshore Structures", *Offshore Technology Conference,* Houston, Texas, 1971, paper no. 1403.

97. Pedersen, B. Egeland, O, and Langfeldt, J.N.:"Calculation of Long-term Values for Motions and Structural Response of Mobile Drilling Rigs", *Offshore Technology Conference,* Houston, Texas, 1973, paper no. 1881.

98. Bell, A.O. and Walker, R.C.:"Stresses Experienced by an Offshore Mobile Drilling Unit", *Offshore Technology Conference*, Houston, Texas, 1971, paper no. 1440.

99. Earle, E.N. and Mandrey, W.L.:"Determination of Dynamic Characteristics of Offshore Platforms from Random Vibrations", *Offshore Technology Conference*, Houston, Texas, 1973, paper no. 1840.

100. Berge, B. and Penzien, J.:"Three-dimensional Stochastic Response of Offshore Towers to Wave Forces", *Offshore Technology Conference*, Houston, Texas, 1974, OTC-paper no. 2050.

101. Vandiever, K.J.:*Structural Evaluation of Fixed Offshore Platforms*, Dissertation, Department of Ocean Engineering, Massachusetts Institute of Technology, 1975.

102. Bell, K.: *A Simplified Dynamic Analysis of the Condeep Platform*, Report STF 71 F 74001, Division of Structural Engineering SINTEF, NTH, STF 71-F74001, Trondheim, 1974.

103. Moan, T.: *Techniques for Stochastic Dynamic Response Analysis of Offshore Platforms*, Division of Ship Structures, The Norwegian Institute of Technology, Trondheim, (Preliminary Version), May 1974.

104. Haver, S, Moan, T. and Vinje, T.:"*RESP - A Program for Stochastic Dynamic Response Analysis of Bottom Supported Platforms*", Division of Ship Structures, The Norwegian Institute of Technology, Trondheim, 1975.

105. Holand, I.:"Dynamic Analysis" (in Norwegian) *Course on Concrete Structures on the Continental Shelf*, The University of Trondheim, The Norwegian Institute of Technology, Trondheim, 1975.

106. Eatock-Taylor, R.:"A Preliminary Study of the Structural Dynamics of Gravity Platforms", *Offshore Technology Conference*,, Houston, Texas, 1975, OTC-paper no. 2406.

107. Moan, T., Haver,S. and Vinje, T.:"Stochastic Dynamic Response Analysis of Offshore Platforms, with Particular Reference to Gravity-Type Platforms", *Offshore Technology Conference*, Houston, Texas, 1975, OTC-paper no. 2407.

108. Sigbjørnson, R.:"Private communication", Division of Structural Engineering, SINTEF, NTH, Trondheim, Aug. 1975.

109. Öner, M.: *A Finite Element Approach to the Equivalent Spring Constant Problem in Soil Dynamics*, Dissertation, Division of Soil Mechanics and Foundations, The University of Trondheim, The Norwegian Institute of Technology, August 1975.

110. Larsen, P.K.:"Dynamic Response of Platforms" (in Norwegian) *Course on Current, Wave, Wind-forces on Marine Structures*. The Norwegian Association of Professional Engineers, Geilo, 1975.

111. Langen, I.: "Dynamisk analyse av konstruksjoner". (in Norwegian). Division of Ship Structures. The University of Trondheim, The Norwegian Institute of Technology, June 1975

APPENDIX A

A.1 EQUIVALENT MODAL DAMPING BY ENERGY CONSIDERATIONS

Soil Damping

The equivalent modal damping due to the soil may also be obtained by energy considerations, Refs.(25,36,56).

Assume that the structure is free to undergo *horizontal* x-z translations u_i and rotation, θ_i, in the vertical plane x·z, Coupled sliding and rocking in the y-z plane is treated in a similar manner. The torsion about a vertical axis is denoted by θ_i. Vertical motion is treated separately. i = 1 corresponds to the point at the interface between soil and structure. Further consider the j'th interaction vibration mode with natural frequency ω_j (equal to that of the undamped system).
The work done during a period of vibration $T = 2\pi/\omega_j$ by the damping forces $P(\dot{x})$

$$A_L = \int_0^T P(\dot{x}) \cdot dx(t) \qquad (A.1)$$

The damping forces P and moments acting at the footing during harmonic motion

$$u_{1_j}(t) = u_{1_j}\sin\omega_j t \qquad \theta_{1_j}(t) = \theta_{1_j}\sin\omega_j t \qquad (A.2\text{, a-c})$$

$$\phi_{1_j}(t) = \phi_{1_j}\sin\omega_j t$$

are

$$\begin{aligned} P_x(\dot{u}) &= c_{xx}\dot{u} = c_{xx}\, u_{1_j}\omega_j\cos\omega_j t \\ M(\dot{\theta}) &= c_{\theta\theta}\dot{\theta} = c_{\theta\theta}\, \theta_{1_j}\omega_j\cos\omega_j t \\ M(\dot{\phi}) &= c_{\phi\phi}\dot{\phi} = c_{\phi\phi}\, \phi_{1_j}\omega_j\cos\omega_j t \\ P(\theta) &= c_{x\theta}\dot{\theta} = c_{x\theta}\, \theta_{1_j}\omega_j\cos\omega_j t \\ M(\dot{u}) &= c_{\theta x}\dot{u} = c_{x\theta}\, u_{1_j}\omega_j\cos\omega_j t \end{aligned} \qquad A.2\text{,d-h)}$$

The total work done by these forces during a period T is

$$A_L = \pi\omega_j(c_{xx}u_{1j}^2 + 2c_{x\theta}\theta_{1j}u_{1j} + c_{\theta\theta}\theta_{1j}^2 + c_{\phi\phi}\phi_{1j}^2) \quad (A.3)$$

The potential energy of the whole structure can be calculated as maximum kinetic energy and is

$$A_T = \sum_{i=1}^{n} \tfrac{1}{2}m_i u_{ij}^2 \omega_j^2 + \sum_{i=1}^{n} \tfrac{1}{2}I_{xi}\theta_{ij}^2\omega_j^2 + \sum_{i=1}^{n} \tfrac{1}{2}J_i\phi_{ij}^2\omega_j^2 \quad (A.4)$$

in which m_i = mass, I_{xi} mass moment of inertia in the vertical plane, J_i = mass moment of inertia about the vertical axis and n the number of masses.

The damping ratio of the structure due to the geometric damping (and equivalent viscous damping due to hysteretic effects) in the soil is defined for the response in the j'th mode as:

$$\bar{D}_j = \frac{A_L}{4\pi A_T} = \frac{1}{2\omega_j M_j}(c_{xx}u_{1j}^2 + c_{\theta\theta}\theta_{1j}^2 + c_{\phi\phi}\phi_{1j}^2 + 2c_{x\theta}u_{1j}\theta_{1j}) \quad (A.5)$$

$$M_j = \sum_n (m_i u_{ij}^2 + I_{xi}\theta_{ij}^2 + J_i\phi_{ij}^2) \approx \underline{\Sigma m_i u_{ij}^2} \quad (A.5a)$$

The effect of the mass moments (I_{xi}) is assumed negligible in Eq.(A.5a).

Similarily, with vertical vibration the equivalent damping ratio for the j'th mode is

$$\bar{D}_j = \frac{1}{2\omega_j M_j} c_{zz}\omega_{ij}^2 \quad (A.6)$$

where

$$M_j = \sum_n m_i\omega_{ij}^2 \quad (A.6a)$$

Eq.(A.5) is equivalent to computing the damping matrix according to $\phi^T C \phi$ and neglecting off-diagonal terms.

Superstructure Damping

The damping in the structure may also be transformed into an equivalent interaction mode damping. The same argumentation as utilized by Novak, Ref.(36) in the case of the soil is adopted. Consider for simplicity the coupled sliding and rocking motion in the x-z plane.

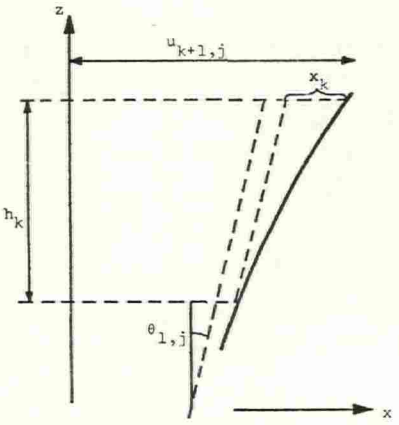

Fig. A.1 Displaced structure in the x-z plane

Assume that the equivalent viscous structural damping is caused by the relative velocity of adjointing stations measured with respect to the translated and rotated axis of the structure.

$$x_k(t) = u_{k+1,j}(t) - u_{kj}(t) - h_k \theta_{1,j}(t) \qquad (A.7)$$

θ_{1j} is the rotation of the footing.

Note that index k is utilized to denote the levels in the vertical direction.

If the structure at a level (k) is equipped with horizontally rigid braces it is necessary to associate only one mass and dashpot to each level. Otherwise, the number of shafts determine the actual number of masses and dashpots.

The work done by all dampers during period $T = 2\pi/\omega_j$ is

$$A_L = \sum_{k=1} \int_0^T \{ c_k(\dot{u}_{k+1,j} - \dot{u}_{kj} - h_k \cdot \dot{\theta}_{1j})^2 \} dt \qquad (A.8)$$

where c_k is the damping constant of the k'th dashpot.

Assume further that the damping constant c_k is proportional to the mass m_{k+1} which is attached to the damper from above, and equal to

$$c_k = 2\alpha m_{k+1} \qquad (A.9)$$

where α is a constant common for the whole structure. Obviously, other damping mechanisms than Eq.(A.9) may be assumed, Refs.(14,16).

The work for the j'th mode then becomes

$$A_L = 2\pi\alpha\omega_j \Sigma_k m_{k+1}(u_{k+1,j} - u_{kj} - h_k \theta_{1j})^2 \qquad (A.10)$$

The maximum potential energy (A_T) of the interaction problem is again given by Eq.(A.4).

The effective interaction modal damping due to the structure is

$$\bar{D}_j = \frac{A_L}{4\pi A_T} = \frac{\alpha}{\omega_j M_j} \Sigma_k m_{k+1}(u_{k+1,j} - u_{kj} - h_k \theta_{1j})^2 \qquad (A.11)$$

Denoting all the magnitudes corresponding to the rigid foundation bt a "cross", and dividing Eq.(A.11) by the same expression written for the rigid footing yields the structural damping ratio for the structure on a flexible foundation

$$\bar{D}_j = \chi_j \bar{D}_j^+)$$

where

$$\chi_j = \frac{\omega_j^+}{\omega_j} \frac{M_j^+}{M_j} (\Sigma m_{k+1} (u_{k+1} - u_{kj} - h_k \theta_{1j})^2$$

$$/(\Sigma m_{k+1} (u_{k+1,j}^+ - u_{kj}^+)^2 \qquad \text{(A.13)}$$

In Eq.(A.13) $\bar{D}_j^+$, ω_j^+ and u_{ij}^+ are the structural damping ratio, natural frequency and displacement amplitude for mode (j) of a structure with *rigid* foundation. $\bar{D}_j$, ω and u_{ij} are the corresponding values for the soil-structure interaction problem. θ_{1j} is the rotation of the foundation. M_j is computed from Eq.(A.5a) with amplitudes u_{ij}, M_j^+ is computed from the same equation but using amplitudes u_{ij}^+.

The coefficient χ_j describes the modification of the structural damping due to foundation flexibility.

Relative Structural Damping in "1 DOF" Model Structure

An important special case is the correction coefficient, χ_1 for the first mode.

For the purpose of quantification consider the simple model problem shown in Fig. A.2.

Consider the simple model problem in Fig. A.2

χ_1 is then given as

$$\chi_1 = \frac{\bar{D}_1}{D_1} = \frac{\omega_1^+}{\omega_1} \frac{(u - h\cdot\theta)^2}{u^2} \simeq \frac{\omega_1^+}{\omega_1} (\frac{u}{u})^2 = (\frac{\omega_1}{\omega_1^+})^3 \qquad \text{(A.14)}$$

where the following formula for the 1 DOF system

$$\omega^2 = \frac{g}{u_{st}} \qquad (A.15)$$

is applied. u_{st} is the static displacement when a force of magnitude $M \cdot g$ is applied at the top of the structure. The formula (A.14) was arrived at by Bielak, Ref.(35) and Veletsos and Meek, Ref.(37) in another manner.

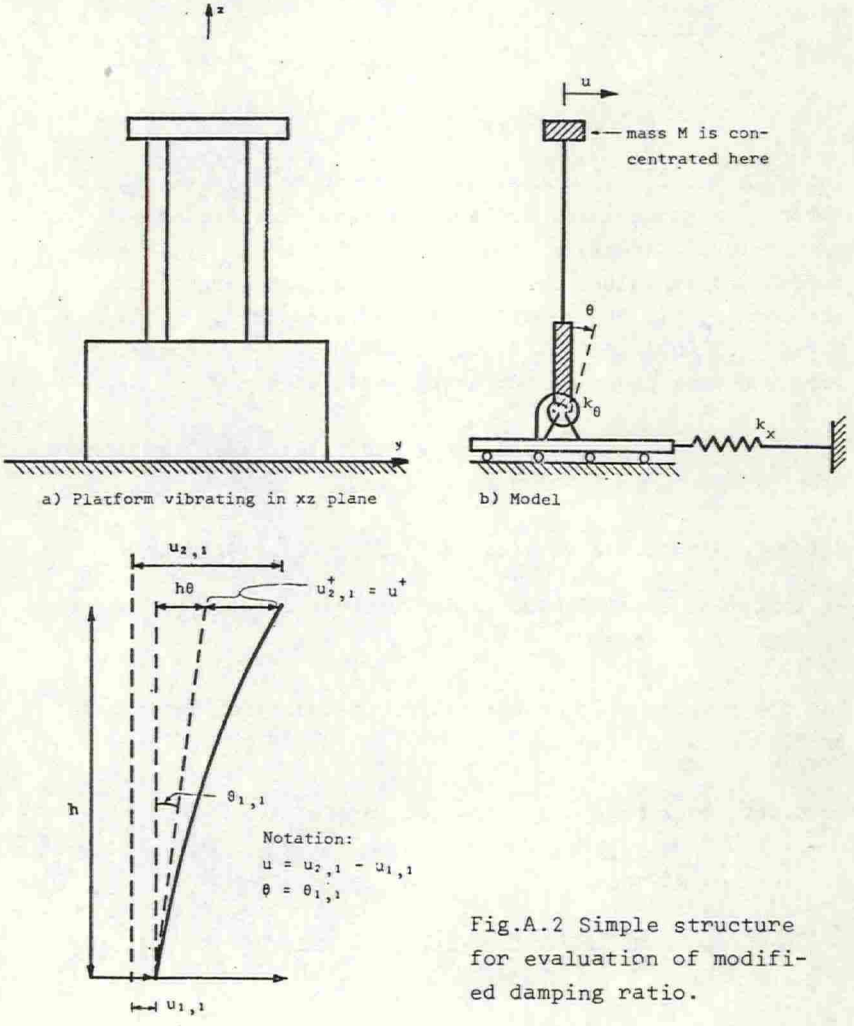

Fig.A.2 Simple structure for evaluation of modified damping ratio.

APPENDIX B

The program "RESP" consists of two independent parts.

I "RESP" - Computation of dynamic response in terms of transferfunctions.

II "LONTIM"- Calculation of the long-term distribution of response.

Simple flowcharts for the two parts are shown on the following pages.

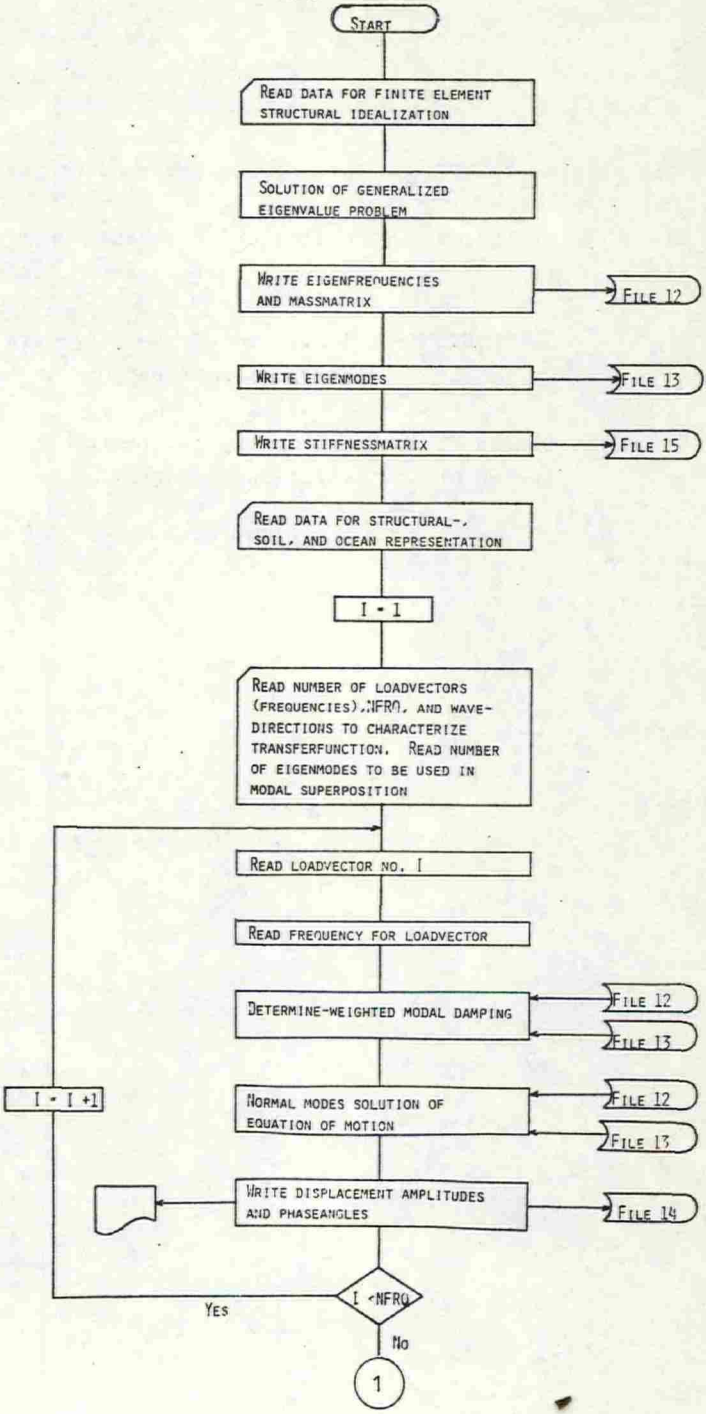
START
READ DATA FOR FINITE ELEMENT STRUCTURAL IDEALIZATION
SOLUTION OF GENERALIZED EIGENVALUE PROBLEM
WRITE EIGENFREQUENCIES AND MASSMATRIX
FILE 12
WRITE EIGENMODES
FILE 13
WRITE STIFFNESSMATRIX
FILE 15
READ DATA FOR STRUCTURAL-, SOIL, AND OCEAN REPRESENTATION
I = 1
READ NUMBER OF LOADVECTORS (FREQUENCIES), NFRQ, AND WAVE-DIRECTIONS TO CHARACTERIZE TRANSFERFUNCTION. READ NUMBER OF EIGENMODES TO BE USED IN MODAL SUPERPOSITION
READ LOADVECTOR NO. I
READ FREQUENCY FOR LOADVECTOR
DETERMINE-WEIGHTED MODAL DAMPING
FILE 12
FILE 13
NORMAL MODES SOLUTION OF EQUATION OF MOTION
FILE 12
FILE 13
WRITE DISPLACEMENT AMPLITUDES AND PHASEANGLES
FILE 14
I = I +1
I <NFRQ
YES
NO
1

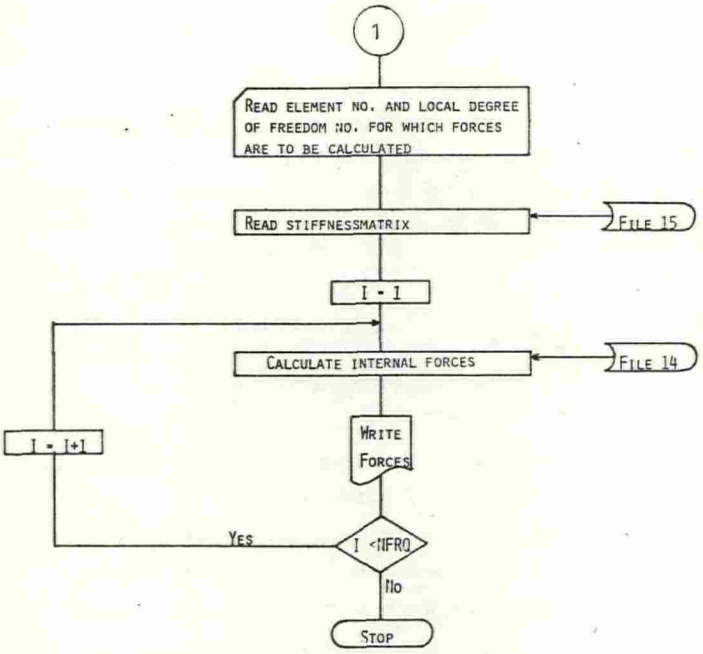

Fig.B.1 Flow chart "RESP" - part 1

APPENDIX C EXAMPLE COMPUTER TIMES

Display of typical time comsumption (CPU-time) is listed in Table C.1. The structural model in the present case consists of 21 beam elements and 6 boundary elements. The total number of degrees of freedom is 102.

Table C.1

Part I

1. Solution of generalized eigenvalue problem, 8 eigenvectors.	23 sec.
2. Calculation of loadvectors by WACUFO, Ref. (36) 20 load conditions.	80 sec.
3. Calculation of transferfunctions for all displacement components (transferfunctions were computed for 20 frequencies.)	43 sec.
4. Calculation of transferfunctions for 6 force components.	23 sec.
	2 min 49 sec.

Part II

Calculation of long-term response. Incoming waves in one direction, long-crested waves, one transferfunction (described by 20 values). Long-term distributions for 6 response quantities were determined.	21 sec.
Calculation of marginal long-term response Incoming waves in 12 directions, separate wave parameters and transferfunctions in all idrections. Long-term distributions for 6 response quantities were computed.	3 min. 50 sec.

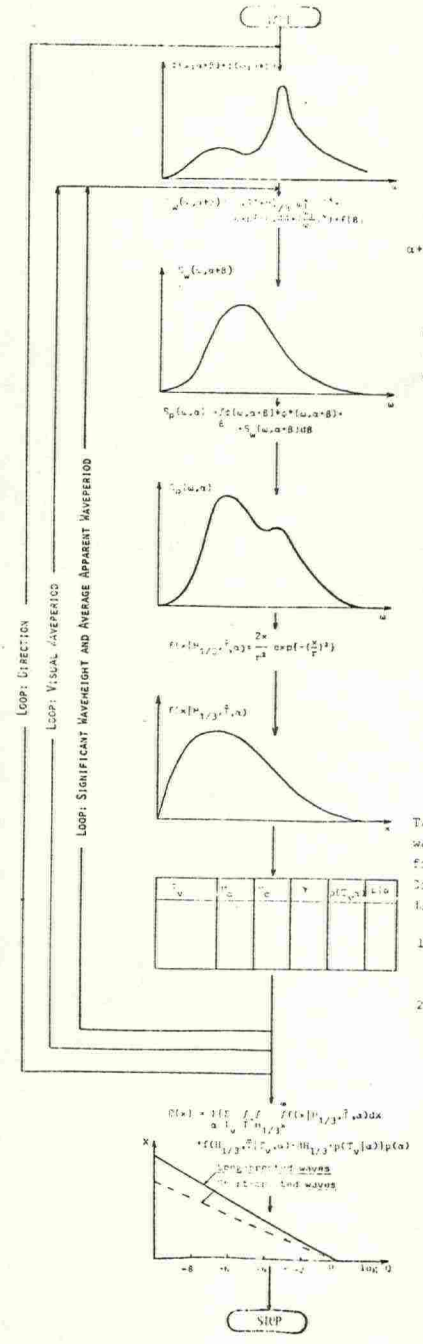

Wave-environment

Response

Transferfunction calculated for various wave-directions

α = main direction of sea

α+β = direction of elementary wave

Wave-spectrum, one- or two-dimensional (long- or shortcrested waves.)

Response-spectrum

Variance:

$$\sigma^2 = \int_0^\infty S_R(\omega,\alpha)d\omega$$

(It is implicit that σ^2 is a function of $H_{1/3}$ and $\bar{T}$ and α)

Short term estimation of response-amplitudes. Rayleigh-distribution is assumed, and the Rayleigh parameter $r^2 = 2\sigma^2$

Tables on long-term wave data, one table for each direction, α. Given interval of T_v late in the form of:

1) Normal-distribution of average apparant period, $\bar{T}$.
2) Weibull-distribution of visual- and significant waveheight.

Long-term estimation of response, Q(x) - probability of exceeding the response amplitude

Fig.B.2 Flow chart "RESP" part 2